Investigation of ultra-high injection fuel sprays and their effect on in-cylinder mixing

A thesis submitted to

The University of Brunel University London

For the degree of

DOCTOR OF PHILOSOPHY

By Christopher Nichols

Principle supervisor Professor Hua Zhao

Secondary supervisor Doctor Changzhao Jiang

December 2023

Abstract

Retarded start of injection is a fuel injection strategy that can be implemented in supressing knocking combustion in the spark ignition (SI) engine, a major limiting factor in raising compression ratio to achieve higher thermal efficiency in such engine. Retarded start of injection requires a more rapid homogeneous fuel and air mixture formation within cylinder, which can be facilitated by the fast atomisation of liquid fuel at higher fuel injection pressure. Thus, in this study, systematic studies were carried out on the fuel injection process and in-cylinder mixture formation at ultra-high injection pressures well above those used in production SI engines. Characterisation of fuel sprays from a multi-hole injector was done by means of the high-speed imaging, Phase Doppler Particle Anemometry (PDPA) and in-cylinder mixture formation in an optical engine by the laser induced fluorescence (LIF) technique. High-Speed Imaging revealed that the momentum of the fuel spray leaving the injector and hence its penetration length increase rapidly at ultra-high injection pressures, which can be an issue using the multi-hole injector in a direct injection spark ignition engine because the injector was designed for compression ignition diesel engines. PDPA was used to assess the D10 and D32 droplet sizes and how diameters of the fuel droplets would be changed with pressures ranging from 20 to 100MPa. D32 droplets progressively reduced till roughly 70MPa beyond which the diameter did not reduce any further whereas the D10 continued to reduce with the increased injection pressure. It is likely that the pressure increase is not the sole cause for a decrease in droplet diameters but rather a turbulent effect brought on by the exiting fuels kinetic energy causing the perimeter of the fuel spray boundary to be increasingly interacting with the surrounding air leading to smaller droplet sizes. Normalised standard deviation in fuel distribution was used to quantify the effects of fuel pressure and end of Injection (EOI) on the in-cylinder fuel and air mixing process in an optical engine by LIF testing at fuel quantities equivalent to 4.5, 7 and 9 Bar BMEP at 1200rpm. The LIF results confirmed wall impingement with earlier EOI as was expected with the earlier high-speed spray imaging results although a reduced standard deviation in fuel distribution was found with later EOI. With the current injector design, the occurrence of wall impingement is a major limiting factor and the geometry, number and distribution of the injector holes need to be optimised in order to be able to implement effectively the retarded injection with ultra-high injection pressures.

Acknowledgements

There have been many people around me that have provided their support in one way or another and without it, the long journey of obtaining a doctorate degree would have been even more challenging. The qualities of curiosity and tenacity distilled in me through my family are attributes I hope never dwindle and without the care of my parents the work in these pages would never have occurred.

To my supervisors Professor Hua Zhao and Dr. Changzhao Jiang, it has been a pleasure to work with you gentleman. Your patience, guidance and understanding are at such high levels it is still unfathomable to me and are attributes I respect deeply. You both are examples to be followed and I am honored to call myself a student of yours.

Without the support and interest of the Ford Motor Company's research team based in Cologne, guided by my industrial supervisor Dr. Helmut Ruhland, this research work would not have happened and I would like to thank you deeply for the opportunity you have given me.

Contents

List of figures

List of tables

Abbreviations

AC	-	Alternating Current
ASOI	-	After Start of Injection
BDC	-	Bottom Dead Centre
CAD	-	Crank Angle Degree
DI	-	Direct Injection
DOA	-	Duration of Activation
DOI	-	Duration of Injection
FPS	-	Frames Per Second
LIF	-	Laser Induced Fluorescence
MAP	-	Manifold Absolute Pressure
MTBE	-	Methyl tert-Butyl Ether
PDPA	-	Phase Doppler Particle Anemometry
PFI	-	Port Fuel Injection
PFV	-	Photron FASTCAM Viewer
PWM	-	Pulse Width Modulation
RPM	-	Revolutions Per Minute
SD	-	Standard Deviation
SI	-	Spark Ignition
TDC	-	Top Dead Centre
TEL	-	Tetraethyllead
UV	-	Ultraviolet

Chapter 1: Introduction

1.1 Background

As a result of the increasing pressures to reduce global vehicle greenhouse gas emissions, automotive manufacturers have supported the development of ever increasingly efficient and cleaner internal combustion engines and the reduction of CO_2. However, the automotive industry still plays a significant contribution to carbon emissions and climate change [1].

The strive for the use of electric vehicles is grounded in the confidence that renewable energy sources will be used to supply the electricity that powers these vehicles. This stipulation is vital for the overall reduction in carbon emissions associated with the automotive and transport sector and is seen by many as a key strategy for sustainability [2]. Even though recent focus in the last decade has been drawn to solely electric vehicles the implementation date of a European ban on the sale of solely petrol and diesel cars has changed several times which brings scrutiny as to whether or not it will be feasible to bring the ban into effect for a variety of reasons not discussed here. With this in mind, there is still an interest in engine development up until the point of the bans' implementation. Additionally, it is worth noting that legislation brought into place by government bodies are a main driving force for societal change and the combat of climate change although research should also be aimed at other areas of study aimed at other applications of internal combustion engines to commercial vehicles, marine vessels, off-road mobile machinery and local power generators.

The European Union has welcomed the concept of 100% renewable electrofuels as part of its policy to achieve carbon neutrality. The production of electrofuels offer a solution for transport sectors that are challenging to electrify where liquid fuel is indispensable, such as aviation, shipping, mining and construction that rely heavily on liquid fuels. Despite the push towards electrification these industries experience major practical and logistical challenges that make high-pressure liquid fuels still a relevant area of study [3]. Recognising that a substantial number of vehicles will still need to be powered by internal combustion engines. There is a continual requirement to reduce emissions and improve efficiency from research and development efforts to obtain a sense of balance between sustainability and practicality to reach net zero [4].

1.2 Research outline

The aim of this project is to assess the characteristics of ultra-high-pressure liquid fuel injection and its implication for use with retarded injection to supress knocking combustion in a spark ignition engine. To complete this main aim, the research needs to be broken down into several key objectives.

To understand the effects fuel pressure and quantity have on the penetration length of the fuel spray, high-speed back lit illumination imaging is required. Images ensembles will need to be processed in MATLAB where a specially formulated code will need to be created to convert the images into tabulated results for examination.

Determining atomisation and velocity characteristics require the use of a PDPA system inside a constant volume chamber. Using this system to measure at different distances from the injector tip quantifies the droplets seen in the initial high-speed imaging along the spray plume and to see the effects fuel pressure has in terms of droplet size and velocity.

To evaluate the effectiveness of high injection pressure on the rapid homogeneous charge formation in an engine, high-speed Laser Induced Fluorescence (LIF) technique is employed to measure the in-cylinder fuel distribution during the fuel injection and the subsequent mixing processes. The first challenge is to mount the injector inside the single cylinder optical engine that is to be used along with the optimum placement of the high repetition laser and high-speed camera. The recorded LIF images for each case need to be processed, by means of Dantec Dynamics BSA flow software and MATLAB, to gather information on the standard deviation of mixture distribution within the cylinder and gain better understanding of the mixture formation process under different injection pressures, injection timings and fuel quantities (loads).

1.3 Thesis structure

This thesis is divided into eight chapters that contain the investigation into the macroscopic and microscopic properties of ultra-high-pressure direct gasoline fuel sprays before exploring in-cylinder fuel distribution inside an optical research engine.

Chapter one provides an overview of the automotive industry and the impact it has on climate change providing the motivation and main objectives of this study.

The literature in chapter two describes the latest in spark ignition engine technologies with regards to performance, fuel economy and emission characteristics before describing a modern automotive common rail direct fuel injection system. The mitigation and justification of how ultra-high direct fuel injection can combat knocking combustion is discussed in detail with the emphasis on fuel spray characteristics from previous studies along with their methods of measurements.

Chapter three provides information regarding the experimental apparatus in regard to the high-pressure fuel system that is required to provide 100MPa of fuel pressure and the electronic control system that operates the injector. The optical engine system and its control are also discussed accompanied by their specifications.

Chapter four begins with information on the camera apparatus and setup used for macroscopic spray characterisation. The post processing procedure is also explained before moving on to the results and discussion of the findings.

Chapter five describes the PDPA equipment used for the study including the triggering of the injector for the measurement acquisition. As the precise position of the PDPAs measurement region is imperative for the quality of results, the description of the experimental procedure is given. The droplet size and velocity results for different injector tip distance and fuel pressure are then discussed as the main content of the Chapter.

Chapter six recounts the apparatus used for the in-cylinder fuel distribution measurements providing details of the laser and camera optics. The experimental procedure is also explained in conjunction to the post processing of images used to extract the standard deviation of the image data sets. The main content of the Chapter is focused on the results of the in-cylinder measurements and their discussion.

Chapter seven provides a summary of the main findings found in the previous chapters for macroscopic spray characteristics, droplet size and velocity measurements and in-cylinder fuel distribution with chapter eight giving several recommendations for future work

Chapter 2: Literature review

2.1 State-of-the-art spark ignition engine technologies: performance, fuel economy and emissions

2.1.1 Downsizing

Engine downsizing has become a popular method for automotive manufacturers and refers to the practice of reducing the displacement of an engine while maintaining or even enhancing the performance and efficiency by using boosted technology strategies. An engine with fewer cylinders offers a reduction in CO2 and fuel consumption by the reducing internal component friction and weight while being optimised so that the engine operation near the minimum BSFC region during normal driving conditions [5] [6]. Originally, the primary function of turbochargers and superchargers was to boost engine performance by pressurising the incoming air, thereby elevating air density. This consequently improved engine efficiency as a result of the reduction in mechanical losses. Typical vehicles of today, petrol or diesel, utilise a single turbocharger that recovers exhaust pressure energy to rotate a turbine. The exhaust turbine is attached via a shaft to a compressor wheel that draws and compresses the intake air. There are different configurations of turbocharger for example, two-stage, twin-turbo and compound systems, depending on their application. Superchargers are compressors driven directly from the engine requiring power to operate them whether they are of positive or negative displacement type. A negative displacement type is similar to a turbocharger in terms of a compressor wheel but however is driven from the crankshaft and not by exhaust energy. A positive displacement supercharger for example a roots type, Lysholm screw or vane type are compressors that push air into the intake with the mechanical energy from the crankshaft. Both methods have traits in which rpm and load they operate effectively but a two-stage system can operate using a combination of supercharger and turbocharger.

Fraser *et al.* [5] used a 1.2 litre downsized engine to explore the impact of various boosting systems. Their findings indicate that a twin charger system is optimal for low-speed load with the best transient response coming from an electric supercharger before transitioning to a turbocharger at higher speeds. The constraints for downsizing are knocking combustion at high loads low engine speed, the mechanical and thermal limits of engine internals as well as external pipework and ancillaries, while still providing reliability and cost effectiveness to a wide range of vehicles.

4

2.1.2 Variable compression

In the last ten years variable compression ratio engines have been explored as a viable technology that can offer efficiency and versatility. Typical internal combustion engines have a fixed compression ratio, a ratio of the amount of swept displacement to cylinder head clearance volume. A variable compression ratio internal combustion engine can adjust this ratio in operation depending on conditions. When at a steady speed and load the compression ratio is increased achieving a better thermal efficiency leading to improved fuel efficiency. With highly boosted engines the compression ratio can be lowered at high loads to reduce the onset of knocking combustion.

This manipulation of compression ratio is achieved by a control system that accounts for engine temperature, speed, load and other inputs to alter a series of linkages altering the connecting rods effective swept geometry as featured in Infiniti's variable compression engine. Due to the inherited relative complexity of a variable compression ratio engine as opposed to a standard engine, the additional moving components and another control system add additional costs to the vehicle buyer that challenges its widespread adoption.

Singh and Shukla [7] undertook a numerical analysis, using specifically Diesel-RK software, to explore performance and emissions of diesel and bio-diesel. Increasing the compression ratio from 16, 17 and 18 at a steady speed of 1500 rpm the numerical analysis results showed as the compression ratio increased the thermal efficiency while the brake specific fuel consumption reduced. It was also noticed that as the compression ratios were raised the higher in-cylinder pressure and heat release rate was observed. As the cylinder exhibits higher pressures and temperatures the increase of NOx and CO2 emissions are the resultant. With extreme EGR dilution it may be possible to reduce these pollutants. However, according to M.H. Shelby *et al.* [8] study into the potential gasoline savings of variable compression ratio engines the fuel economy benefit could be up to 3.3%. Although savings in fuel economy is beneficial the overall cost and resources to create such a technology and implement into vehicles have been limited to a couple of vehicles produced by Nissan in the V6 engine for their Infinium brand and the most recent range extender engine for their e-Power system.

2.1.3 Pre-chamber ignition

Pre-chamber ignition is an engine ignition method where a smaller supplementary chamber, known as a pre-chamber, is used in combination with the main combustion chamber of an engine. Some of the cylinder's fuel/ air mixture is introduced to the pre-chamber via passageways to the main chamber in a passive pre-chamber set up or a dedicated fuel injector in an active-pre-chamber system, before a sparkplug ignites the pre-chamber mixture causing jets of high energy gasses to exit the openings of the pre-chamber into the main combustion chamber. These jets of free radicals initiate the combustion of the main combustion chambers air fuel mixture.

An advantage of this method of high ignition energy is that an improved combustion efficiency can be had by extending the lean limits of an air/ fuel mixture when employed with EGR mixture dilution, reducing pollutants such as NOx. The mixtures dilution to achieve an overall lean fuel/ air mixture has the caveat that it requires higher ignition energy to combust. This has led to development of pre-chamber ignition sources containing several smaller orifices for the high temperature pre-chamber flame radicals to initiate the main chamber charge. Toulson, E. *et al.* [9] experimented with jet ignition and found that smaller jets, rather than a large singular jet, penetrate further into the main combustion chamber creating faster burn rates due to the multiple distributed ignition sites caused by the pre-chamber radicals allowing the use of higher levels of EGR dilution and lean burn operation. The additional ignition surfaces several small orifices bring by creating more jets exiting the pre-chamber enable a faster flame front speed and result in a quicker and higher pressure rise over a traditional spark enhancing performance.

The necessity for a high ignition source can be tied to lean burn combustion, a method that sees the cylinder less than lambda 1. Lean burn operation requires a high level of ignition energy to commence combustion. By reducing the amount of fuel in the cylinder not only is fuel saved but the susceptibility of knock is reduced due to the lower combustion temperatures. Many engines on the market today utilise overhead camshafts that act upon multiple valves. With the addition of direct injection, the space required to supplement a pre-chamber is not always possible. However, a recent surge in rotary engine design for unmanned aerial vehicles may implement such an ignition method as to aid combustion efficiency as there is more free space to implement this ignition technique.

As an incompatibility with the efficiencies of the three way catalectic converters has led automotive companies to steer away from lean burn technologies the need for pre-chamber at this current time has swayed. Another reason why focus has moved away from pre-chambers is that the locally rich pre-chamber mixture and poor passive scavenging leads to more soot production within the pre-chamber. With more active pre-chambers making an appearance and

more research into catalytic converters the pre-chamber and lean burn can once again be explored

Overall, pre-chamber ignition is a method that aims to improve upon the traditional single spark plug process that has changed very little since the widespread use of automobiles over 100 years ago. In Figure 1 the pressure traces of a traditional and a pre-chamber spark plug can be seen and were produced by the author. As the pre-chamber spark plug has more ignition surface area it can react faster with the fuel mixture in the cylinder. A traditional spark plug has an ignition kernel that grow outwardly throughout the cylinder, reacting the fuel mixture as it spreads across the cylinder as a flame front and has a much slower ignition time. The visual differences between the two ignition methods can be seen in Figure 2 where high-speed imagery captured both ignition events in an image ensemble but is presented as an extract and were again produced by the author to visually and quantify the differenced in the two different types of ignition methods.
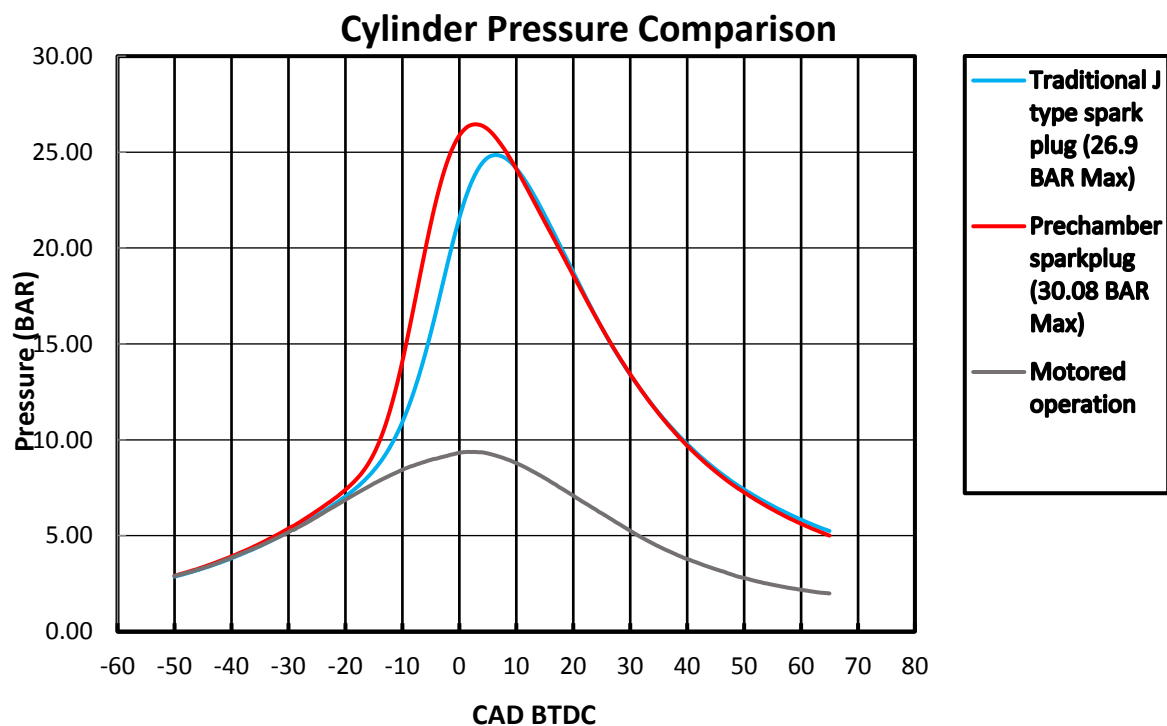
Figure 1: Cylinder pressure comparison of a traditional and a pre-chamber spark plug

CAD (BTDC)	Normal spark plug	Pre-chamber spark plug
10°		
6°		
3°		

Figure 2: An extract of a high-speed imagery ensemble taken of a traditional sparkplug and a pre-chamber sparkplug

2.1.4 Alternative fuels

As it stands, oil is the predominant fuel source in the transport sector significantly contributing to GHG and pollutants. The use of alternative fuels, as opposed to gasoline, has the potential to reduce the dependence of fossil fuels. The move away from fossil fuels to more renewable energy sources as a method to reducing emissions involves the introduction of new fuels and vehicle technologies and its mainstream adoption. This section provides an insight of some alternative fuel options that have the ability to be used as transport fuels. The relevance, manufacture and emission characteristics of ethanol, methanol, ammonia and hydrogen are explored.

Since the early days of automotive transport ethanol has been considered as an appropriate fuel for spark ignition engines with Henry Ford requiring the Model T to have the ability to utilise ethanol distilled from corn from local farms under the guise of self-sufficiency. Brazil has adopted this ideology in the seventies to minimise the reliance of imported oil with ethanol fuel being widely available throughout the country. A major advantage of an ethanol fuel source is it can ready be produced by using a well-known technology and with relative ease can be adopted by vehicle manufacturers as a flex vehicle fuel before being utilised as a sole fuel source.

The primary method for production is by the fermentation of feedstocks such as corn or sugar being the most popular. Almost any source of starch or sugar can be used with potatoes even being a potential source for ethanol. The choice of feedstock is governed largely by cost and the scalability for production. In Brazil sugar cane is the preferred source while in France grapes that are of inadequate quality for wine production. As of January 2022, the United States of America has reached 21 billion US gallons a year from 275 locations with the majority of them located in the Midwest where the largest amount of corn is produced [10]. Ethanol fuel production has been on the rise in America since the 1980s, encouraged by tax subsidies. To put the rise of ethanol production into perspective, in 1978 only 10 million US gallons of ethanol was sold. In 1991, America produced 875 million US gallons and sold 50 million US gallon to Brazil [11]. The step up in production is down to facilities meant to cater on a world-scale where smaller facilities do not have the efficiencies that the economics of scale can bring to produce ethanol at an even lower, competitive price of the larger scale producers. However, the production of crops for the explicit use of generating ethanol as a fuel source depends on its relative value to that of gasoline, aided by tax reliefs, and also the value that ethanol fuel has to the production of food.

Engines operating on pure ethanol suffer from more problematic cold starts in cooler climates in comparison to engines operating on gasoline. This is due to its lower vapor pressure but when combined in small amounts with gasoline this effect is reduced, hotter climates such as Brazil are able to forgo this to an extent. The neat use of ethanol can improve thermal efficiency and torque output providing the correct engine conditions are met and optimised to use such a fuel with a higher knock tolerance. Vehicles optimised to use ethanol typically command higher compression ratios or with boosting technologies being employed to counter the lower calorific value that ethanol provides. In 1996 Ford tested their flex fuel Ford Taurus with E85 and did not find any significant difference in engine out emissions when using gasoline [11]. In the experiment the E85 produced lower NOx and HC but were also convinced that the resulting lower exhaust gas temperatures of the ethanol reduced catalyst efficiency resulting in the tailpipe emissions being

the same as there control. Many studies have been conducted since suggest that there is notable variation in NOx and CO emissions [12] [13] [14] whilst Wallner *et al.* [15] found that NOx emissions decreased as the percentage of ethanol increases even at low percentages. When using ethanol, even in conjunction with gasoline as a blend, there are some apparent differences in vehicle driveability. The reduced calorific value of ethanol might initially suggest a rise in fuel consumption as it is less energy dense in comparison to gasoline. However, the benefits of charge cooling resulting from its increased latent heat of evaporation can lead to a 5% enhancement alone. Additionally, the higher-octane rating of ethanol permits the optimization of engines to employ a higher compression ratio and more aggressive spark timing, resulting in increased engine power [11]. From 2023 and onwards the American IndyCar series most notable for the Indianapolis 500 is aiming for the use of 100% ethanol as fuel in a move to be more renewable. As with many cases in racing, rules that govern the teams often lead to improvements in technology that filter down to the consumer market.

Methanol

The thought of utilising methanol as a motor fuel only gained prominence once it had established itself as a widely known and used industrial chemical. Its application as an automotive fuel dates back to the 1930s, where it served to supplement or substitute gasoline supplies. During this time methanol was used in high-performance engines and even saw use as a Grand Prix racing fuel. Although the use as the fuel for the Indianapolis 500 moved away from methanol as the exclusive permitted fuel in the late 2000s over safety concerns as the flame that comes from a methanol vehicle fire is indiscernible [11]. More attention was put into the research of methanol as a fuel source in the late 1960s but was expanded in the 1970s when the Western world faced a substantial energy crisis and gasoline shortages. Just as with ethanol, methanol can readily be manufactured, and can be adopted into vehicles gradually with fuel flex vehicles. However, considerations into its fire safety in case of accidents would need to be addressed along with handling instruction over toxicity [16].

Methanol is an industrial solvent commonly used in the chemical industry and is a colourless liquid. One of the main uses for this solvent is to manufacture MTBE which is used as an additive for gasoline as it increases its oxygen levels. An old name for methanol is "wood alcohol" as methanol was originally made from the distillation of wood. A large-scale manufacturing method was developed by Badische Anilin and Soda Fabrik, also known as the BASF chemicals company, in Germany in 1924 [16]. The process of producing methanol is by the steam reformation of de-sulphured natural gas. Under high heat and pressure the natural gas is reacted with the steam in the presence of a catalyst to form carbon monoxide and hydrogen. These

10

compounds are subsequently subjected to a methanol producing catalyst, resulting in the generation of liquid methanol. With the efficiencies involved in the manufacturing process larger production plans are more efficient than smaller ones. If the demand for methanol were to rise the investment for more production plants is essential.

As mentioned, the burning of methanol creates a nearly invisible flame to the eye that has always been a safety concern with its use. However, this demonstrated that methanol does not produce smoke or soot when combusted and makes it an alluring fuel for use in compression ignition engines. Unlike diesel fuel, no fuel particulates are formed which is the justification for the introduction and widening of London Ultra Low Emission Zones to reduce passenger diesel vehicles.

The advantageous physical and chemical properties of methanol can be harnessed in engines to yield lower emissions. Methanol, having a higher latent heat of vaporization consequently leads to a lowering of peak combustion temperatures and consequently a decrease in NOx emissions. In addition, methanol's higher oxygen content facilitates leaner combustion, resulting in reduced CO formation [17]. Initial tests of early model methanol flexible fuel vehicles showed increased emissions per mile compared to gasoline use, negating the reactivity advantage of methanol. However, recent flexible fuel vehicles have demonstrated the ability to achieve emissions per mile similar to those when using gasoline. With comparable vehicles, a methanol powered vehicle theoretically produces 94% of the emissions of their petroleum-fuelled counterparts in terms of CO_2 emissions. However, the production of methanol by the steam reformation of de-sulphured natural gas releases significantly fewer greenhouse gases compared to the production of gasoline. When considering the entire well to wheel fuel cycle, from extraction to combustion, methanol from natural gas exhibits very similar greenhouse gas emissions compared to gasoline [18] [19].

Methanol spark-ignition engines have the potential to exhibit a 15-20% higher efficiency compared to their gasoline counterparts. This enhanced efficiency is attainable due to the exploitation of methanol's broad flammability range for lean-burn technology as well as its high octane number The improved thermal efficiency of lean-burn engines means the production of fewer emissions, although it has been observed that lean-burn vehicles exhibit significantly reduced emissions of HC and CO but NOx emissions remaining roughly on par with those from current gasoline vehicles [20]. Advancements in 3-way catalytic converter efficiency could see the reduction of NOx from tail pipe emissions.

Flex fuel vehicles operating on a gasoline/ methanol mix, can adjust ignition timing and AFR on the fly with just the one fuel tank to save for convenience just as with ethanol flex fuel vehicles.

This is done via a concentration sensor in the fuel system that monitors the ratio of gasoline to methanol and adjusts base AFR and timing tables. This flexibility gives the customer freedom of a novel fuel source without depending solely on its availability which will be a major factor to the early adopting motorist [11].

<u>Ammonia</u>

Just as with methanol, ammonia is in some cases corrosive to some materials and possesses a health risk when inhaled but is easily detected due to its obscenely piercing odour.

The Haber-Bosch process is used to synthesise ammonia by combining nitrogen and hydrogen gas under high pressure in a reaction chamber. A catalyst inside the camber promotes the production of ammonia when the temperature is elevated to roughly 450 °C. In these high temperature and pressure conditions the molecules of hydrogen and nitrogen collide into each other and react to form ammonia molecules. When the successful process of ammonia production was found it transformed the agricultural sector around the world as ammonia was used in the manufacture of fertiliser with Fritz Haber being awarded the Nobel Prize in Chemistry for 1918.

When used as a fuel source ammonia has a higher energy density than other alternative fuels such as hydrogen and natural gas. With ammonia having a higher octane number of 110, it can also sport engines with increased compression ratios to raise thermal efficiencies [21] [22]. The low auto-ignition aptitude of ammonia suggests that it is suitable for SI engines but due to the narrow flammability limits and low flame speed it has a trend of incomplete combustion and results in the incomplete combustion and the presence of ammonia in the exhaust. To combat this the use of a promoter is used to increase cylinder temperature, with the best promoter being hydrogen as it is carbon free and has a higher combustion velocity and wider flammability range [23]. Although, if complete combustion occurs the products of combusting solely ammonia is nitrogen and water vapor, but NOx emissions are still a concern though there are no carbon containing emissions at all. The interest in ammonia as a fuel source is on the rise although traditionally it has been used when gasoline shortages have been extreme with one of the first well known instances of vehicles using ammonia is during World War II where a fleet of busses in Belgium were converted to use a mixture of liquid ammonia and coal gas [24]. Depending on fleet vehicle costs and the use of NOx traps the use of ammonia as a transport fuel could be on the rise. In particular, ammonia fuel is being considered as one of the most viable zero carbon fuels for large marine vessels.

<u>Electrofuels (E-Fuels)</u>

E-fuels are considered to be part of a broader effort to reduce CO2 emission in the transport sector as it offers a carbon neutral alternative. However, for their widespread adoption economical and technical challenges need to be addressed in its early phase if widespread adoption is to be a success. The idea of synthesising hydrocarbon-based fuels has roots in Germany during World War II but as climate change has gained notoriety the manufacture of these fuels is being considered as an option as a net zero carbon strategy.

E-Fuels are synthetic fuels fashioned from combining captured CO2 from the atmosphere with hydrogen that is produced using a renewable electricity source. The European Commission has allowed the sale of combustion engines after 2035, creating a new vehicle category, as long as they are able to operate solely on carbon neutral fuels created with a renewable electricity source. Hydrogen can be collected using electrolysis from water with the carbon dioxide molecules being captured from industrial applications or gathered from the air. The hydrogen and carbon dioxide are mixed together in a reaction vessel and subjected to a catalyst with heat and pressure known as the Fischer-Tropsch Synthesis to form methanol. The resulting methanol is dehydrated to from dimethyl ether before being converted into unsaturated hydrocarbons called Olefins. Further catalectic relations are used to form longer chains of hydrocarbons found in gasoline [25]. Currently Porsche has participated in a consortium in the production of E-Fuels in Punta Arenas, Chile and are aiming to "produce around 130,000 litres of E-Fuel annually" [26].

Since gasoline E-Fuel is essentially the same as regular gasoline vehicle performance and tailpipe emissions are the same. With this though there is no mitigation for NOx and so this would be on the rise in the atmosphere. The emissions characteristic of this fuel comes from the production method and that the carbon is sourced in carbon neutral technique. As long as the method to produce this fuel is carbon neutral then so are the tailpipe emissions of the vehicle although more large-scale production facilities need to be built in order to see the true effect E-Fuels have on climate change. With the aim of reducing emissions from combustion engines, many companies from around the word are creating and developing new technologies to improve components, overall engine design and the possibilities of using fuel other than crude oil distilled products.

<u>Hydrogen</u>

Over the decades Hydrogen has been hailed as a fuel of the future that could help end the globes dependence of fossil fuels in an effort to transition into net zero as it is an energy source that does not contain carbon. There is much discussion surrounding hydrogen fuel as there are obstacles to overcome for its widespread adoption from its manufacture and its safety concerns. Hydrogen is the most abundant element in the universe and on earth it is mainly found combined with other atoms in the form of water with much of the controversy has been about how to manufacture pure hydrogen. As hydrogen is combined in molecules, such as water, energy is needed to break the bonds between the hydrogen and oxygen atoms. The discussions have been about surrounding where this energy is originating from. When the hydrogen was produced with older coal or gas power stations though electrolysis or with methane steam reforming, the incentives to use it as a fuel source was never there as it was much more expensive and overall produced more emissions than other fuels. When climate changed became a major issue and more development was put into renewable energy sources the creation of hydrogen can now be viable in instances where the energy source is renewable.

Hydrogen when used in a fuel cell combines with oxygen and generates electricity producing water and heat that can be used to power vehicles with the benefit of the refuelling time is much shorter, minutes as opposed to hours, that is an obstacle for many people and transport companies. Hydrogen also has the ability to be retrofitted into conventional gasoline vehicles that are already present on the road as there are many vehicles in Europe are equipped to use compressed natural gas or liquified petroleum gas as a fuel source.

With the additional focus that has been placed on hydrogen over the recent years that has led to improved hydrogen cells and production efficiency, coupled with more renewable energy sources. Hydrogen could very well be the next widespread fuel source for transport in an effort to reach net zero. However, many obstacles are in place that need to be considered for the adoption of hydrogen even with conventual power sources that used as a stop gap until more renewable sources are implemented. Could see a long-term reduction in emissions that are desperately needed to avoid climate change.

2.2 Knocking combustion

2.2.1 Normal combustion

The normal combustion process commences between the spark plug electrode where the discharging spark creates an initial focal flame in the unburnt air fuel mixture. This small flame propagates though the unburnt mixture and releases the energy of the combustion mixture [27]. Since the flame front takes a finite time to propagate and create sufficient cylinder pressure the mixture is ignited just before TDC on the compression stroke. After ignition, the cylinder sees increased pressure due to the propagating flame penetrating the unburnt mixture while the piston is still compressing the mixture increasing the compression and the negative work [27]. While the engine is being ran at high rpm the peak pressure happens 15° after TDC allowing the maximum energy to be obtained from the expansion of the combustion gasses providing the engine positive work, as depicted in Figure 3. There is a balance to provide optimum ignition timing so that the peak pressure happens close to TDC to extract the most energy without experiencing abnormal combustion.

The delay between the initial creation of the focal flame to the time it takes for the flame to start propagating is called the ignition lag stage. The pressure rise after the ignition lag is the flame front propagating within the cylinder, ideally peak pressure should be closest to TDC where theoretically the most work can be extracted [27]. A representation of cylinder pressure is given in Figure 3.
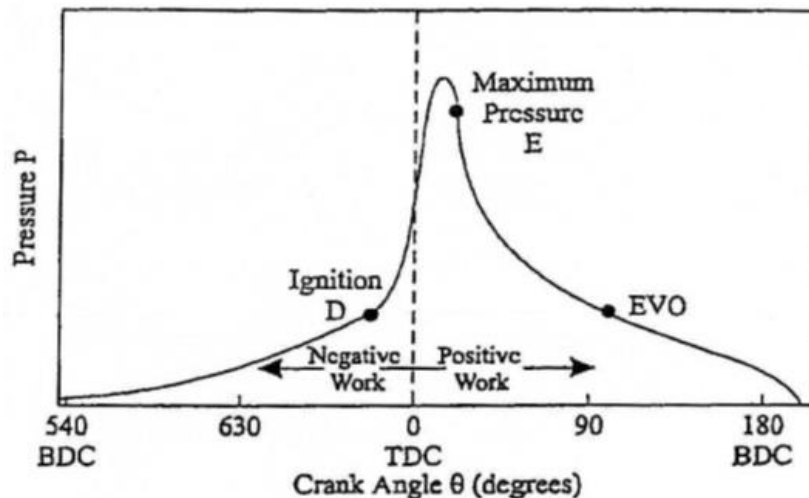
Figure 3: Stages of combustion for a reciprocating engine [28]

15

2.2.2 Abnormal combustion

Abnormal combustion can be prompted by numerous mechanisms, oil-fuel droplets can create new flame kernels at their location sites [29] just as with carbon deposits, gas-phase autoignition of the fuel-air mixture. Early pioneering in aviation led way to higher pre-ignition resistance of fuel being used as this alleviates the risk of engine damage. Overheated internal engine components can cause the temperature of the fuel and air mixture to be raised high enough that the mixture will self-ignite independently of an external ignition source. This temperature threshold is called the self-ignition temperature and varies between fuels [30]. High temperatures can be brought on by a combination of having too high an intake charge temperature, compression ratio, end gas compression or hot spots within the combustion chamber or on the piston surface. Cylinder bore size is also has a factor that needs to be considered when the engine is initially designed. Having the fuel air mixture self-ignite uncontrollably within an engine designed for SI operation is an undesirable trait as the resulting pressure wave pulses caused by the self-igniting fuel collide with the propagating flame front. This phenomenon is often called knock or ping due to the auditable sound the colliding wave pulses produce resonating on the cylinder wall [27]. High levels of knock can lead to higher peak pressures, that can cause damage within the combustion chamber. Figure 4 shows how destructive and undesirable combustion knock can be for engine internals. As can be seen the piston dome has been damaged due to extreme prolonged engine knocking overheating the aluminium piston and melting material over time, eventually leading to a 'holed' piston. Therefore, prolonged exposure to knock should be avoided.
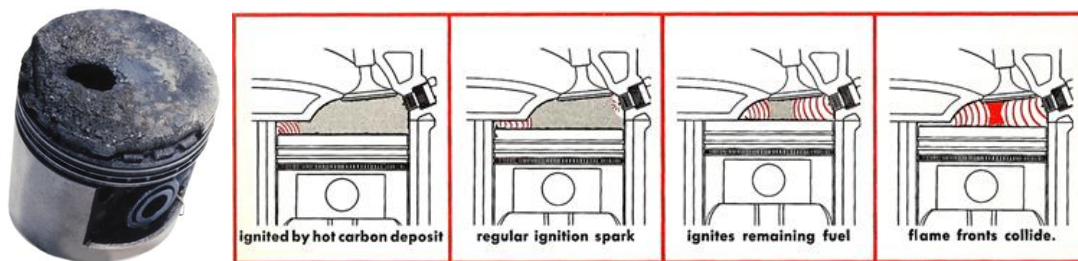
Figure 4: (left) Piston crown damaged caused by knock [31]
(right) colliding pressure waves in combustion chamber [32]

For knock to occur, the self-ignition temperature of the end gasses needs to be reached for an adequate amount time. The Livengood-Wu integral is the simplest model for describing self-ignition and can be described in equation (1), The Linengood and Wu integral [33].

$$\int_0^{tai} \frac{1}{\tau} dt = 1$$

where tai is the auto ignition temperature of the fuel; τ is the induction time at a certain pressure and temperature would lead to self-ignition the induction time (τ) can be calculated in (2), Induction Time, where Ap, B and n are fuel constants.

(2)

$$\tau = Ap^{-n} exp\left(\frac{B}{T}\right)$$

2.2.3 Knock detection

Since the colliding pressure waves pulses of knock vibrate the cylinder wall at typically between 6-10kHz it is possible to use an accelerometer as a knock sensor [34]. With computerised engine control, knock sensors can detect the onset of knock and factor in a safety margin into the ignition timing map, retarding the ignition where necessary whilst the engine is running to prevent engine damage. The alternative method for non-electronically controlled engines is to permanently retard ignition timing or reducing the compression ratio.

Meyer et al examined the fuel consumption of a vehicle designed to use 98 octane fuel equipped with a programmed ignition system utilising a knock sensor. Meyer et al results [35] in Figure 5 show that there was no significant change in fuel consumption for different driving conditions. However, some slight decline was noticed in the full load fuel economy test.

Fig 11 Fuel consumption versus octane rating for various drive conditions
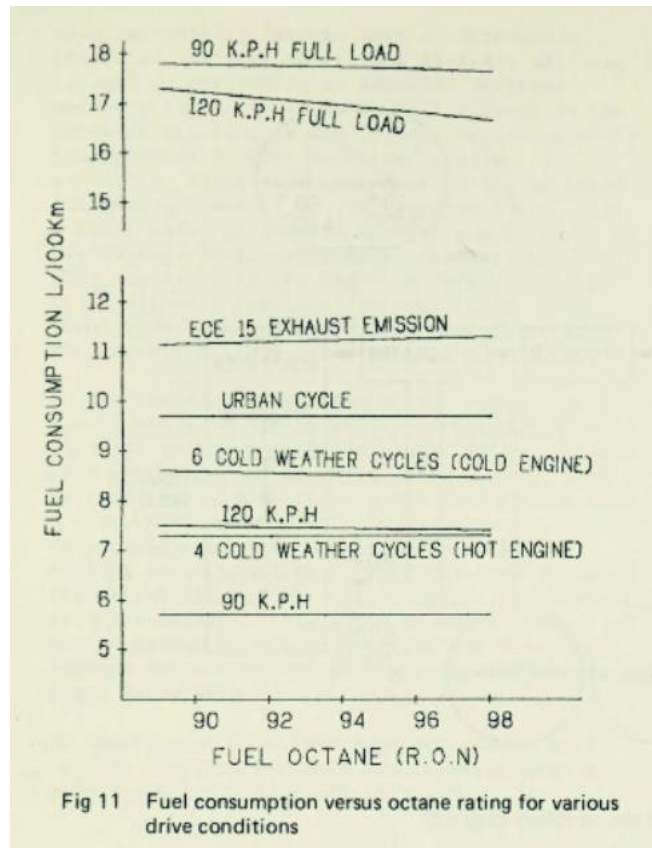
Figure 5: Fuel consumption with electronic ignition equipped with knock sensor [35]

Knock has always been a limiting factor in engine performance and efficiency with early relocations of this being found in the infancy of aviation where the inconsistent and low octane fuel available would damage engine internals. Although reasonably adequate for the day, a maturing in the refining process and development of more sophisticated engine designs saw greater efficiency and power gains. Tetraethyllead (TEL) was introduced into the market in the 1920s to raise the fuel octane to counter knock and worked remarkably well. However, the health and environmental concerns saw the gradual decline of lead in gasoline from 1986 in the United Kingdom. With the sale of leaded gasoline being fully banned in January 2000 in favour for other additive packages and more advanced engine components and designs. To meet the future emissions and fuel economy regulations, knock needed to be understood for the use of high efficiency engines. Downsizing has been a popular method employed by automotive manufactures to gain efficiency as the increased air density that comes with forced induction allows a smaller engine capacity to be used while maintaining the same level of performance. A smaller engine operating at higher loads, results in lower throttle losses under normal driving conditions. The higher induction densities results in higher combustion pressures that ultimately cause a temperature rise of the mixture charge ahead of the flame front leading to a rise in detonation. Before the rise of downsizing manufactures typically reduced engine compression

ratio as a means of a counter measure although this reduces any efficiency gains. With GDI and altering injection strategies over previous PFI, or even carburettor systems allow greater control methods to reduce in cylinder temperature and mixture exposure time [36]. Even with these countermeasures derived from electronic fuel injection, engine knock still plays a pivotal role in the quest for ever increasingly efficient engines.

2.3 Direct fuel injection

2.3.1 Introduction to Direct fuel injection

The ever-constant demand for reduced fuel consumption and emission formation has led the way for DI for SI engines. However, DI can first be seen the early 20th century pioneered by early aviation necessitating high output light aircraft engines. The first instance of fuel injection being introduced to the automotive sector was in 1952 by Goliath and Gutbord where the aim was to increase engine output by exploiting the effects of charge cooling [37]. The two-stroke powered Goliath GP700E and Gutbrod Superior 600 boasted Bosch fuel injectors located centrally near spark plug locations for the purpose of utilising evaporative cooling to increase power output in some models. Figure 6 shows the engine of a Goliath GP 900, the difference being the larger displacement between the engines, the mechanical injectors are clearly visible alongside the spark plugs.
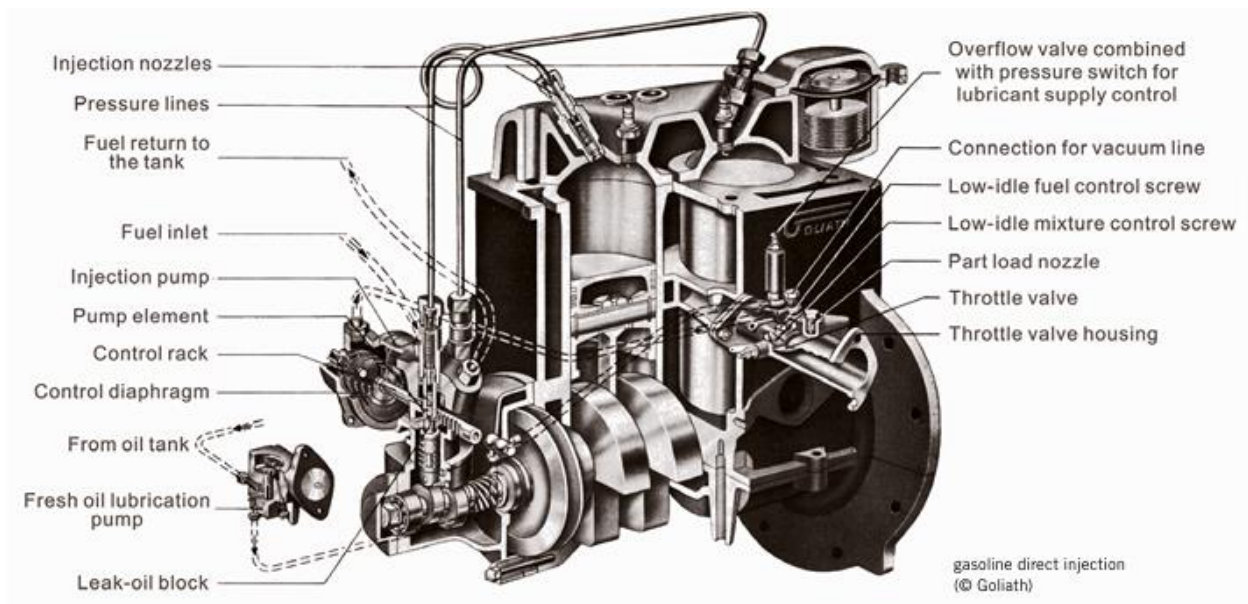
Figure 6: Engine of a Goliath GP 900 [38]

With the limited success of mechanical fuel injection and fuel spray behaviour it would not be until the late 1990s when the subject was more widely understood [39]. The improvements to fuel

injection technology meant that automobile engines could transition from an overall lean stratified operation at low to mid loads to a homogeneous stoichiometric operation at mid to high loads. These mixture formations are available with DI as a result of the placement of the injector and sophisticated ECUs that control injector timing and duration. Stratified operation necessitates late injection. This is where fuel injection to take place nearing the end of the compression stroke limiting the degree in which the fuel and air mix to the vicinity of the spark plug electrode. Homogenous operation requires early injection timing though the intake stroke permitting time to create a well-mixed fuel and air charge.

The application of DI of recent have been more focused to homogeneous operation with stoichiometric mixtures due to the effectiveness of three-way catalysts at this ratio. Coupled with the benefits of turbochargers, homogeneous DI can still provide low emissions and much improved fuel economy. These two classifications of DI are now widely used, though a stratified approach can provide decreased fuel consumption at a lighter load as it can provide an overall lean fuel air ratio in the cylinder but maintain a locally rich mixture near the sparkplug to maintain ignition. Though the increased NOx emissions call for effective after treatment with an included cost.

2.3.2 Description of the Direct fuel injection system

Modern high-pressure common rail direct fuel injection systems can be seen in both gasoline and diesel engines although the emphasis for this work is on gasoline systems. Figure 7 is a simple representation of how fuel is supplied to the injectors by means of a shared high-pressure fuel rail. In these cases, fuel is lifted from the fuel tank (1) under relatively low pressure from a small electric pump (2) to the engine bay of the vehicle where it is filtered (3). A mechanically driven pump (4) creates high pressure in the supply rail (5). As the ECU signals for the injectors (6) to trigger, fuel is gradually drawn from the common rail. A pressure sensor (7) and fuel pressure regulator (8) monitor and maintain constant pressure of the fuel supply.
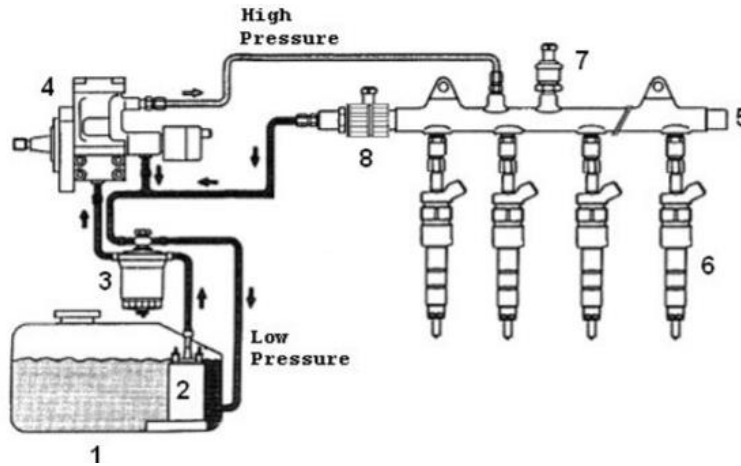
Figure 7: Simple depiction of a common rail fuel supply [40]

The fuel quantity delivered to the cylinder depends on the amount of time the injector needle is open and the difference in pressure between the fuel rail and cylinder gas pressure. For precise metering of the injector it is necessary to calibrate the needles voltage profile enabling pulsed current to maintain energising time and truss fuel flow. A short needle opening and closing time is necessary to maintain precision over different operating conditions. To operate a modern electrical fuel injector the engine control unit's logic sends an electrical signal to the injector driver unit, usually located in a powertrain control, module before a current is passed to the injector. Depending on the load and RPM of the engine a pulse of current of a specified length is sent to the injector to open the needle. The pulse sent to the injector typically has a higher initial current to rapidly move the needle off its seat before lowering and pulsing the current to maintain its open position.

High pressure fuel injectors have been specifically developed for spark ignition direct injection engines as the liquid fuel must be atomised into very fine droplets and dispersed in the desired region of the cylinder, piston or combustion chamber. Any variations in injection pressure can cause a change in the cone dispersion angle of the fuel spray. Sometimes this technique is used to alter the transition from narrow spray used for a stratified operation to a wider spray pattern used for a homogeneous spray formation when required [39]. As this would mean the injectors would need to be located directly in the combustion chamber this makes it essential that Injectors be able to withstand cylinder pressure and heat, although this makes them more expensive to produce over the PFI counterparts as they reside outside of the combustion chamber in the inlet tract and don't need to be able to withstand the same temperatures. Developments in technology have led to faster responding and more precise piezoelectric needle actuators, the mixture preparation is able to respond to changes in engine conditions faster since the fuel transport delay

though the majority of the intake stroke as experienced in PFI equipped vehicles is eliminated [39].

2.3.3 DI mixture preparation

DI has the ability to vary the fuel delivery time considerably quickly, changing the mixture formation within the cylinder. For homogeneous operation, a uniform distribution of fuel mixture within the cylinder is desired. An early injection produces a homogenous mixture when the piston is at the beginning of its intake stroke, similarly to that of a PFI, and is usually predominantly used for high load cases higher in the rpm range. For a stratified injection technique, the injected fuel mass must provide a near stoichiometric ratio in the vicinity of the spark plug electrode to facilitate stable ignition and combustion of the mixture charge within a limited combustion chamber volume.

Fuel vaporisation inside the cylinder in an injection strategy after the intake valve closure cools the air charge sufficiently to allow for a greater compression ratio as the subsequent cooling postpones the onset of knock. With injection timing advanced before the intake valve closure during the intake process a cooler and more condensed air charge can be optimised for WOT applications resulting in increased torque values. In certain low speed high load applications, the addition of fuel as an enrichment can be used to absorb in cylinder heat. As the fuel mass evaporates it removes heat energy from the surrounding surfaces the mixture where it is effectively cooling the mixture mitigating knock. The tighter mixture preparation control given by DI can improve the specific fuel consumption of an engine, raise engine output by offering higher compression ratios with improved fuel conversion efficiency although at higher fuel-system cost due to additional parts and overall system complexity [39].

Late injection when occurs on the compression stroke and can create stratified charge to achieve remarkably greater overall lean air fuel ratios under part load conditions. Coupled with a de-throttled intake can provide thermodynamic benefits favouring fuel consumption due to a reduction in pumping loss [39]. It is worth noting that the progression of three-way catalytic converter technology has hindered the widespread use of lean burn engines.
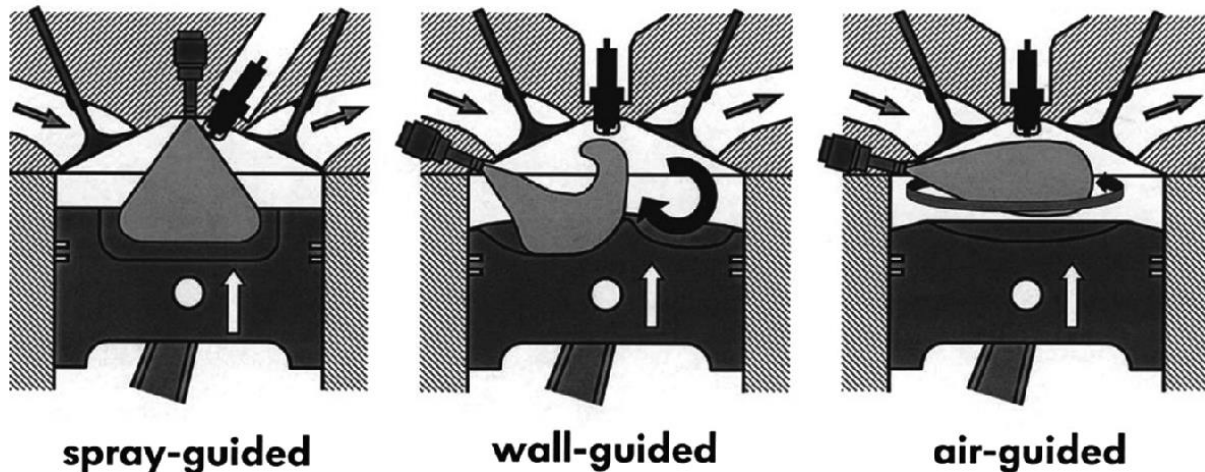
Figure 8: Illustrating the different methods of DI [41]

There are number of distanced types of direct injection, jet guided, wall guided, and air guided. Each with a different method of aiding the combustion process and are illustrated above in Figure 8.

When the combustion process is directed with a jet approach, the formation and development of the mixture charge are governed by the features of the fuel jet. As the fuel is propelled and propagates though the air, an ignitable layer of fuel and air mixture is formed on the outer boundaries of the jet. Spark plug and fuel injector positing need to be precise in order to ignite the mixture correctly just as the mixture reaches the plug at the time of ignition. As a result of this method this process is sensitive to the quality of the injection system and the spray provided. Satisfying this function as adequately providing consistent mixture formation in the upper part load range is problematic [39].

For a wall guided combustion arrangement, fuel spray is directed into a recess on the piston to evaporate the fuel droplets and designed to work in conjunction with the tumble movement of the incoming air charge to generate a good mixture formation. A drawback to this arrangement is that it compromises cold start emissions as the surface temperature of the recess is well below operating temperature hindering the clean burning of the fuel [39]. However, the excessive partial emissions upon cold start outweighs the overall benefits of improved fuel economy and reduction of greenhouse gasses [42].

With the advancement in fuel injection evolving from PFI where a typical a typical pressure of 6MPa is seen. A typical direct injection petrol vehicle on the road today can be observed using up to 14MPa of pressure. This has developed as the higher pressures have resulted in finer atomisation than their PFI counterparts along with the increased injection strategy methods. In

summary the adoption of direct injection plays many roles in preventing knock while being able to increase power and reducing tail pipe emissions.

2.3.4 Cold start emissions

GDI engines are well known for having increased specific output and efficiency. Although so too are the elevated levels of particulates while compared to PFI equipped engines [43]. Badshah, Kittelson & Northrop, (2016) conducted a study continuing several laboratory experiments into the increased amount of particulate emissions upon cold start conditions as the lower temperatures of fuel influence the volatility characteristics experiments along with many other studies [39] [44] [45] [46] [47]. To counter this, engines are forced to operate in fuel-rich conditions upon initial start-up ensuing that an adequate amount of the fuel fraction has evaporated, and thus is ignited [48] [49] [50]. In recent years the production of PFI systems has eased to make way for GDI, with apparent lower implementation cost, however in colder conditions fuel atomisation in wall-guided injection are hampered by the cold engine internals allowing for fuel to impinge on combustion chamber surfaces limiting vaporisation and having adverse effects on particulate emissions by flame quenching, pool burning culminating to incomplete combustion [51] [52]. This is less of a prominent problem in PFI as the fuel is sprayed on to the back of the intake valve. The fuel that impinges onto the cold surfaces of the intake port and backside of the valve is re-atomised by a shearing action with the influx of air once the intake valve is opened again. The objective of this study was to examine particle numbers, size distribution and mass during and after severe cold starts for PFI, GDI equipped cars. To mimic real life sample conditions a selection of newer vehicles with less than 50k miles, were chosen from a vehicle rental agency giving a total number of 10 GDI and 11 PFI. Vehicles were left overnight for a duration of 12 hours at roughly -20⁰C with them being tested in the morning. It is worth noting that the testing equipment had to be kept in a warmer environment, because of their minimum operating temperatures, and resided in a building while the testing probes were extended outside to the test vehicles.

Badshah *et al.* [42] tests found out that there was a significant difference between GDI and PFI Particulate emissions where the PFI vehicles where had a high initial spike upon start up and then gradually decreased while the GDI equipped vehicles had a lower initial peak but the production of particulates continued for a greater amount of time. Once a GDI engine has warmed up the characteristics of evaporative cooling benefiting the volumetric efficient and knock resistance can be attained although localised rich regions with slower evaporation hinder the, mixing of the fuel leading to the development of soot [51].

Even though GDI engines can offer increased fuel economy with a reduced emission output, work has highlighted the need for greater emission controls upon engine start up to meet upcoming standards, especially with the cold ambient temperatures that can be found in some countries [42]. The study selected a variety of already mass-produced automotive engines that can be found on the road today. Although this could be described more of an applied comparison of GDI and PFI in the modern vehicle. The differences between the manufactures and the subtle differences in manufacturer engine technology found within the engine bays does not enable a like for like experiment for the comparison of GDI and PFI.

With the considerably cold temperatures the study was conducted in it was necessity to have equipment remotely. Having equipment this far away from the subject is not ideal as partials may not be able to be sufficiently read by the apparatus. This was countered by forcing the particles to the machine via an airtube in order to read by the machine but it still remains that the analyser equipment was not in the ideal position although the results did show the variance in types of injection and followed the traits that were found in their literature review. It is essential to understand the mixture preparation process in order to control and minimise soot partials emission. Insights into GDI mixture preparation and combustion can be achieved using Optical engines to study and gather data for flow predictions, spray formations and AFR distributions [43].

2.4 Ultra-high injection Pressure

2.4.1 Concept of Knock Prevention by Retarded Injection

With the advancement in fuel delivery from carburettors to direct injection not only delivering better atomisation, electronically controlled fuel injection has the added benefit of precise fuel delivery timing under much greater injection pressure. To achieve the benefits of retarded injection, direct fuel injection must be utilised to rapidly form a homogenous fuel mixture while avoiding wall wetting to achieve optimum combustion [53]. Studies have shown that with a delayed injection approach does not give enough time for form a uniformly distributed mixture within the combustion chamber on the compression stroke [54] [55]. The studies mentioned advocate the avoidance of wall wetting to maximise combustion efficiency and minimize unburned fuels. Increasing fuel pressure is one way that would enable a faster fuel traversal in the combustion chamber. With a retarded but rapid mixture formation the end gas exposure time is greatly minimalised and with the aid of fuel cooling the chances of auto ignition occurring in the end gases is significantly reduced [56].

2.4.2 Reduction of in-cylinder temperature

Electronically controlled direct injection can supress knock by means of charge cooling. An injection of fuel into the cylinder at the early stages of the compression stroke reduces the temperature of the cylinder due to the latent heat of evaporation by the introduced high pressure fuel. In turn this will decrease the auto-ignition reactions of the premixed fuel and air mixture. Other than reducing knock in turbocharged or normally aspirated engines, taking advantage of latent heat of evaporation can also increase engine volume efficiency or compression ratio [4] [57] [58].

2.4.3 Reduction of temperature exposure time

Knock limits the maximum compression ratio and hence the efficiency of the engine. Therefore by delaying the SOI to occur later in the compression stroke the fuels exposure time to environmental heat inside the cylinder greatly reduces the knock phenomenon as it is governed by the temperature and pressure history of the end gas region [59] [60]. This reduction of contact time reduces the precursor of knock by preventing early oxidation of the end gas as there is less time for the mixture to create hotspots triggering ignition [61] [62]. With the additional high fuel pressure and velocity needed to inject fuel close to top dead centre, additional turbulence is created by small vortices from the injector's orifices leading to an increase in fuel distribution. Before these vortices diminish and dissipate it is possible to use its induced turbulence to aid in the speed of the combustion process when the mixture is ignited [56].

2.4.4 Previous ultra-high injection pressure research

Gasoline direct injection and other strategies have been implemented along with an increasing trend for higher compression ratios to achieve a higher thermal efficiency [63]. Knock has always been a major limiting factor in raising compression ratios and what can be safely be achieved. One method to combat this limitation is retarded start of injection where gasoline is injected directly into the cylinder late on the compression stroke shortening the fuels exposer to in-cylinder heat and by means of evaporative fuel cooling [56]. This method of injection requires a rapid homogeneous formation of the fuel/ air ratio to benefit the combustion process. However, thermal efficiency would be hampered by higher fuel momentum from higher injection pressures. This increases the likelihood of fuel impingement on cylinder surfaces translating to the creation of soot producing combustion [64] [65] [66] [67] which will be exacerbated by cold start conditions [68]. The effects of gasoline/diesel fuel blends were conducted by Z. Feng *et. al* [69] to investigate the atomisation characteristics with a diesel injector and a maximum common rail injection system

suitable of up to 140MPa. It is worth noting that the cone angle of the fuel spray did not fluctuate largely and remained rather consistent and as the gasoline ratios increased it was observed that significantly smaller droplet sizes were found. By using a similar methodology with solely gasoline, the droplet size should also decrease with high injection pressures which is beneficial as to produce high atomisation rates improving mixture formation that is used with retarded injection strategies.

In order to take full advantage of retarded start of injection a thorough understanding of the fuel mixing process needs to be understood. Fuel injector technology has improved significantly since the widespread implementation of electronic direct fuel injection. Initially increasing the number of holes an injector has a benefit on the creation of a more homogeneous fuel mixture with a decreased droplet size increasing the contact surface between the liquid-gas and as the need for better atomisation arises higher pressures are required [70]. With the high injection momentum from higher fuel pressures creates a growth in the turbulent diffusion as the smaller droplets migrate away from the centre of the plume at a higher rate than those of the larger droplets [71]. Advancing from PFI where fuel rail pressure is generally been in the region of between 0.3 to 0.5MPa. Direct injection pressures of 5, 10 and 20MPA were examined by S. Lee *et al.* [72] and is shown to reduce the SMD with increasing pressure. Diameter statistics also show that the highest pressure of 20MPa tends to produce a higher count of smaller droplets by at least 30%. Although these experiments were performed with a PFI a trend of higher fuel pressure against droplet diameter is expressed. S. Lee and S. Park [73] performed similar visualisation and PDPA experimental studies of a GDI injector with pressures up to 30MPa and found that injector pressure plays an important role in reducing the SMD up to 20MPa before plateauing where there after there was not a significant reduction in droplet diameter. With higher fuel pressures a similar trend in droplet diameter should present itself although at the risk of high injection momentum runs the risk of wall impingement.

An analysis of different methods for reducing fuel consumption conducted by Stiebels *et al.* [74] demonstrated that direct injection has the greatest single potential to reduce fuel consumption when compared to other concepts such as variable compression ratio, variable valve timing, engine downsizing of selective cylinder shut off. With this incentive Volkswagen have decided to focus its engine developments into direct injection so that the benefits can be combined with other appropriate fuel saving technologies. Richardson *et al.* [56] reviewed the potential of using high pressure fuel injection with retarded injection and successfully verified the theory by supressing knock. The study carried out by Richardson *et al.* shows that retarded start of injection is an effective measure for reducing the in-cylinder temperature and avoiding auto ignition through reducing exposure time. It was noted that retarded injection induced turbulence can release a

faster propagating flame, but the issues associated with high pressure mixture formation were confirmed. The fuel spray must rapidly penetrate the cylinder while avoiding wall impingement, which is one of the main worries with retarded injection as it can reduce the influence of the sprays turbulent effect and increase emissions. A homogenous mixture formed in a short amount of time has the potential to supress knock and remains a key ingredient in efficient combustion. Richardson *et al*. [56] conducted combustion experiments at 35, 60 and 120MPa fuel rail pressure with 35MPa having more wall wetting than the tests carried out at 120MPa. It was concluded that the spray characteristics for the 12 hole centrally mounted injector favoured the higher fuel pressures and showing higher atomisation, faster breakup, dispersal and a faster combustion. A reason for this could be because the injector that was used could have been a diesel injector with the injector's orifices being better suited to the characteristics of diesel fuel although this is not stated, similar characteristics could be observed with the Ford injector used in this study as its original design was for diesel application. The research and tests carried out in this paper has proven to deepen the understanding for knock prevention with retarded injection and Richardson *et al*. continue to undertake research into mixture formation. A study into a high pressure centrally located direct injection spark ignition engine by Hiraya *et al*. [75] used a multiple-hole fuel injector similar to the ones employed by diesel engines at the time in bowled piston and visualised the in-cylinder behaviour of the fuel using laser induced fluorescents. Isooctane was the fuel used for the optical tests, which is transparent to ultraviolet light, with dimethylaniline being added to the fuel as the fluorescent tracer. Using laser induced fluorescents Hiraya *et al.* was able to observe the effects of fuel injection pressure and spray angle had on mixture formation. To form a turbulent yet circulatory flow inside the piston bowl the fuel spray needed to be narrow and concentrated to the centre of the bowl. Higher fuel pressures of 30MPa or more were needed to create sufficiently stable combustion and with this, higher fuel pressures lead to better evaporation to prevent fuel wall flow. A laser Doppler velocimetry system can be used to measure the velocity of the fluid flow inside the AVL optical engines cylinder by means of measuring the Doppler shift in the convergence of the laser beams. This technique was used for fluid flow and spray investigations by Karaiskos *et al*. [76] to measure the spray formation generated by two swirl atomisers under various engine conditions. laser Doppler velocimetry was able to measure the decay of the turbulent vorticial structures that were created by the Cosworth cylinder head and observed strong tumble characteristics around the central axis upon and though the compression stroke. Using laser induced fluorescents and laser Doppler velocimetry it is possible to visualise Fords ultra-high-pressure injector in operation inside the spray test tank and AVL optical engine to view the characteristics of mixture formation for the study of retarded SOI.

Gradual improvements to high pressure fuel injectors have enabled better fuel spray diffusion, atomisation and according to the research of Saltoh *et al.* [77], high injection pressure is effective in reducing wall wetting. Fuel injection pressures researched here are mostly limited to below 35MPa although Postrioti *et al.* [78] comprehensively tested spray development of fuel pressures of 5MPa to 60MPa using high-speed imaging and PDPA concluding a decreasing trend for SMD that benefits in terms of soot reduction. There are some exceptions to fuel pressures of near 100MPa although they were for use in commercial diesel engines and exhibit a longer spray break up distance but remain relevant due to the measurement techniques. As such, ultra-high-pressure gasoline fuel injection is an extreme novelty in the automotive sector and require the study of the droplet size and velocities that are produced for future reference as little material exists on gasoline fuel injection of 100MPa. With the resources and equipment available, the in-cylinder mixture formation of ultra-high-pressure gasoline direct fuel injection can be studied by means of high-speed LIF giving a fine resolution to spray development.

2.5 Liquid fuel injection and spray measurement techniques

2.5.1 Back lit High-speed imaging

Initial characterisation of fuel injectors to determine their penetration lengths can be determined by defining the outline of the spray by creating a silhouette, forming shadowgraph images. Light scattering images by means of Mie scattering is where a front or side illumination is conducted. There is no significant end result of the two different methods although it has been reported using shadowgraphs it is found to distinguish the spray boundary easier [79]. Both methods require the use of a high-speed camera at a known distance to create a spatial calibration, the length of the fuel spray can be calculated by the individual camera frames.

The experimental setup consists of a light source to illuminate the measurement region. Care must be taken so that the alternating current (AC) from the power socket does not affect the light source by creating a pulsing effect. LED light sources are a good foundation as they provide ample bright light and do not get affected by the AC outlet power. To create even lighting on the measurement region the emitting light must be diffused to avoid an area of oversaturation for the high-speed camera. Any oversaturation of the camera can be dealt with by changing the lens aperture. To isolate the spray being measured a narrow depth of field is adventures as objects with little significance will be blurred out making the post processing of the spray boundary in the acquired images easier to detect. Post processing of the image ensemble to determine the sprays penetration length requires the isolation of the spray boundary in order to track the number of pixels it has travelled from the injector tip. The total number of pixels travelled in a frame can be

expressed as millimetres using the spatial calibration and plotted against time as the frame rate of the camera is also known.

High-speed imaging is a low-cost solution for visualising liquid spray formations for characterisation. The macroscopic characterisation of a fuel jet between 60 – 140MPa were presented in a study by Shao and Yan [80]. Their experiments focused on the effect of injection pressure had on the diesel spray characteristics in a pressurised constant volume chamber. The experiment revealed variations in luminosity intensity from image to image which could lead to the over exposure of the fuel spray boundary leading to errors. Although the experiment was conducted with a flashlight source and the energy stored should be equal a non-interrupted high intensity light source should be used in future experiments as to minimise luminosity variation in the resultant images. The results from Shao and Yan's study however revel that the diesel spray penetrated further and faster with wider cone angles being observed as the pressure raised which is expected due to the higher kinetic energy in the fuel.

S. Lee & S. Park [81] performed a similar visualisation technique in their experiment but used two metal-halide lamps instead of an LED light source, but even so similar images can still be had with a different light source as long as it is bright enough and does not pulse with the main grid AC current from the power outlet to keep the luminosity constant.

To improve the quality of the image ensembles Hwang *et al.* [82] averaged 30 recordings for an experimental condition. While the study conducted by Shao and Yan was derived from six repetitions of each case. Due to the fewer repetitions of samples the standard deviation (SD) presented is relatively large leading to an increased margin of error. Although the technical limitations in equipment experienced have been greatly surpassed. It is now possible to collect many thousands of images by a high-speed camera and process them with faster computers and memory. With this advantage in computing power, the repetition of experiments is an important factor in acquiring accurate results.

2.5.2 Phase Doppler Particle Anemometry

PDPA is an instrument that uses the Doppler effect and phase difference between scattered lights to measure and analyse the velocity and size of small droplets. This piece of equipment is used in research and industrial applications to study spray droplet formations such as aerosols, spray coatings and can be employed to study fuel injectors spray droplet characterisation. As a droplet passes though the laser beam measurement volume the light scattering from it can be detected and analysed to give droplet distribution and velocity.
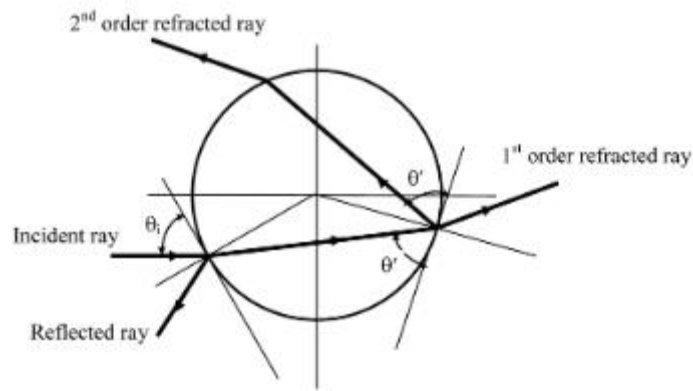
Figure 9: Geometric ray trace of incident ray though a spherical droplet [83]

Figure 9 is an illustration of an incident light rays' movement as it traverses though a liquid droplet. At the boundary layer of the droplet, light is reflected off the surface of the droplet and are known substituent as reflected rays. Light that passes through the boundary layer is refracted by the inner surface of the spherical droplet and are referred to as first order refracted rays. Rays that reflect from the inner surface of the droplet and refract outwards are called second-order refracted rays. Using the light scattering ability of the liquid droplet, when it passes the measurement volume it scatters the two laser beams causing interference. This interference creates a variation in intensity and a phase difference relative to the hypothetical wave which is proportional to size and partial position inside the measurement region. By examining the intensity and phase changes the droplet velocity and size can be calculated.

As shown in Figure 10 a single component PDPA system compromises of a laser source to emit a coherent and monochromatic light before being split by a dividing beam splitter. The two laser beams are then focused by a spherical lens to form a measurement volume at their intersection where the two laser beams' waist are. As a particle travels through the measurement volume where fringes of bright and dark regions are formed by the two identical laser light waves. The scattered light is characterised with a fluctuating signal from a photodetector, which frequency is directly related to the particle's velocity. As shown in Figure 11, when two photodetectors positioned at different angles, a phase shift is observed which is directly related to the particle size (assuming the particle is spherical). For gasoline and diesel fuel measurements, the two photodetectors are typically positioned around 120° to the beam splitter optics to capture the 2nd order refracted light by the passing liquid droplets in the measurement volume. By analysing this information, the size and velocity of spray droplets can be quantified non-intrusively and used as a valuable tool to characterise and quantify the spray from a fuel injector.
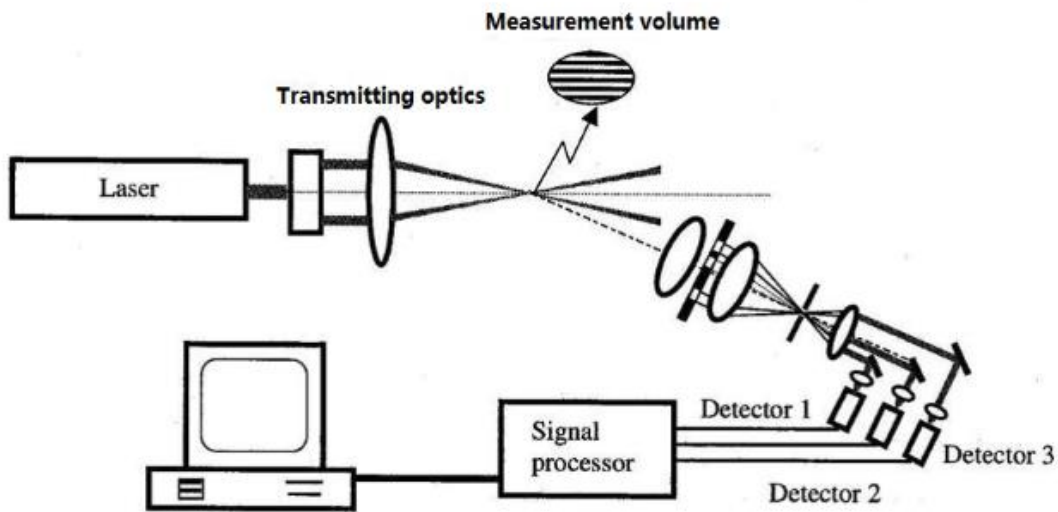
Figure 10: Diagram of a theoretical PDPA arrangement [83]
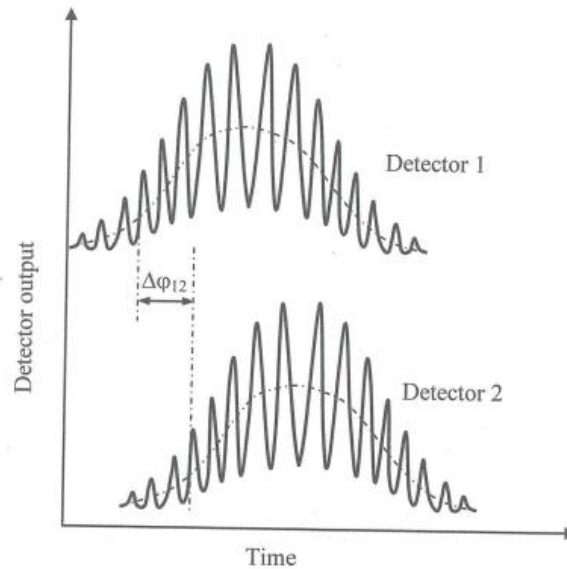
Figure 11: Representation of interference fridge patterns [83]

This technique for measuring fuel sprays, however, can become difficult due to high fuel droplet concentrations near the injector tip. Droplet validation and velocity measurements can also suffer as the measurement volumes size is large enough allowing more than one droplet inside at once [84] [83].

Poatrioti *et al.* [78] conducted investigations into the spray characteristics of a direct injection fuel injector with fuel pressures from 5 to 60 MPa with a Dantec PDPA system. Data was collected

from 360 consecutive injection samples for each injection case and reported low deviation in their testing. Injection rate profiles of the pressures tested at 1.5ms exhibits low fluctuations in the average velocity of the fuel spray droplets. Lower velocities were seen with the lower injection pressures with higher pressures reviling higher average velocities. With the slower, lower pressures tested, the tail of the fuel spray is longer as it takes more time for the tail to traverse the PDPA measurement volume. The spray head of the higher pressures, 50 and 60MPa, have a notable spike in velocity denoting that at these higher pressures the fuel spray is moving out of the measurement region due to the kinetic energy and it is possible that these pressures studied by Poatrioti *et al.* are actually at a much higher velocity as suggested. The placement of the PDPA measurement volume inside the jet plume is critical as deviation from the centre can cause a lowering of the average velocity [71] [85]. Using a sequential grid pattern similar to Jiang *et al.* and Araneo *et al.* the centre of the fuel plume can be assessed appropriately inside a PDPA system.,

2.5.3 LIF

Laser-Induced Fluorescence (LIF) is a measurement technique that detects the emission of light from a molecule following excitation from a laser source. In an optical engine LIF experiment the fuel is mixed with a tracer dopant that can be excited by a laser with the appropriate wavelength.
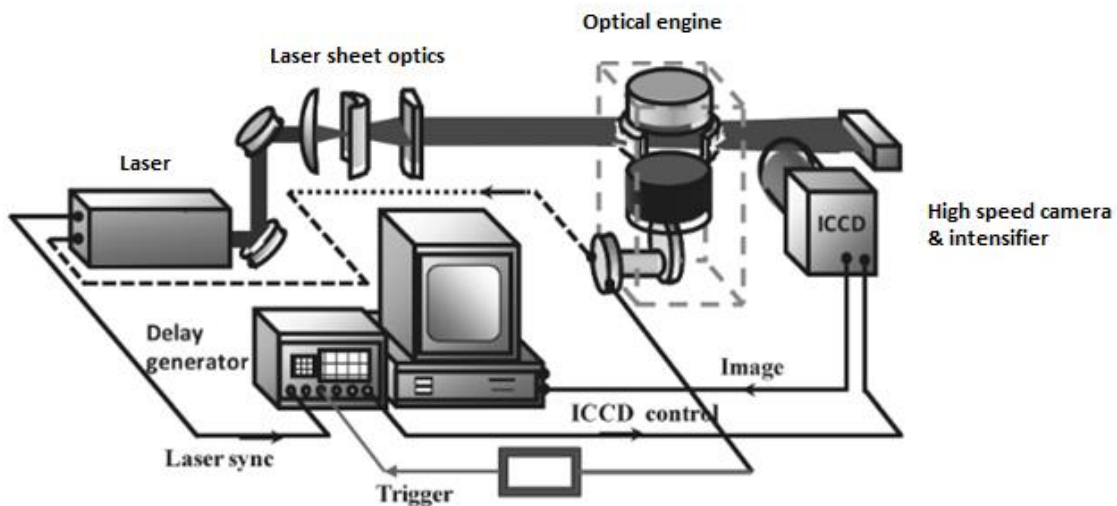

Figure 10: Diagram of an optical engine setup for LIF experiments [83]

In a typical LIF setup, a high-energy pulsed ultraviolet laser source is triggered to produce a pulse of laser light at a specific crank angle that is driven from an encoder mounted directly to the engine crank shaft. Using a combination of optics, the laser light is manipulated into a sheet of light and directed at a right angle to the region of interest to form an image plane for the high-speed intensifier and camera. In front of the recording equipment a band pass filter, or a UV coated lens, may be used to reject any elastic scattering of light that may occur from items in the field of view, allowing only the fluorescence light of the dopant to pass though. As the excitation and electrical equipment experience an operational delay a delay generator in conjunction with an oscilloscope is used to synchronise the operations of the laser, intensifier and camera to ascertain correct image acquisition from a desktop data acquisition computer. This is a crucial step as all systems have variance in their operation, the amount of time for the laser to produce a pulse and the delay from its trigger signal need to be measured and accounted for. The intensifier gating of roughly 100μs needs to occur after the laser pulse to differentiate against background light and phosphorescence with a representation is shown in Figure 11. The dopant such as biacetyl creates a yellow stain on the optical engine glass and it is important to only operate the fuel

injector when measurements are to commence, periodically it is necessary to clean the optical access of the engine to maintain image clarity.
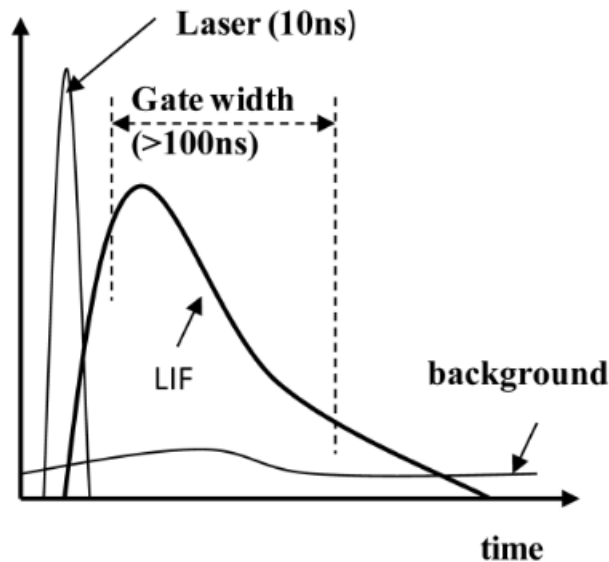

Figure 11: Timing events of LIF signal and laser emission [83]

LIF imaging is a widely used laser-based imaging diagnostics to provide insight into the fuel distribution inside an internal combustion engine and has been used in multiple studies [86] [87] [88]. Previous experiments use a relatively low frequency repetition laser and frame rate camera that is unable to capture cylinder evolution as it unfolds in the same injection cycle but rather capture events from many cycles. This would cause a large detachment in between images when quantifying an experiment making it more difficult to demine clear outcomes. M.A. Attar et al [57] research into GDI charge cooling needed to avoid reducing the resolution of the camera measurement area, 1024x1024 at 4Hz, instead opting to use an external counter/divider unit to skip some injection events to avoid window fouling. Their experiment had the potential to utilise the higher repetition rate of the laser but were limited in frame rate resolution by the 4Hz of the camera. With the correct optical positioning a vertical laser sheet can be provided from the piston with video recordings being side on the cylinder rather than the inverse from M.A. Attar *et al.* Having near full side optical axis with a higher camera frame rate of 6800fps can provide an insight to understanding to mixture characteristics late on the compression stroke at a near 1 CAD temporal resolution at 1200RPM. J.D. Smith and Volker Sick [89] elected for a higher temporal resolution at 2000rpm of 12kHz at 384x328 pixels over the full pixel resolution of 600x800 pixels at 4.8kHz. To compromise for reduction of image resolution would have a negative impact on in cylinder measurements as fine gaseous phase droplets and other information could be lost and effect the image processing to gather in cylinder distribution measurements.

2.6 Summary

In summary, this chapter discusses state-of-the-art engine technologies including engine downsizing; variable compression ratio engines; pre-chamber ignition systems and possible future alternatives fuel options looking into their characteristics and manufacturing methods. As engine knocking is a major issue that faces engine efficiency normal and abnormal combustion was discussed in section two along with how knock is detected with computerised control. The third part introduces direct fuel injection starting with its history and a descriptive overview of the fuel injection system components. As the understanding of DI mixture preparation plays a significant role in this work different DI injection methods are reviewed as to develop further comprehension. The third part ends with a review on vehicle cold start emissions as much emphasis has been placed on this area of study. However, direct injection vehicles fair worse than other injection methods due to impingement and localised rich zones causing soot formation highlighting the need for emissions control upon start up.

Ultra-high injection pressure is introduced in section four providing information on the concept of using a retarded injection strategy for the prevention of engine knock. This gives information about the reduction of in-cylinder temperature that gives way to the reduction time of the fuel's exposure to temperature. Previous studies into high pressure fuel injection were discussed at length in this section as to create a deeper understanding into a retarded injection strategy. Several experimental studies tested late injection strategies requiring fast forming homogeneous mixtures although found wall impingement to be an issue. To take full advantage of late injection strategies a high injection pressure needs to be employed so that the atomisation rate of the fuel spray can be increased within a small amount of time. With fuel pressures of up to 100MPa, a vast increase over many of the studies, the atomisation rate of the fuel should lend to be much improved at these heightened pressures.

To evaluate the characterisation of ultra-high injection pressure, spray measurement techniques were evaluated in the final, fifth, section of the literature review. Previous work that characterised spray evolution used highspeed imaging to determine penetration lengths; PDPA has been used extensively for previous droplet size and velocity measurements of fuel sprays; With in-cylinder measurements for droplet distribution using LIF. Using these three measurement methods the concept of ultra-high fuel injection pressure can be explored and investigated.

Chapter 3: Experimental equipment

3.1 Fuel injection system and Control

3.1.1 Fuel system

The fuel injection system comprises of an eight-hole direct injection diesel injector (A Bosch JX6Q-9F593-AB) as it can reliably achieve 100MPa, each nozzle has a diameter of 0.108mm. The injector is controlled through a National instruments NI9751 injection driver module. Fuel pressure is provided by a Hi-Pro P4203 air driven Sprague pump that utilises the principle of differential area to increase liquid fuel pressure with the aid of an 80PSI air supply. With an air regulator the fuel pressure can be governed as the internal air shuttle cylinder reciprocates until the set fuel pressure has been met. The pump apparatus to supply the high-pressure fuel is shown in Figure 12.
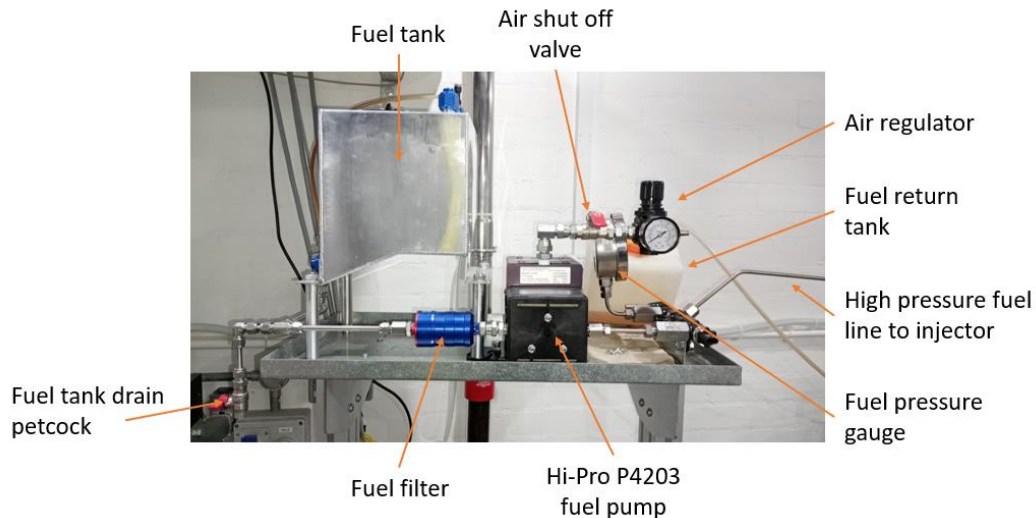

Figure 12: Fuel pump delivery apparatus

3.1.2 Injector driver and calibration

To calibrate the injector's flow rate, a National Instruments direct injector 9751 driver system was used in conjunction with a National Instruments CRIO 9066. The control system is depicted in Figure 13
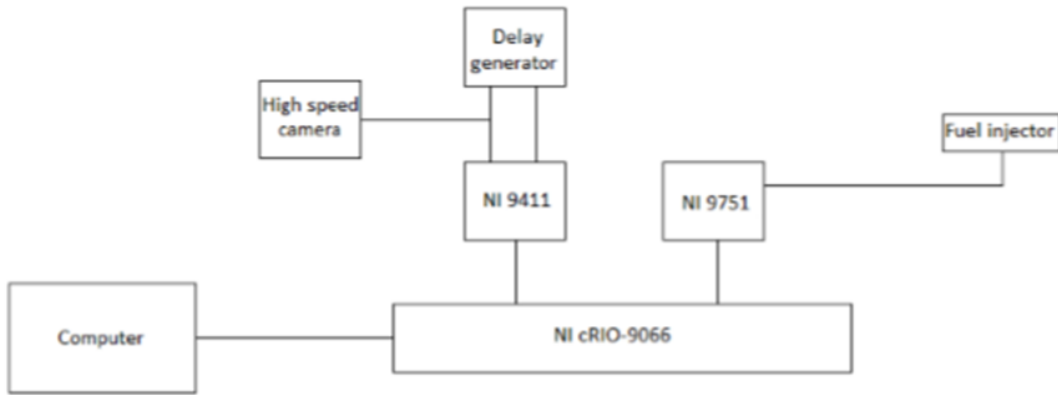
Figure 13: Block diagram of injector control

To operate the injector, the voltage/current profiles required are generated after the initial lift and hold constraints are entered into the CRIO as shown in Figure 16 and Figure 17.
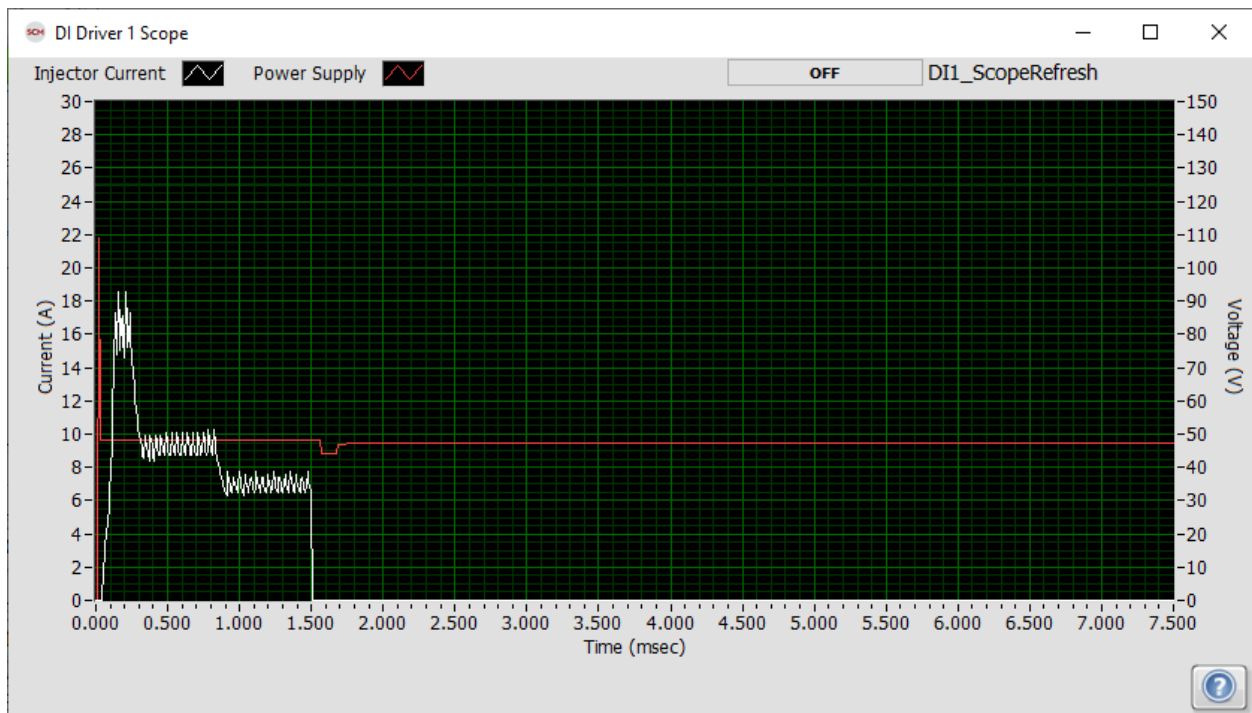

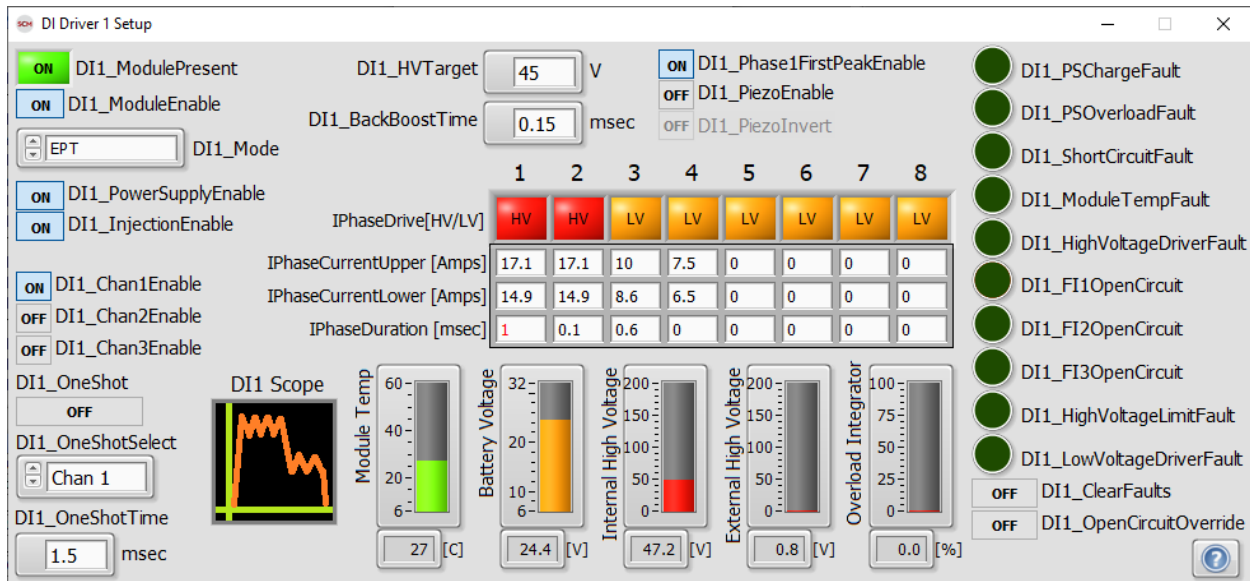*Figure 14: Voltage profile for the DI injector*

Figure 15: Injector driver voltage profile arrangement

Calibration of the injector was performed by quantitative mass measurements using the National Instruments Software Calibration Management toolkit utility. This toolkit was used to trigger the injector 2000 times with varying pulse widths from 100-1000μs at different pressures using 95 RON Gasoline at ambient temperature and pressure. The injection test cases are provided in Table 1 and shows a duration of pulse width against an operating pressure. The injected mass for each case was collected in a beaker and weighed using an MKS euro products nhv-30 precision scale. The collection for each case was repeated 5 times to create an average quantity totalling to 10,000 injections. Dividing the injected weight by the number of injection cycles yields the injection quantity per injection event along with its SD also being determined.

Table 1: Injection calibration quantities for pressure and pulse width

Fuel presssure (Mpa)	Injector pulse width (µs)									
	200	300	400	500	600	700	800	900	1000	
100	0.00333333	0.0093333	0.016	0.0206667	0.0266667	0.032	0.038	0.0433333	0.05	
90	0.00266667	0.0073333	0.0126667	0.018	0.0226667	0.0286667	0.0333333	0.0393333	0.0446667	
80	0.00266667	0.0053333	0.014	0.0166667	0.022	0.0273333	0.0313333	0.036	0.0406667	
70	0.002	0.006	0.0066667	0.0153333	0.0193333	0.024	0.0273333	0.032	0.0353333	
60	0.002	0.004	0.008	0.012	0.0166667	0.0193333	0.0233333	0.028	0.032	Quantity (mm^3)
50	0.00133333	0.004	0.0073333	0.0113333	0.0133333	0.0173333	0.0226667	0.0233333	0.0273333	
40	0.00133333	0.0026667	0.006	0.008	0.0106667	0.014	0.0193333	0.02	0.0233333	
30	0.00066667	0.002	0.0033333	0.0066667	0.0073333	0.0106667	0.0133333	0.0146667	0.0166667	
20	0	0.0006667	0.002	0.002	0.004	0.006	0.006	0.0093333	0.0093333	
15	0	0	0.0013333	0.002	0.002	0.004	0.004	0.0053333	0.006	
10	0	0	0	0	0	0	0	0	0	

This was done at different pulse widths and pressures from 10-100MPa to generate an injector calibration chart show in Figure 16. To authenticate the calibration, Bosch, the supplier provided

a calibration flow rate for 100MPa. If any significant discrepancy were to be found, the repetition of the calibration would be conducted.
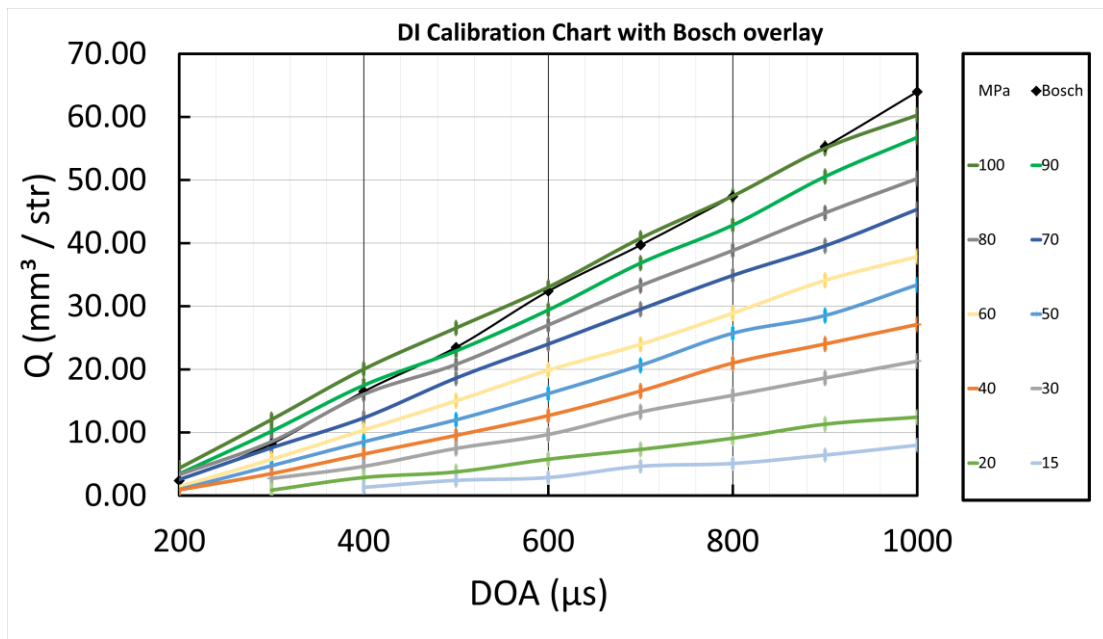

Figure 16: Calibration of fuel quantity for different pulse widths at different pressures

3.2 Optical engine system

Table 2: Key engine specifications

Cylinder bore	82mm
Stroke	86mm
Swept volume	454cc
Compression ratio	10.5
Maximum speed	3000RPM
Test speed	1200RPM
DI Injector location	Central, vertical

For in cylinder LIF experiments a four-stroke, spark ignition, single cylinder optical research engine was used. This engine is manufactured by AVL and differs from thermo dynamic engines

vastly as the cylinder compromises of durable fused silica glass as opposed to a steel liner in a cooling jacket. The fused silica glass enables the visual studies of in cylinder conditions possible. The AVL optical engine is equipped with a quickly removable cylinder glass which forgoes the disassembly of the engine top end for cleaning and relubrication like other research engines. The quick removable cylinder glass permits the conducting of experiments considerably quicker.
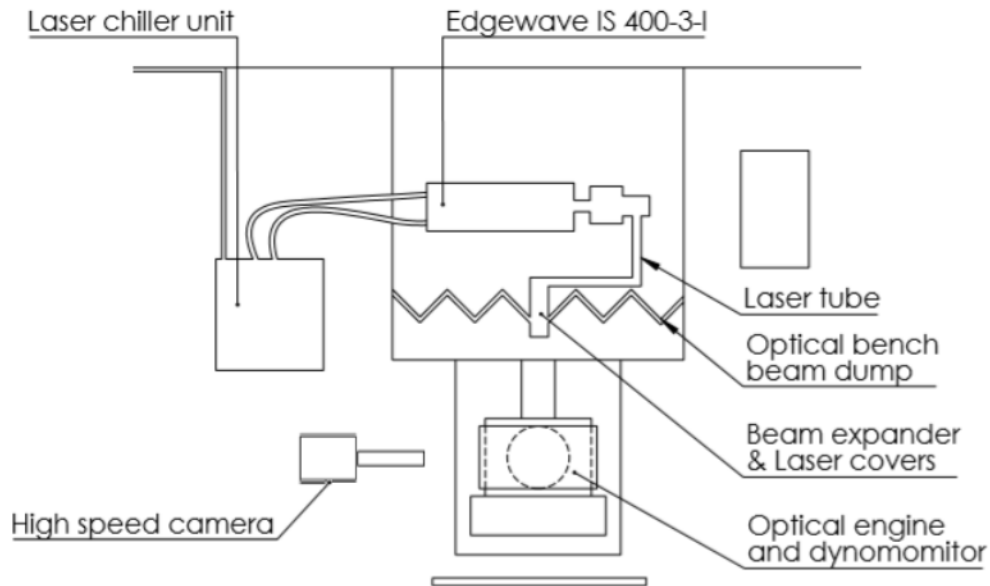

Figure 17: Diagram of optical engine setup

3.2.1 Load control

Engine load is controlled by an intake throttle butterfly valve operated via a servo remotely controlled from the dynamometers operators compartment. Using a PWM signal from a rotary dial the electrical signals are sent to the servo that acts on a bell crank lever to open and close the throttle. As the throttle opens and closes it has an effect of the pressure within the manifold in turn effecting the engine load. To measure the intake pressure, a Manifold Absolute Pressure (MAP) sensor is used and is calibrated to the mass air flow of the engine. From there and by measuring the engine load on the dynamometer control at different throttle positions, the fuel quantity per cycle can be calculated.

3.2.2 Cylinder head & In-cylinder pressure transducer

As previously mentioned, the optical engine is equipped with a quick removal cylinder liner that with the aid of 130PSI hydraulic pressure can be lifted into position under the cylinder head sealing the cylinder. This method of operation vastly decreases down time when performing optical

experiments allowing for easily cleaning of the optical access, piston skirt and rings that is needed for optimum image quality. Within the cylinder head resides an AVL GU22C Piezo-electric pressure transducer that measures the in-cylinder pressure traces as the engines goes through its cycles. The high frequency electrical fluctuations caused by the rising and falling of pressure are communicated to a Piezo amplifier where the pressure information is converted into a voltage profile for the combustion analyser to be displayed as a pressure trace.

3.2.3 Lubrication and cooling systems

The optical engine needs to be pre-warmed before operation and uses separate pumps to circulate pre-heated oil and coolant though the engine. The engine operates on a dry sump recirculating oil supply of straight 30W oil maintained at 4Bar to lubricate the main bearings, connecting rod and valves. Engine coolant compromises of de-mineralised water and 25% ethylene glycol in a closed system that circulates though the lower engine block and cylinder head. The coolant system is unconventional to automobiles and uses a large reservoir to store the coolant mixture. A thermostatically controlled heating element is also housed in the coolant reservoir and warms the coolant mixture and intern warming the engine to 50°C for operation. Since no radiator is present the coolant should not be allowed to exceed 60°C, if temperatures begin to climb with prolonged use the engine has to be stopped until the large coolant reservoir has to cool down to 50°C whereby the thermostatically controlled heating element will maintain this temperature. Since the quartz cylinder and piston are not equipped with liquid cooling a supply of compressed are is passed through an orifice directed under the piston attached to the mirror carriage. This supply of compressed air sufficiently cools the piston and avoids binding.

3.2.4 Dynamometer

The dynamometer used to motor the engine is manufactured by McClure and operates on direct current voltage from an inverter or is used as a generator under fired conditions to load the engine. The dyno is cooled with a squirrel cage blower fan that pushes air though the motor to cool it. As the dynamometer needs to operate at specific speeds, the control system incorporates a closed loop speed controller that monitors the dyno shaft speed and adjusts accordingly. This is done in order to counter fluctuations in engine load, conditions etc. engine torque and the initial start-up current is also monitored on the dynamometer controller and is used to determine BMEP for calculations.

Manufacture	McClure
Operation method	Shunt wound DC
Rating	30kW
Maximum speed	6000RPM
Max armature	400Volts, 65Amps
Cooling	Air cooled - Centrifugal blower fan
Loading control	KTK type 6P4Q30

3.2.5 Angle encoder

An angle encoder on the end of the crankshaft provides precise angle positional information that is used for signal triggering and positional data used in conjunction with the in-cylinder pressure sensor. The AVL 365C optical angle encoder uses patterns on a rotating disk attached to the crankshaft with an optical sensor to create an absolute rotary encoder to provide a unique angular position without additional referencing ensuring it can determent the exact crank angle with a high degree of accuracy. The optical output from the encoder is transformed into a trigger pulse by a pulse converter in the engine timing unit that is able to produce 720 pulses per revolution creating a crank angle resolution of 0.5° for use in data acquisition and the combustion analyser. This level of precision exceeds requirements for the triggering of recording equipment but is useful in controlling the duration of components that require duration signals such as injectors.

3.2.6 Engine timing unit

The engine timing unit (ETU), the AVL 427 ETU, is an essential piece of equipment that performs as a hub for timing related and dependant equipment acting as the main interface between the sensors installed on the engine to the data acquisition systems. Input and outputs TTL channels are connected around the back of the ETU and are controlled in a crank resolved fashion by ETU software based on a local computer, represented with a block diagram in Figure 18. The proprietary software enables the control of outputs that are matched with injection timing, camera triggering and even spark timing for motored tests. Slight synchronisation of equipment, such as the camera trigger, may be needed and can be adjusted based on crank degrees or time. Outputs

such as the intake pressure, in-cylinder pressure, exhaust lambda sensor were forwarded to the separate data acquisition software and resolved on a crank angle basis.
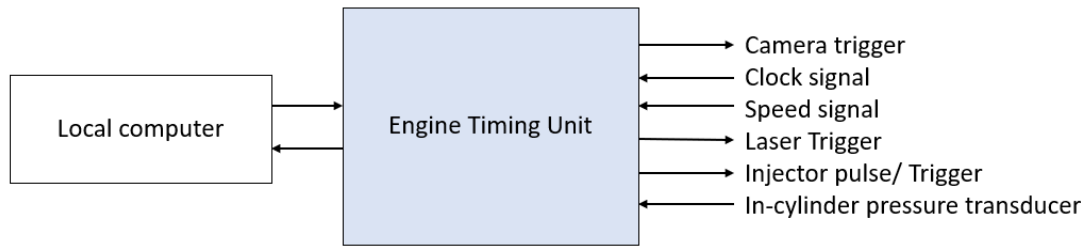

Figure 18: Inputs/ Outputs of ETU

The fuel injectors pulse width is programmed into the ETU. When an injection event is required, a signal from the ETU is sent to the NI DI driver 9751 module which in turn operates the injector at its set voltage profile. A TTL trigger signal for the camera to start recoding is also controlled by the ETU and is in tandem to the injector. A gated Lambert image intensifier is attached to the cameras sync connector, ensuring synchronised operation of the camera frame rate and gated shutter. Recording is completed once the cameras internal memory is filled, with the current resolution of 512x384 and frame rate of 6800fps this gives enough space for the acquisition of 44 complete injection cycles.

3.2.7 Data acquisition and combustion analyser

Acquisition and monitoring of engine parameters are accomplished by two National Instruments data acquisition cards, one high-speed for high frequency instruments and one low speed card for low frequency instruments. Information received from the data acquisition cards is relayed to the combustion analyser software that displays the different required parameters. The National Instruments USB-6353 high-speed card allows a single channel sample rate of 1.25MS/s and is operated at a slower sample rate of the shaft angle encoder output, which is used as the timing clock. This card is used to acquire pressure readings such as in-cylinder and intake pressure readings along with the previously mentioned angle encoder used display the engine crank angle of the engine and to determine the engine speed. The National Instruments USB-6218 low speed data acquisition card records the exhaust/ intake pressure conditions and the various temperature sensors as the sample rate can be much slower but still provides a 250kS/s sample rate.

The data acquisition cards are coupled to the engine combustion analyser software that was developed internally at Brunel University, and is used to monitor the parameters of the engine. Additionally, it is also used to record in-cylinder pressures over 300 cycles.
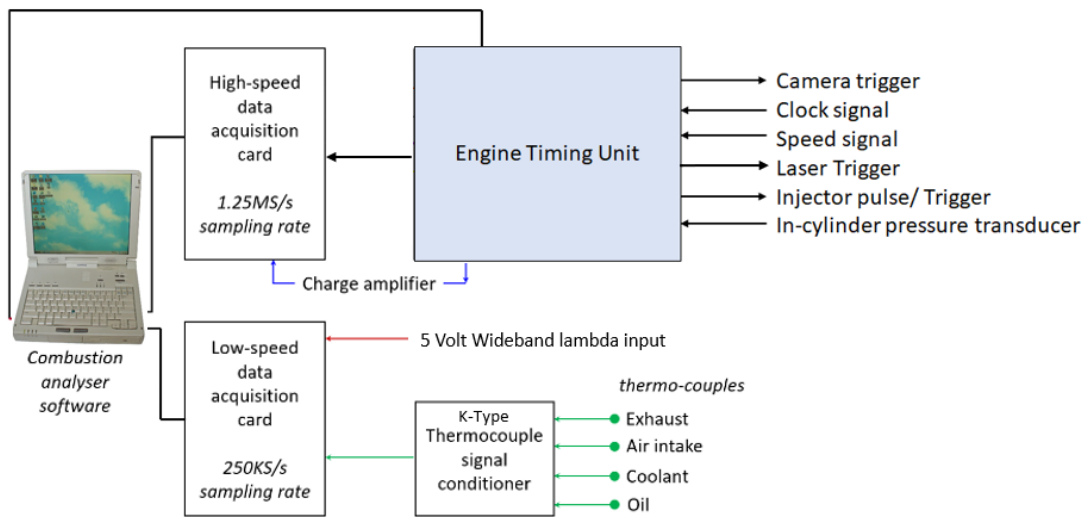
Figure 19: Block diagram of the data acquisition setup

3.2.8 Injector fitment

A major hurdle for in-cylinder testing is mounting the injector in the cylinder head as the machining of the cylinder head is prohibited due permanently altering the cylinder head. Using the cylinder head and injector drawings, a CAD model for the injector mounting can be created along with a model of the injector. With this the material interference can be visualised and is displayed in Figure 20, the red highlighted area represents material from the injector that is residing in the cylinder head. Using CAD helps anticipate the material removal from the injector that can be done with a lathe and in doing so allowed the fitment of the high-pressure DI injector without altering the cylinder head injector seat dimensions.
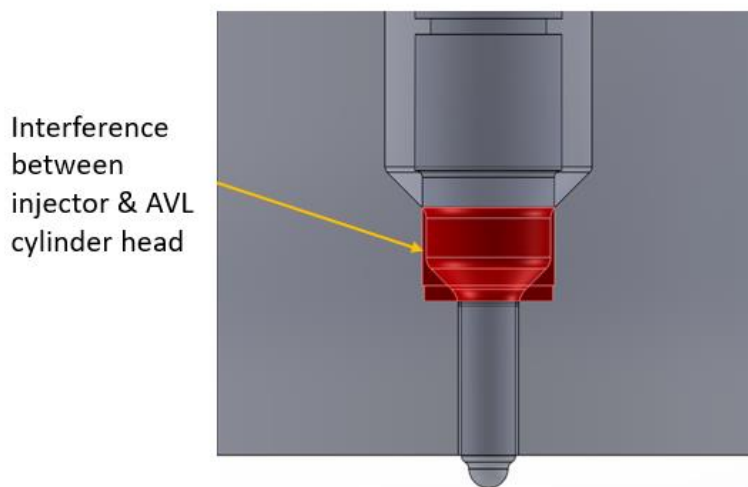

Figure 20: Interference of the injector and cylinder head

Figure 21: Left - machined injector collar, Right – standard injector collar

3.3 Summary

This chapter highlights the experimental test apparatus for the high-pressure fuel system capable of 100MPa; the injector driver setup for the DI injector that electronically controls the trigger pulse widths for operation; the calibration of the injector to from pressures ranging from 20MPa to 100MPa against DOA. The optical engine and its main components are also discussed along with and data acquisition. Furthermore, the DI injectors fitment into the cylinder head is also reviewed as LIF experimentation could not have happened without the simple yet effective machining of the injector tip fastening collar using a lathe and a collet chuck.

Chapter 4: Macroscopic spray characterisation

4.1 High-speed imaging setup

Measurements were undertaken inside a covered glass tank with dimensions of 380mm in length, 240mm in width, with a height of 255mm. To capture back lit high-speed images, various equipment was used and can be seen in Figure 22. An LED light source manufactured by GSVITEC was positioned on the other side of the glass tank. In order to avoid overexposure spots, the 4mm thick acrylic light diffuser panel was placed between the LED and the glass tank. The LED light source was operated in the continuous light mode. The injector was mounted vertically and in a central position on the lid of the tank with the measurements undertaken at atmospheric conditions.
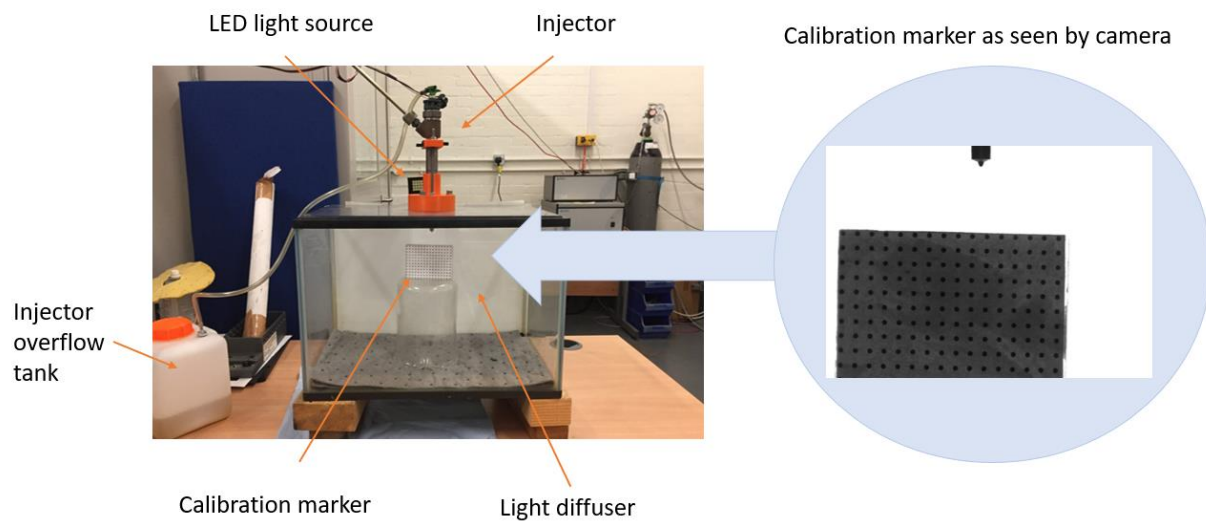

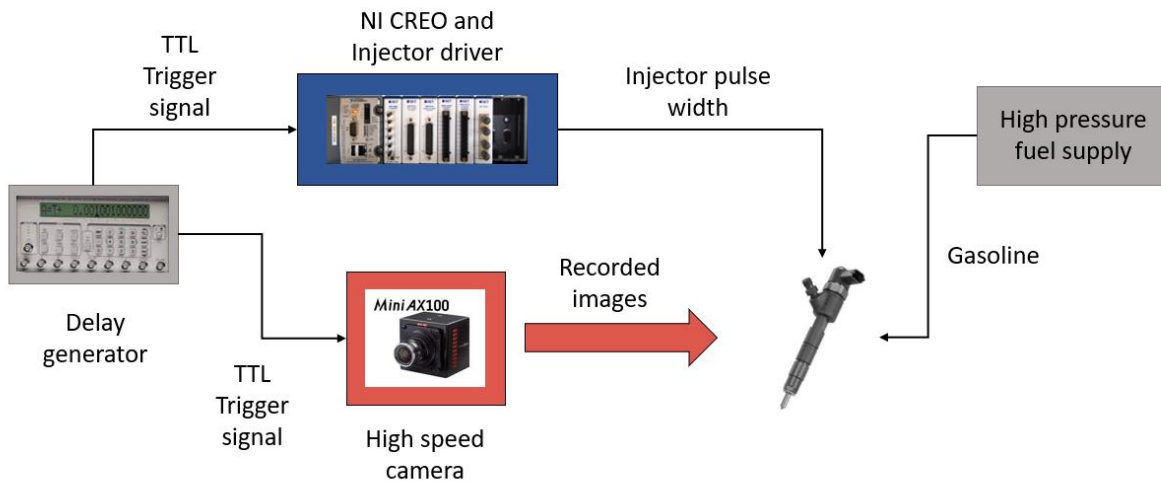*Figure 22: High-speed imagery apparatus*

Figure 23: Block diagram of high-speed imagery setup

Positioned in front of the tank was the high-speed imaging system that entailed a 28-70mm AF-s NIKKOR ED Nikon lens attached to a Photron FASTCAM mini AX100 high-speed camera. Using the Stanford delay generator, the injector and camera were triggered to record just before the spray event and until the memory was full. Then the images were transferred to the Photron FASTCAM Viewer (PFV) for review. In this way the whole of the injector's spray evolution was captured along with start buffer frames if needed. Figure 24 is a depiction of the trigger sequence used and illustrates how the camera trigger is activated before the injector pulse with Figure 23 depicting a block diagram of the wiring for the setup. The recording window needs to span the entire length of time it takes for the complete spray evolution to occur. The collected image ensembles for each case are repeated 30 times and processed in MATLAB to determine the penetration length.
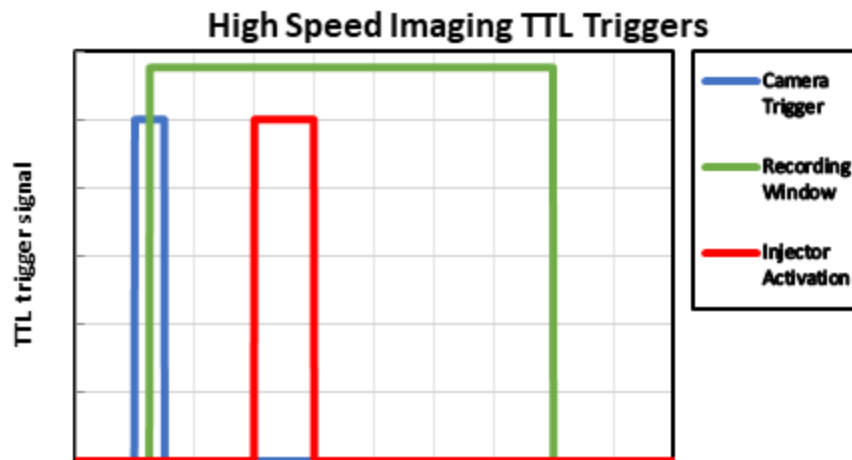

Figure 24: Back lit high-speed imaging trigger sequence depiction

48

Table 4: Optical parameters used in high-speed imagery acquisition

High-speed camera	FASTCAM Mini AX100
Pixel resolution	768x528
Frame rate	10,000fps
Shutter speed	1/20,000
Lens	Nikkon ED 28-70mm AF-s NIKKOR
Aperture	F8
Backlight illumination	GSVITEC LED (in continuous mode)

4.2 Experimental procedure

High-speed shadowgraph imagery was employed to study the penetration length macroscopic spray characteristics for fuel quantities of 0.01,0.02,0.03,0.04 and 0.05g of gasoline. Since a pressure increase results in an increase in fuel quantity, the use of the calibration chart made earlier comes into force to make an experiment plan that gives the parameters to fulfil the fuel quantities at the different pressures. The experiment parameters including the corresponding pulse widths can be seen in Table 5.

Table 5: High-speed imaging pulse widths for fuel quantities at varying pressures

	Fuel quantity for single injection event				
g / str (mm^3/ str)	0.01 (13.33)	0.02 (26.67)	0.03 (40.00)	0.04 (53.33)	0.05 (66.67)
Pressure (MPa)	Required pulse width for given fuel quantity (µs)				
20	1049.3	1847.735	2646.138	3444.541	4242.944
30	710.7	1200.94	1691.136	2181.332	2671.528
40	593.8	989.5361	1385.184	1780.832	2176.48
50	515.6	843.1908	1170.791	1498.391	1825.992
60	461.7	750.8821	1040.108	1329.335	1618.561
70	404.8	652.2127	899.5844	1146.956	1394.328
80	369.0	594.9689	820.9576	1046.946	1272.935
90	348.3	548.801	749.3023	949.8035	1150.305
100	316.2	505.8914	695.5548	885.2181	1074.881

4.2.1 Camera

Optical camera parameters were focused on creating high picture quality and high frame rate. With this a frame rate of 10,000 fps and a 1/20000th of a second shutter speed was selected as to give many sharp images of the spray evolution at a 768x528 pixel resolution. Specifications of this nature require a lot of light shining on the recording subject. To balance the mixture of

background and spray boundary overexposure against too little light to clearly see the developing spray border, the lens aperture was used to control the exposure. Closing the aperture towards f22 creates a darker image and larger depth of field while opening the iris creates a lighter image and a shallower depth of field. Since the background is a uniform colour and the close proximity of the equipment the depth of field is largely irrelevant and so the aperture to regulate light intake is justified and remained constant throughout the experiments.

4.2.2 Spatial resolution

To ascertain the spatial resolution of the imaging setup by converting pixels into millimetres for later measurement image post processing, a calibration image needs to be taken with known dimensional metrics. To determine the resolution a calibration marker sheet consisting of 2mm diameter dots 5mm apart from centre to centre was placed under the injector in a parallel plane to the camera. After taking the calibration images MATLAB was used to determine the spatial resolution calibration to be 0.25 mm to each pixel.
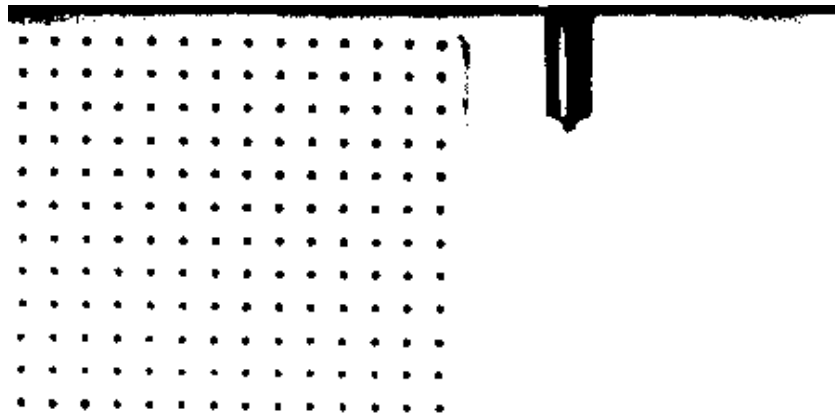

Figure 25: Injector tip and calibration marker used to assess spatial resolution

4.2.3 MATLAB processing procedure

Once the high-speed shadowgraph images have been acquired in line with the experiment procedure and repeated thirty times to form a good statistical average known as the central limit theorem. MATLAB code was created to retrieve the image ensembles from numbered folders and create one average image sample for each injection setup. The averaged image ensemble is then binarized. Using the injector tip as a zero point, the number of pixels was counted throughout the spray evolution. Since each image had a growing pixel count as the spray progressed a table of spray evolution can be fashioned. Using the spatial calibration, each pixel count in the table can be converted into millimetres giving penetration length in time based on the camera frame rate. Post-processing followed the guidelines outlined in "JSAE 2715 a new recommended practice" [90].

4.3 Results and Discussion

Back lit high-speed images were taken to view the effects of increased fuel pressure has on the penetration length of the fuel spray. Raising the injection pressure allows additional fuel delivery for a given pulse width, to counter this previous calibration was used. Pulse widths tested corresponded to 0.01, 0.02, 0.03, 0.04 and 0.05g per injection event that would relate to the fuel delivery of an engine operating between low and high load.

4.3.1 Macroscopic Spray Characteristics

Table 6: Expanding fuel spray images of a 0.03g fuel quantity at 20, 60, 100MPa

(12ms images have been cropped to show the start of injection)

ms (DOA After Trigger)	20MPa (0.03g)	60MPa (0.03g)	100MPa (0.03g)
12			
16			
22			
28			
36			
46			

Images of from the penetration length test have been assembled in Table 6 they show that the cone angle is substantially hampered at 20MPa after 20° where thereafter it increases with fuel pressure. After the initial injection there is distinctively a liquid fuel jet as the centre of the evolving sprays at all pressures shown by a very dark area. With higher pressures more kinetic energy is transferred to creating finer fuel droplets on the peripheral as they get evicted from the main plume and entrained with the surrounding air before losing momentum. The confirmation of how this relates to droplet size will be confirmed quantitatively using PDPA, although possible ligamentation experienced in these images could present a challenge. These early characterisation images can help understand future results by acting as a base line showing the basic features of the initial breakup of the liquid fuel jet, the development of droplets, and their distribution in space without any outside influences. For example, before numerically post processing these images demonstrate that penetration length will result in cylinder wall impingement that harms engine efficiency and likely, although not tested in this study, will result in substantial unburned hydrocarbon and soot exhaust emissions.

4.3.2 Penetration length

30 repetitions of each injection case were conducted using the high-speed camera and processed in MATLAB. Each case was averaged to form a reliable representation of the injection event complete with its SD. A representation of the penetration length and its SD is given in Figure 26. It is seen, in this case and other cases, that while the injector is open and activated the position of the leading edge of the fuel spray is consistent equating to a stable gradient. This changes however, when the injection event has stopped and the leading edge increases due to the built up momentum before beginning to fluctuate as the head of the spray begins to break up. Leading to broader SD at 250mm as the penetration length begins to flatten off. An explanation of this is can be concluded in the MATLAB image process used to determine the penetration length. As the spray head begins to break apart the boundary between fuel and air becomes less clear. If the droplet at the edge diffuses and blocks enough light the pixel is counted and if not, it is not added to the pixel count that determines the penetration length. It is when a mixture of these light and dark pixels as the head atomises that causes the variation in penetration lengths that can be seen by the increase in SD and by the digressive behaviour of the average penetration length presented. Figure 27 shows inverse spray images that are then binarised showing that the boundary definition of the fuel spray is worsening while the main body is clearly made up of white pixels that are used for the penetration length count.
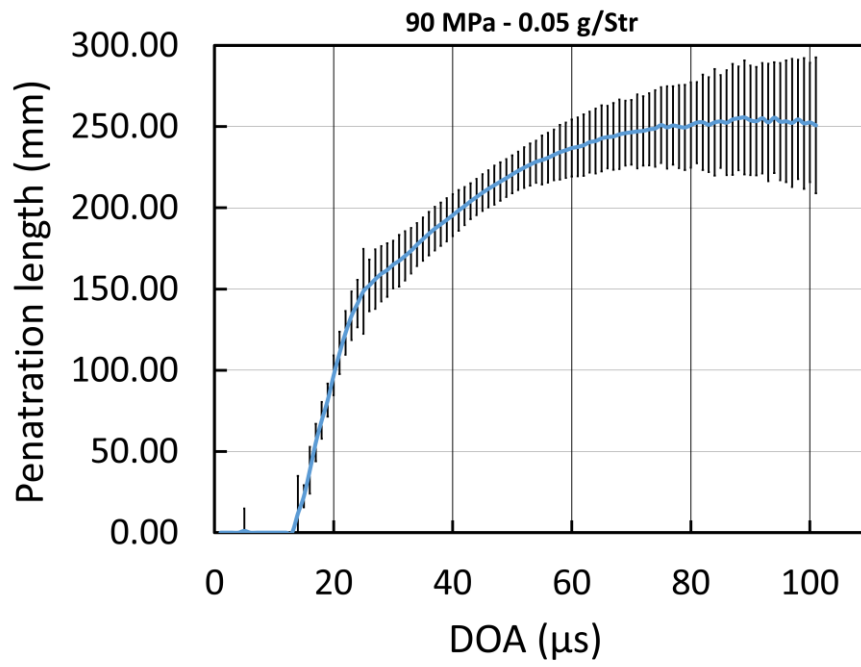
Figure 26: Example of penetration length and its deviation over 30 repetitions
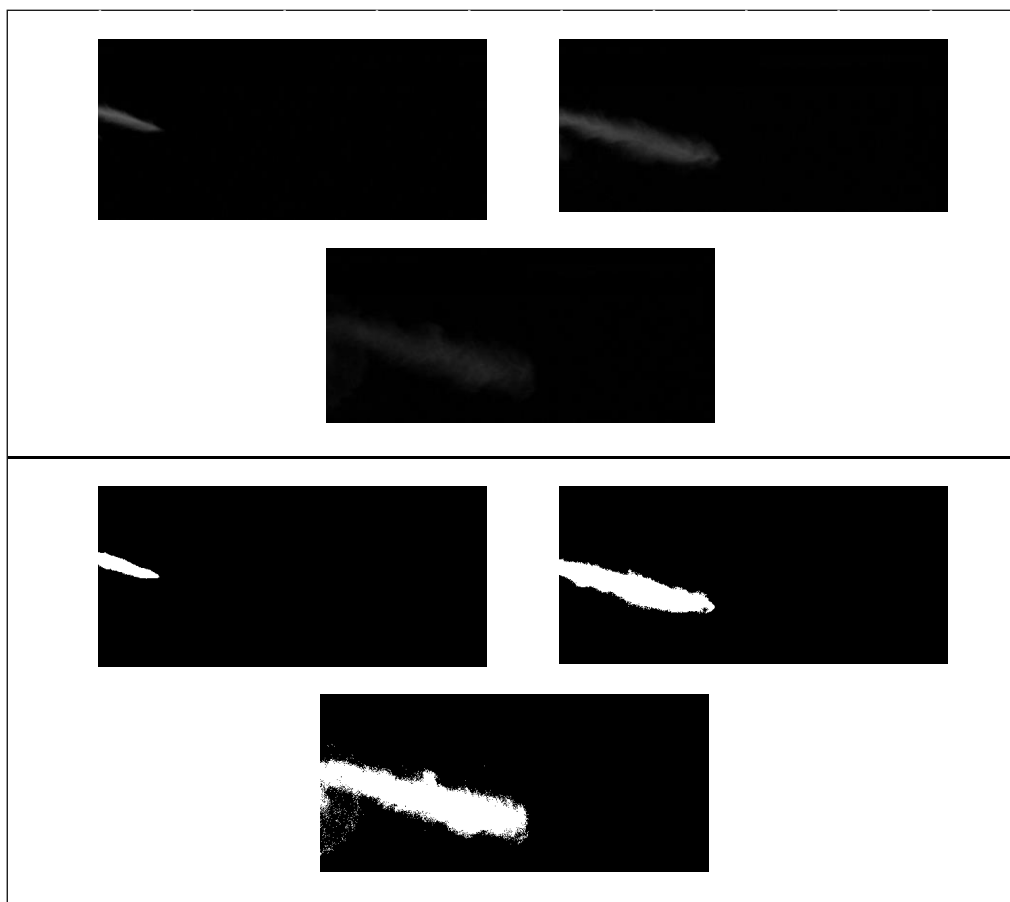
Figure 27: Example of spray boundary dispersion in penetration length measurements for a given greyscale and binary injection image

Figure 28, Figure 29 and Figure 30 depict the penatration lengths for different quantities of fuel at 20, 60 and 100MPa, respectively. In all cases the penatration lengths behave almost the same manner in the initial stages of injection. It is only when the needle closes for the different pulse width does a change in the figures appear. The figures show that there is very little effect on penatration length for an increased amount of fuel pressure while delivering the same amount of fuel. Examining 0.01g from 20 to 100MPa, at 20us the penatration length is roughly 100mm and it is at this point the penatration length begins to fall. This trend can be seen with all cases just as the maximum penatration length is aproximatly the same and is shown quite clearly for 0.05, 0.04 and 0.03g. The results reflecting each other could originate from the fact that the same fuel quantities were used for each case. With higher energy behind the fuel the injector needs to open less to provide the same amount of fuel but provides the same characteristics. The benefit of higher injection pressure should be the reduction in dropplet diameter and will be explored in the coming chapter. Figure 28 to Figure 34 also display this behaiviour after the penatration length flattens out after roughly 60µs, the decreasing penetration length signifies that the momentum in the spray plume is depleting leading to a decrease of overall penetration length after the initial injector trigger event exacerbated by the variability in SD that come with spray plume breakup.
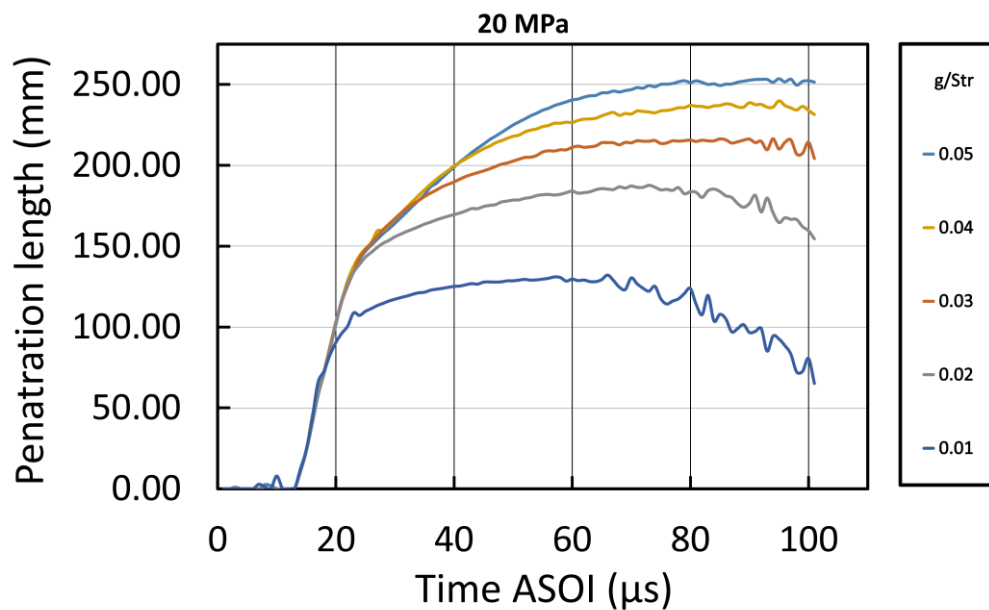
Figure 28: 20MPa penatration lengths
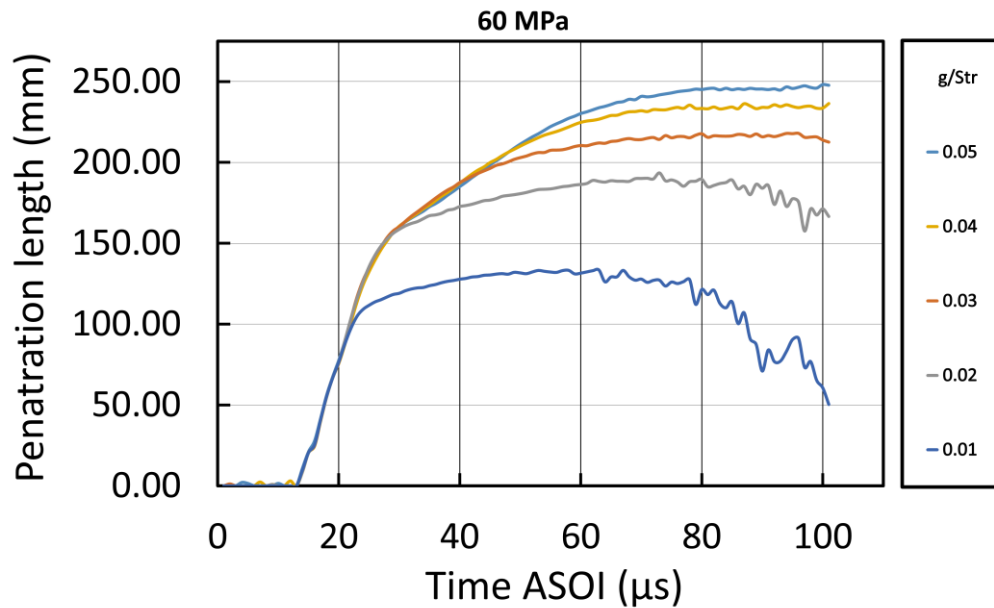
Figure 29: 60MPa penatration lengths
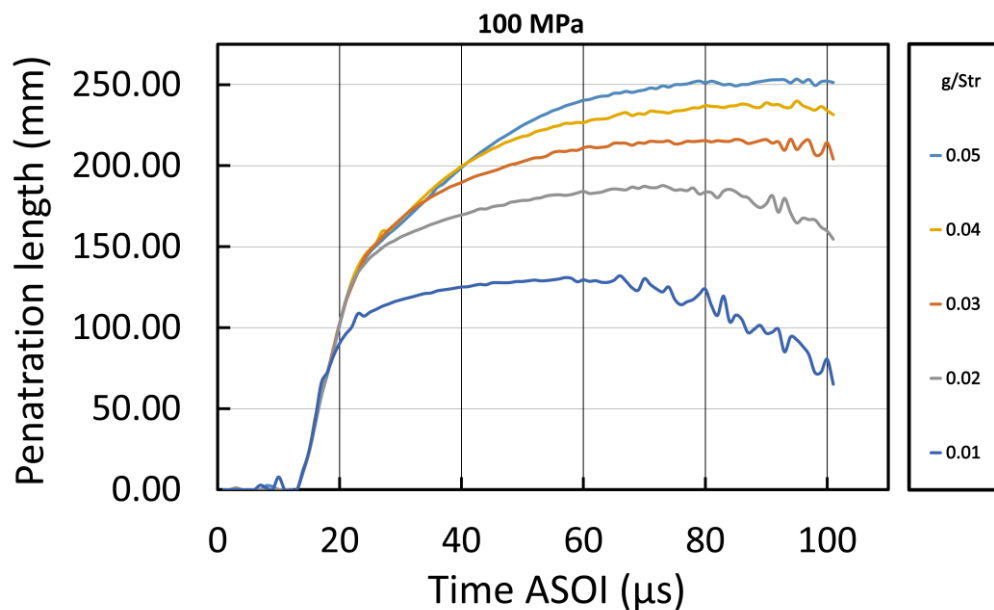
Figure 30: 100MPa penatration lengths

When plotting the different injection pressures for a given fuel quantity presented in Figure 31 Figure 33 Figure 34, we can see that as the pressure increases, the gradient of the initial spray head becomes steeper denoting that the fuel spray is evacuating quicker out of the injector tip with each increase in pressure. The resulting increase in kinetic energy does not translate however to further penetration lengths due to the correction of fuel quantity.

57
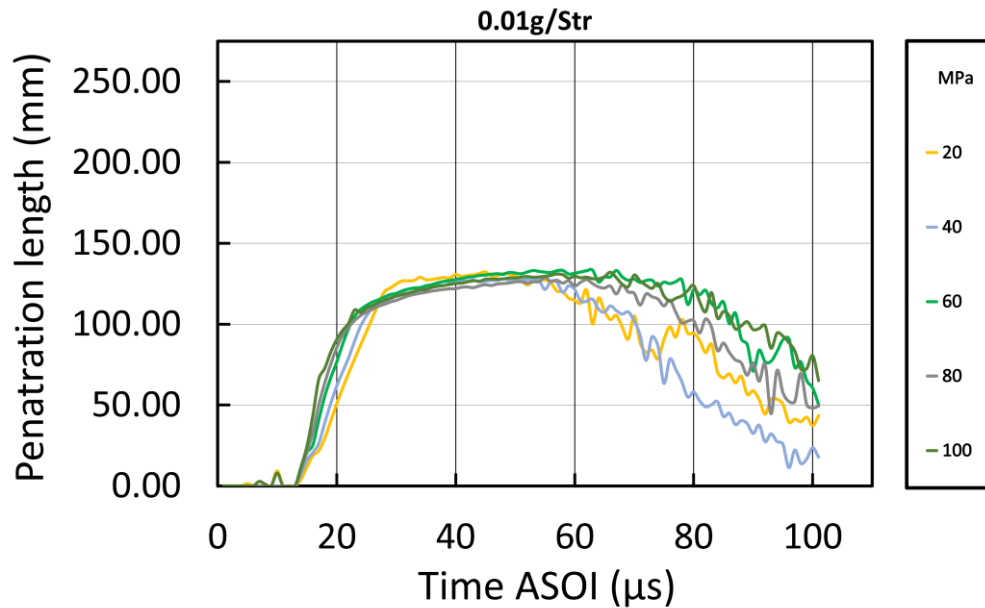
Figure 31: 0.01g/Str penatration lengths

0.01 and 0.02g fuel quantities illustrate divergence in the SD at the tail end of the injections, representing that the spray boundary is more susceptible to break up. Fuel quantities of 0.03, 0.04 and 0.05g do not exhibit this behaviour alluding to the fuel quantities being the cause of this divergence and truss boundary layer breakup that can be seen in this initial characterisation experiment. The increased fuel quantities in this particular injector are producing more of a visual stream of fuel as opposed to a more atomised spray. PDPA characteristics in the next chapter will be able to show more detail into the velocities and droplet structures.
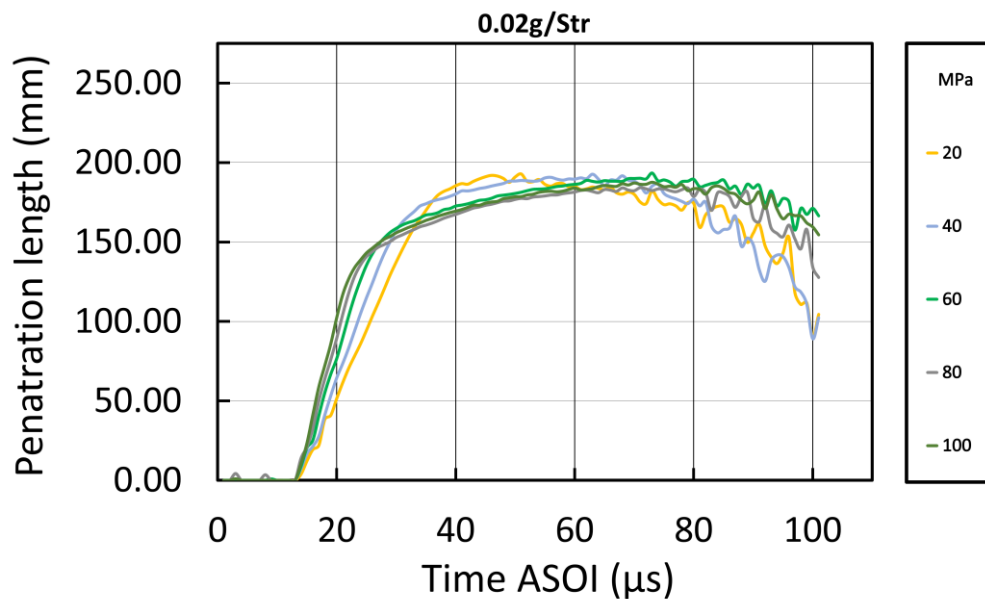
Figure 32: 0.02g/Str penatration lengths

58
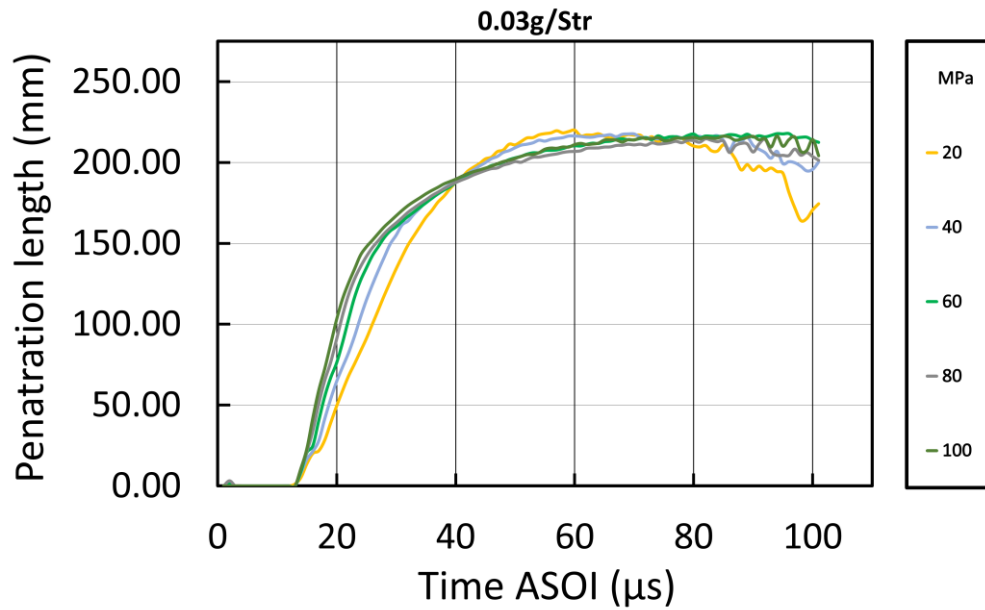
Figure 33: 0.03g/Str penatration lengths
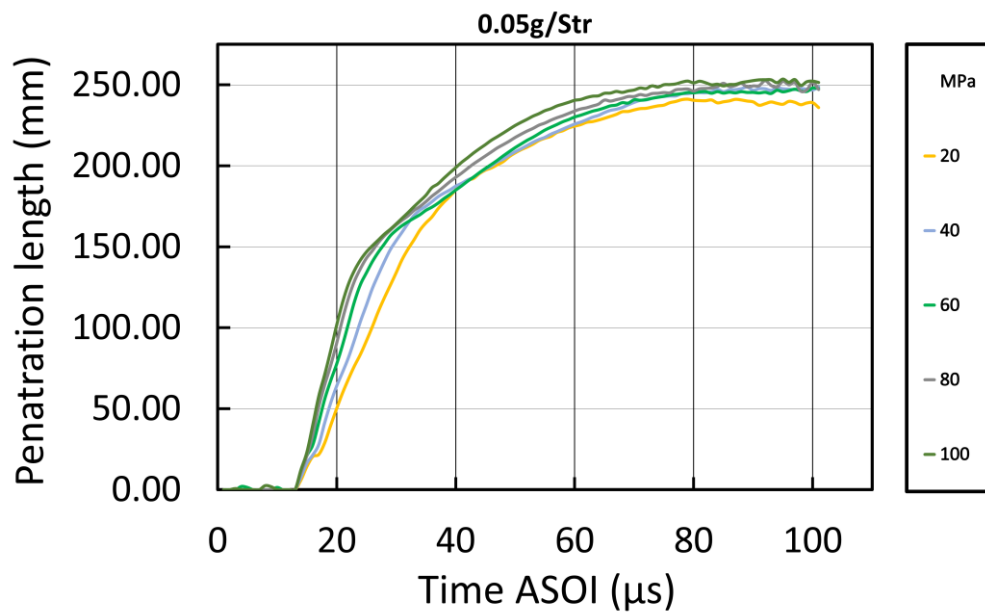
Figure 34: 0.05g/Str penatration lengths

When examining the outcomes of the experiment, increasing the injection pressure shows negligible change in penetration length is observed. Figure 28 to Figure 34 shows fuel quantities at increasing pressure and inspecting the maximum penetration length of each case they are quite even and almost featureless apart from the transition area where the injector is closing. This step change from Figure 28 to Figure 30 can also be observed in Figure 31 to Figure 34 where it is the consequence of a change in momentum as the needle closes due to the fuel pressure. With higher pressure the step is more aggressive than that of lower pressures where it is more uniform

as the lower spray momentum can easily change its velocity in comparison to the higher momentum of higher pressures it is harder to change its velocity so suddenly creating a smoother transition. This larger amount of momentum can also be seen in the maximum penetration lengths for 60Mpa and 100MPa as when the injector pulse has finished and the needle closed the maximum length still has not been observed and occurring much later in the time scale.

With an increased repetition rate of 30 as opposed to six, seen in high-speed imagery experiments from Shao and Yan [80], have created penetration length information with low deviation and a greater regard for accuracy. Comparing penetration lengths results with work conducted by M. Danji [91] and C. Jiang [92] that used similar high-speed imagery test methods. The penetration length of the DI injector tested here is far greater than those tested at pressures of 35MPa and 15MPa respectively even with the slight differences in DOA used in the test methods and at the lowest pressure and injected fuel quantity tested here. Changes in fuel density and injection pressures would also lead to differences in entrainment effects affecting penetration length. The main contributing factor that causes the penetration length here to be vastly increased is that these tests are conducted with an injector that is designed to introduce diesel fuel into a compression ignition combustion chamber where its spray characteristics are best suited to fuel rich regions in a propagating flame as opposed to a wider fan or cone spray formation seen in previous gasoline studies. This is also confirmed by the high-speed imagery and penetration length experiments performed in this study even at the lowest pressure and pulse widths tested.

4.3 Summary

High-speed imaging was used to study the macroscopic spray behaviour of a high-pressure spray evolution from a DI fuel injector. Using a recording frame rate of 10,000 fps, mean averaging of 30 injections has created consistent penetration length data with a high temporal resolution. Test cases focused on pressures between 20MPa and 100 MPa for fuel quantities of 0.01 to 0.05g per injection.

Averaged fuel injection images exhibit distinguishing features resulting from fuel pressure changes in the liquid penetration length and initial breakup and the development of droplets. The understanding of these can help anticipate challenges of cylinder wall impingement that are typical of DI that harms efficiency and emissions. Visual comparisons of the fuel pressures tested suggest that at the centre of the spray is a liquid fuel jet but it formation diminishes when fuel pressure rises to 10MPa. With this raised pressure the liquid fuel on the boundary entrains with the surrounding air to create a visually wider cone angle. Initial high-speed imaging suggests that the increased fuel pressure creates smaller fuel droplets but the chances of wall impingement in future in cylinder experiments are highly likely.

MATLAB was used to process each test case over 30 injections to from a mean averaged image to determine the resultant penetration length graphs. Differences in penetration length can be seen when increasing fuel quantities, this stems from a longer injector pulse duration allowing the fuel to use more of its kinetic energy to use in traveling further. As the fuel quantities are identical for each test case, as the pressure is increased the pulse width needs to be reduced. This gives the fuel spray equivalent kinetic energy to give comparable penetration lengths. Using the gathered information, it is observed that increasing the fuel pressure does not notably increase the total penetration length for a given amount of fuel but does however eject the fuel at a faster rate when the injector is open due to the larger amount of kinetic energy acting upon the fuel and injector. The verification of the velocity increase will be able to be analysed in further PDPA experimentation.

Chapter 5: Droplet size and velocity measurements

5.1 PDPA setup

Droplet sizes and velocities measurement were conducted using a one-component 112mm fibre PDPA system by Dantec Dynamics. The PDPA system was mounted on a motorised 3-dimensional traverse system to precisely move the measurement volume within the spray. The 3D traverse system co-ordinates with the PDPA Processing software and is able to collect data at different points with 0.01mm accuracy.
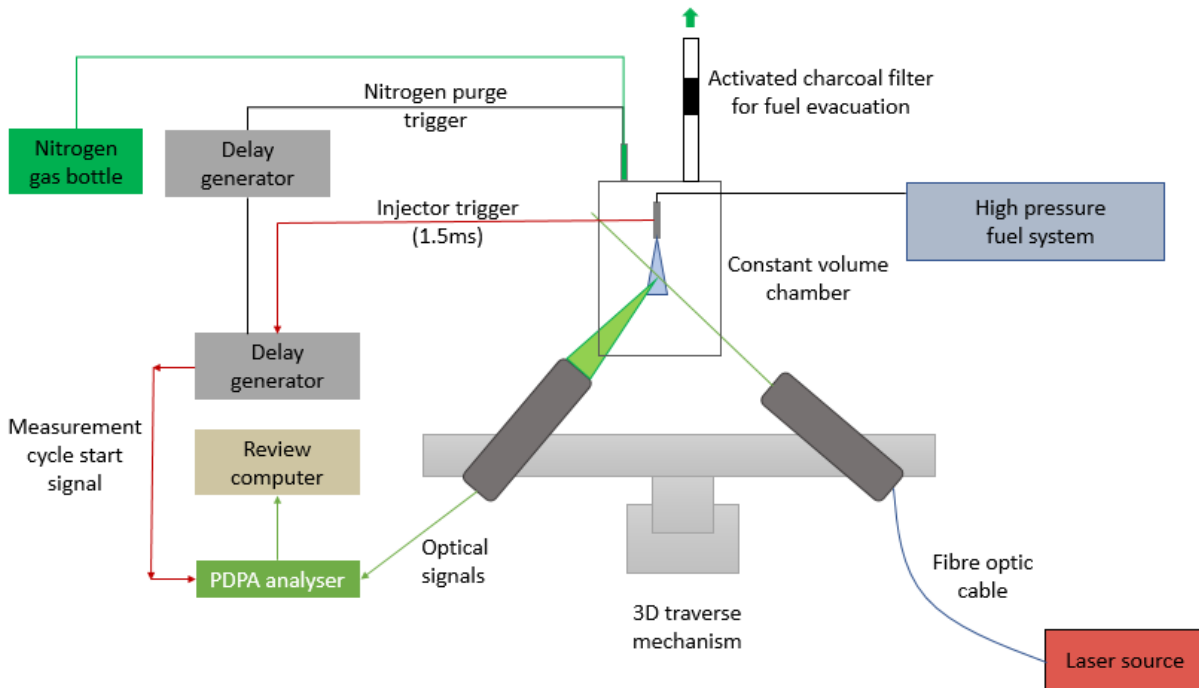
Figure 35: Block diagram of the PDPA setup used

5.1.1 Laser source

An mpc6000 power supply controls a Dantec Dynamic DopplerPower laser head that produces beam diameter of 2.2 mm at a wavelength of 532nm. The maximum output power is 1000mW, although as the spray formation would be fuel dense the laser power was set to 750mW as not to oversaturate the photomultipliers which is denoted as anode current in the BSA Flow monitoring software. The laser power can be adjusted from the power supply unit by adjusting the main dial.

5.1.2 Beam splitter

Immediately after the laser source was a Dantec Dynamics Fibre flow 40MHz Bragg cell that was used to split the single beam into two 2.2mm beams while additionally producing a variable frequency shift before being conveyed to the PDPA transmitter optic using a fibre optic cable.

5.1.3 PDPA laser optic

A beam expander is used to increase the spacing of the beams being emitted from the beam splitter before passing though the final optical lens that converges the separate beams at a focal length 310mm to form the measurement volume. Within the volume contained of 21 fringes with a spacing of 2.208μm denoting an appropriate resolution to distinguish particles and precisely perceive velocities.

Table 7: PDPA parameters used in acquisition

Beam spacing	38mm
Number of fringes	21
Fringe spacing	2.208μm
Fringe direction	Negative
Probe volume	dX 0.04856 dY 0.04821 dZ 0.40010
PDPA receiver	112mm fibre PDA
PDPA detector angle (in respect to the laser path)	70°
Aperture mask	A
Spatial filter slit	0.22mm
Maximum particle diameter	40.8μm

5.1.4 Constant volume spray chamber

Measurements were carried out in a constant volume spray chamber at atmospheric pressure and with consistent room temperature. The spray chamber is made out of glass and has dimensions of 380mm in length, 240mm in width, with a height of 255mm and has injector and nitrogen purging access at the top. The constant volume spray chamber was connected to a heavy steel frame to ensure the positioning of the injector did not more during testing and its position relative to the 3D traverse system is depicted in Figure 35. As the chamber was not

designed for pressurised experiments droplet evolution with increased pressure above atmospheric conditions could not be tested.

5.1.5 Triggering of injector and purging

The triggering of the injector is controlled by the delay generator and drivers explained in the earlier section along with the high-pressure fuel system. In between the 2Hz fuel pulse another trigger is sent by an additional delay generator attached to the first to trigger a gas solenoid to inject nitrogen to purge the constant volume of excessive fuel. A block diagram in Figure 36 displays the TTL wiring. To create a cyclic measurement event for the BSA processor to build statistical data on the spray evolution, a start measurement TTL signal is sent to a programmable input on the back of the processor. When in operation the delay generator sends a "start measurement pulse" signal to the processor before the delay generator triggers the injector at the specified pulse width. After these pulses have been sent and the spray evolution is complete, the delay generator sends a trigger signal to another delay generator that sends an operating pulse to a gas solenoid to completely purge the constant volume chamber. The reasoning for the additional use of a delay generator is because of the additional channels needed to create an operating pulse.

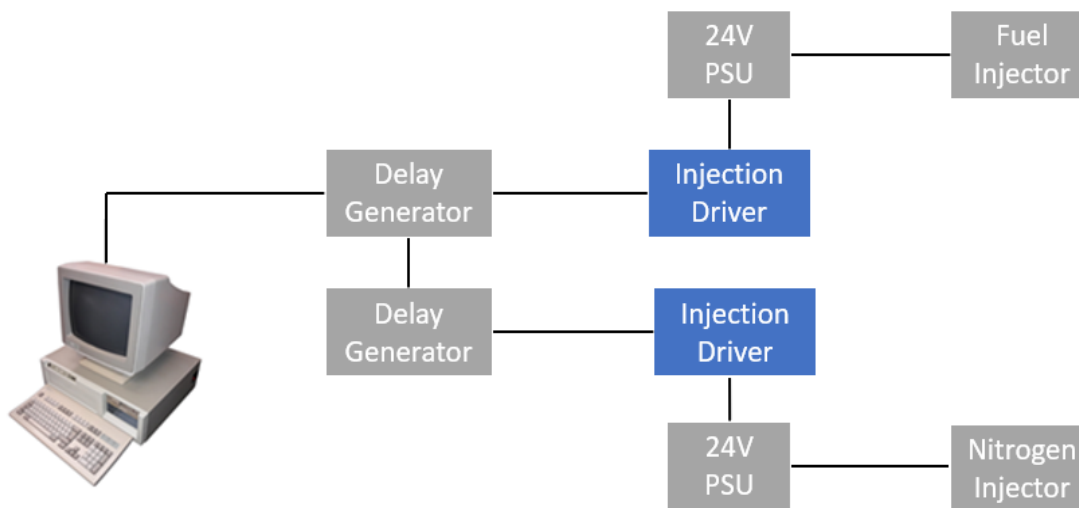*Figure 36: TTL block wiring of the injection setup that uses delay generators to operate the "start measurement" event, trigger the injector and purge the chamber.*

5.1.6 PDPA detector and Signal processing

As the light scatters from a fuel droplet, it is detected by the PDPAs 60mm receiving probe focused on the measurement volume. The receiver was positioned 70° with respect to the laser's path in

order to capture the dominant first order refraction mode from the fuel droplets. An aperture plate in the receiving probe has three divisions that divide the scattered light for three photo multipliers. The received light is passed through a fibre optic cable to the Dantec FibreFlow PDPA processor where the photo detectors and multipliers are housed and transformed into an electrical voltage signal for the processing unit to recognise. The fluctuations in voltage signals are then subsequently analysed by the processing unit to construct particle size and velocity information to be displayed on a local computer.

5.1.7 Test fuel

The JSAE 2715 standards [72] advise the use of N-Heptane as the test fluid as its chemical stability and volatility means it can quickly evaporate and is less volatile than other fluids. Gasoline is a complex mixture of hydrocarbons, additives, and other compounds that vary around the world while the commercially available N-Heptane has a high purity and its constant composition makes it a known control condition. Gasoline, however, was used as the test fluid as the refractive index and vaporisation characteristics of N-Heptane and gasoline are similar. The refractive index of N-Heptane is typically around 1.387 with gasoline being around 1.427. The difference in refractive index is not significant. Although when measuring droplet size differences, the refractive index is able to affect a measurement by causing error in the sizing determination. Gasoline emissions from testing are purged though an activated charcoal canister and exited to an external source. 95 RON Gasoline was also used in other experiments conducted and to be comparative to each other gasoline was selected to be a constant as the fuel source for all experiments was the same throughout.

5.2 Experimental procedure

To acquire respectable number of droplet counts for the PDPA experiments, above 30,000 accepted counts, the measurement volume was precisely aligned using a 3D printed camera mount made for an Olympus EPL8. Using this method an exposed image would reveal if adjustments need to be made until the measurement volume fell seamlessly within the 50µm slit marker, although a 250µm slit width was used for the experiments. To learn the coordinates centre of the spray plume for the 3D traverse system, initial tests were carried out using a grid formation to seek the highest velocity fount in the velocity plots. These began with a 1mm spacing before narrowing to 0.25mm.
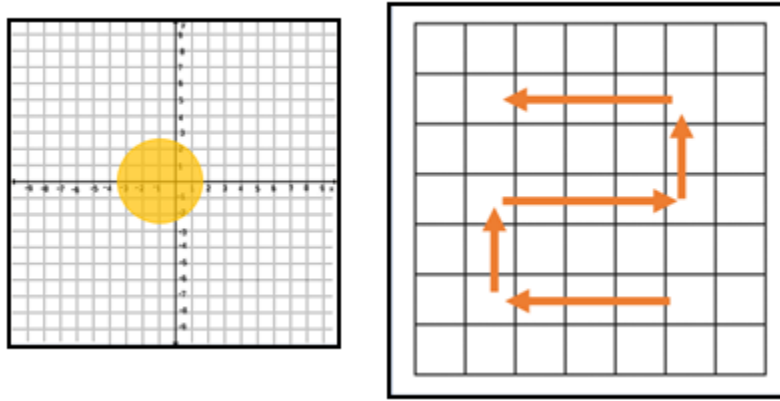
Figure 37: Representation of a narrowing grid structure used to in preliminary PDPA testing to determine coordinates for the fuel spray

The combination of the precise alignment of the receiver to the measurement region and the measurement region to the fuel spray allowed for an accepted droplet count of between 100,000 and 60,000 depending on pressure and proximity to the injector tip. The injection frequency used was 2Hz and also incorporates a burst of nitrogen in order to purge in between injections. To achieve a higher number of injections for the experiment the acquisition time was made longer to 200 seconds. With this, the minimum injections for a case was 400, although some cases exceeded this number under repeat conditions due to the lower accepted droplet threshold the closer measurements were taken to the injector tip. Using the BSA flow software on a cyclic measurement event basis and using the PDPA processers TTL inputs, velocity plots can be developed every time the injector has been triggered.

From the earlier study using high-speed image shadowgraph, it was known that there was a high likelihood of the liquid fuel ligament in the centre of the spray plume and near the injector tip region, which resulted in an accepted sphericity of the droplets in the mid to high 70% range. Although, due to the high number of counts this still leaves a large number of validated droplet samples that can be used.

	X [mm]	Y [mm]	Z [mm]	Counts	Spherical Validation [%]	D10 [μm]	D20 [μm]	D21 [μm]	D30 [μm]	D31 [μm]	D32 [μm]	D43 [μm]
1	412.50	455.00	437.00	58786	74.38	4.0	4.8	5.9	5.9	7.1	8.6	14.6
2	411.50	465.50	420.00	55319	73.53	3.6	4.5	5.6	5.6	7.1	8.9	16.3
3	410.50	474.50	405.00	66739	76.57	3.6	4.5	5.5	5.5	6.7	8.2	14.1
4	410.00	486.00	387.00	77377	75.38	3.0	3.8	4.7	4.9	6.2	8.0	15.9
5	0.00	0.00	0.00	70084	75.74	3.2	4.0	5.1	5.2	6.6	8.6	16.3
1	412.50	455.00	437.00	67786	79.47	5.0	5.9	6.9	6.8	7.8	9.0	12.3
2	411.50	465.50	420.00	51812	75.30	4.4	5.4	6.5	6.4	7.6	8.9	12.8
3	410.50	474.50	405.00	56254	77.16	4.6	5.5	6.7	6.5	7.7	9.0	12.7
4	410.00	486.00	387.00	74743	77.51	3.6	4.5	5.6	5.7	7.1	9.1	15.6
5	0.00	0.00	0.00	55183	78.86	4.2	5.0	5.9	6.0	7.2	8.6	14.0
6	0.00	0.25	0.00	66432	80.51	3.7	4.6	5.6	5.6	6.9	8.6	14.7
1	412.50	455.00	437.00	71928	82.76	6.5	7.5	8.5	8.4	9.5	10.6	13.4
2	411.50	465.50	420.00	58105	73.94	5.1	6.2	7.6	7.3	8.7	10.0	13.5
3	410.50	474.50	405.00	52047	73.42	5.0	6.2	7.7	7.4	9.0	10.5	14.1
4	410.00	486.00	387.00	66188	74.82	4.1	5.2	6.7	6.5	8.2	10.2	15.5
5	0.00	0.00	0.00	53624	79.28	5.1	6.0	7.0	7.0	8.2	9.6	14.1
1	412.50	455.00	437.00	97605	83.31	6.7	8.0	9.5	9.3	10.9	12.5	15.7
2	411.50	465.50	420.00	101112	84.72	6.2	7.3	8.7	8.5	10.1	11.6	14.8
3	410.50	474.50	405.00	94335	82.67	6.2	7.5	9.0	8.8	10.6	12.4	16.4
4	410.00	486.00	387.00	90763	78.69	5.0	6.2	7.8	7.6	9.4	11.3	15.7
5	0.00	0.00	0.00	55615	78.65	5.9	6.8	7.9	7.8	8.9	10.2	13.6
1	412.50	455.00	437.00	91833	79.86	6.9	8.9	11.5	10.9	13.7	16.3	20.6
2	411.50	465.50	420.00	84322	78.23	6.1	8.0	10.4	9.9	12.5	15.2	19.8
3	410.50	474.50	405.00	79658	77.35	6.2	8.0	10.5	10.0	12.7	15.3	20.1
4	410.00	486.00	387.00	76134	75.45	6.6	8.3	10.3	10.0	12.3	14.6	19.3

Figure 38: Dantec Dynamics PDPA software showing droplet counts and spherical validation

To confirm the quality of the setup, the BSA flow software has an inbuilt oscilloscope display to inspect the Doppler signals. Figure 39 is a screen capture of the doppler bursts that were seen in the initial setup and data acquisition of the PDPA experiment While Figure 40 shows a noisy signal which would result in poor data acquisition and so is not satisfactory for use in the investigation.
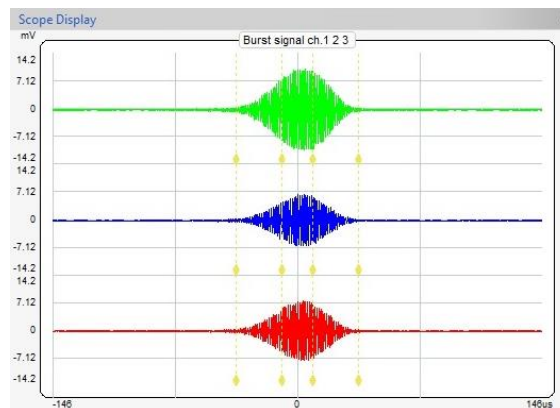
Figure 39: BSA Flow software in built scope display showing little signal noise

67
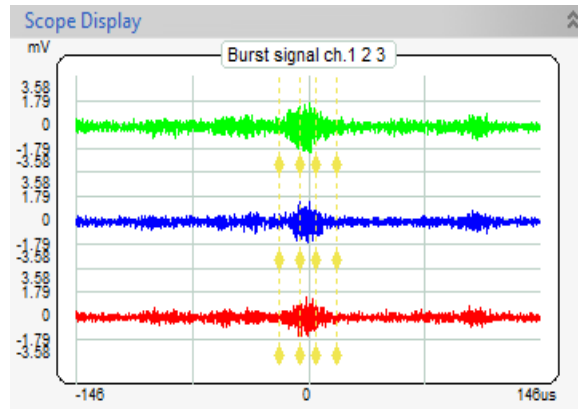
Figure 40: Noisy doppler bursts showing a poor data signal

Table 8 lists the test conditions for the PDPA investigation into the injector characteristics. As a 1.5ms pulse duration is recommended and widely used this simplifies the data acquisition. As the initial calibration and high-speed imaging revealed that the injectors fuel delivery seemed rather linear and predictable, the pressures to be analysed were reduced from every 10MPa to what is seen in the table. based on the previous research in Chapter 2, the measurement points were selected to be between 40 and 100mm away from the tip in order to avoid errors caused by multiple scattering and non-spherical droplets. A representation of the how the distances interact with the fuel spray are given in Figure 41 and are located in the centre axis of the fuel spray.

Table 8: PDPA test conditions

Pressure (MPa)	Pulse width (ms)	Distance from injector tip (mm)
20	1.5	40,60,80,100
40		
60		
80		
100		
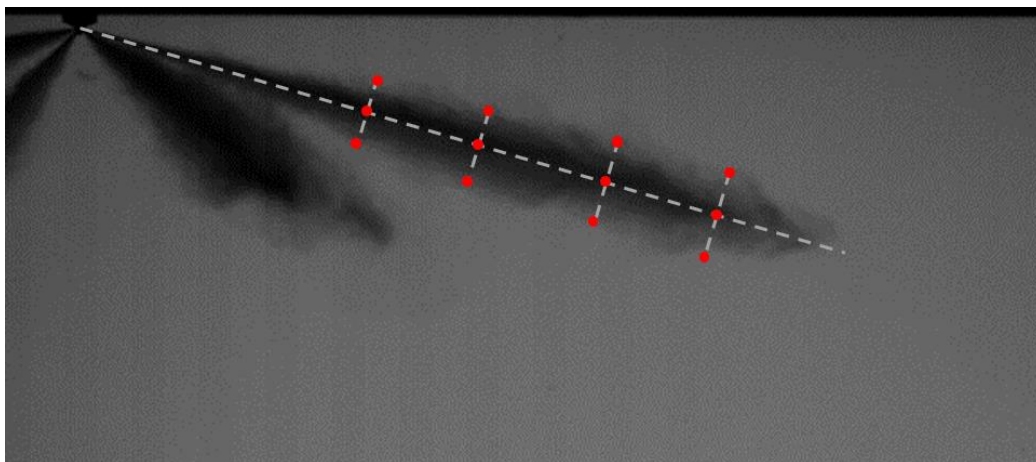
Figure 41: Measurement distances from the injector tip

5.3 Results and Discussion

5.3.1 Spray Structure against time

The typical distribution of overall droplet diameters and droplet velocity seen for an injection are exhibited in Figure 42 and are plotted against the time after the start of injection. The measurement for this figure were undertaken in ambient temperature and pressure conditions using an injection pressure of 60MPa. The injection duration was 1.5ms and the measurement point was at a distance of 60mm away from the injector tip. After the injection trigger has been sent, the fuel spray rapidly moves towards the measurement point of the PDPA system. There is a slight delay from when the fuel spray evacuates the injector tip to when it reaches the measurement volume, and this is what is known as injection delay that includes the solenoid delay time to raise the injector needle. As there are a high number of droplets counted for the measurements it is practical to create mean average droplet data to compare the differences for each test case. Figure 42 shows the initial delay in injection as predicted before sharply rising as the spray head passes through the measurement region at approximately 1ms. This is presented in the form of average velocity trend within the tens of thousands of confirmed droplet counts. The uniformity in velocity between 1-3ms denotes the measurement of the main body of the fuel spray. The tail, after 3ms, quickly decelerates without the fuel pressure momentum acting upon it. Using the mean average of the droplet data the development of the velocity and diameter characteristics are clearly indicated and subsequently will be presented in this form.
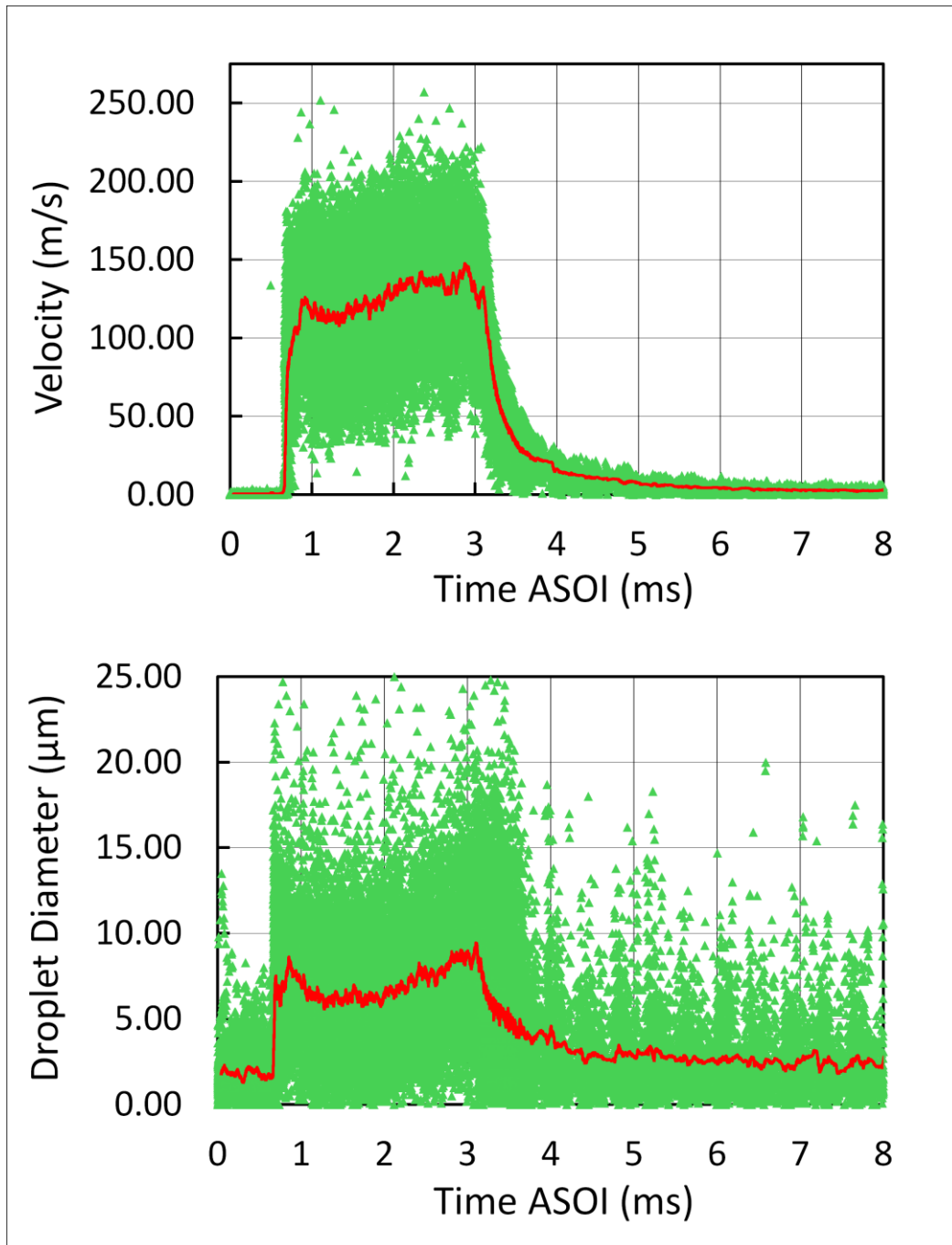
Figure 42: Droplet velocity and diameter plots of 60MPa injection pressure at a 1.5ms pulse width
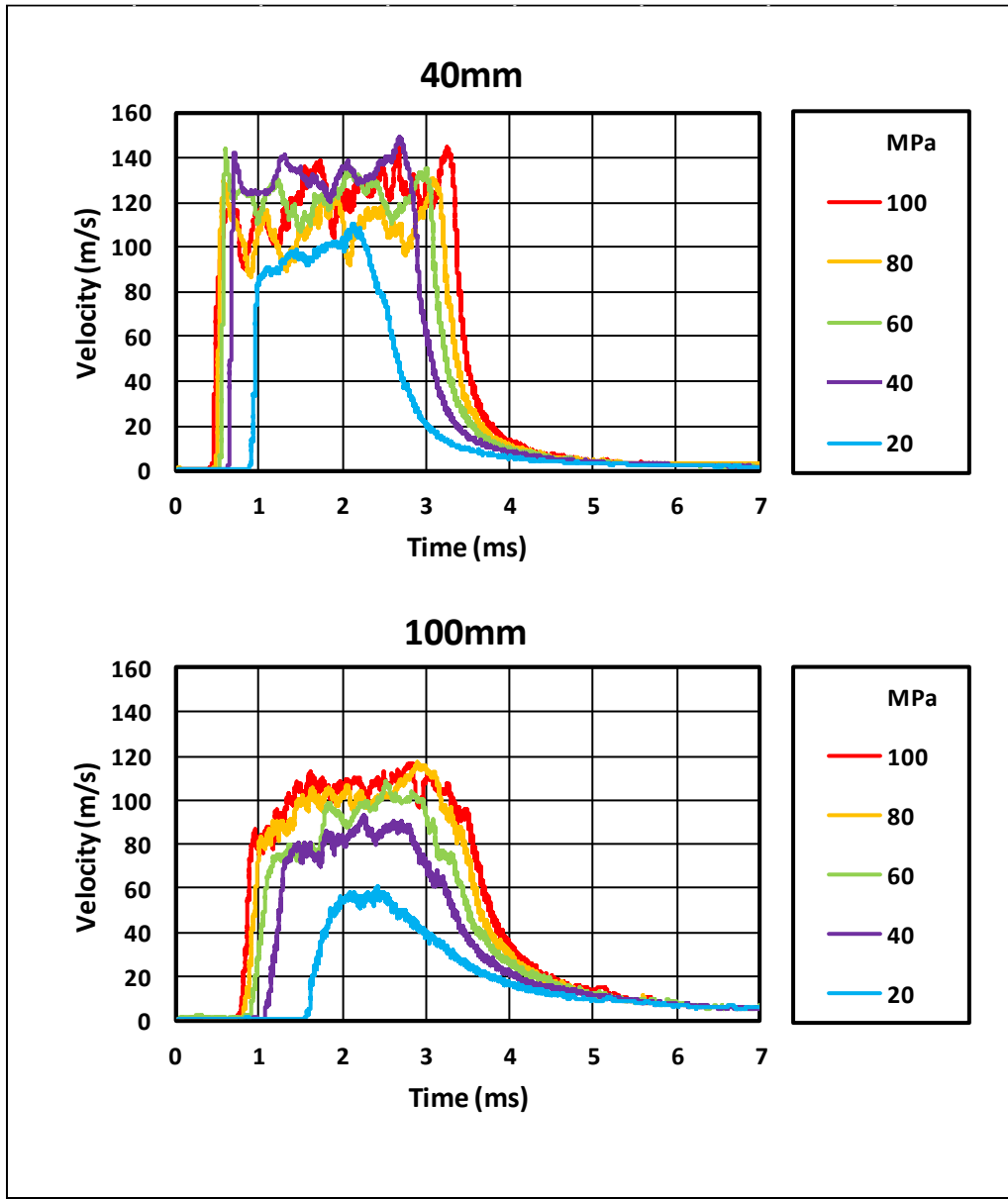
Figure 43: Spray velocity at 40mm and 100mm away from the injector tip

As experienced from the high-speed imaging experiment, the velocity of the injection spray increases with raised injection pressure. Figure 43 shows the velocity profiles from 20 to 100 MPa at the closest and furthest distances from the injector. There is a surge in velocity from 20 to 40 MPa while after 40 MPa the progression still increases but at a much-reduced rate. If pressures were continuing to rise the resulting terminal velocity of the fuel spray could be around 120 to 140ms at 60MPa at 40mm away from the injector tip but are not likely to stray far from seen in the figure. The injection delay for 20MPa is significantly longer to any other pressure tested. Apart from the spray traveling much slower from the outset and takes longer to get to the measurement region. Another could be a result of the operation of the injector, the internal needle that releases the fuel spray uses the principle of differential pressure change to use its own fuel to open the

72

needle and thus release the fuel. Having less pressure, and the energy that it would bring, would have the side effect of a slower needle reaction time that would result in a delay in fuel delivery. Incidentally, since the fuel injector was calibrated for fuel delivery the quantity would be correct for future LIF testing but a timing delay in operation may be a cause for discussion.

Looking at the velocity profiles in Figure 43, every case has a clearly defined leading edge, head and tail typical of spray structures. The leading edge can be seen as the initial increase in velocity where the droplets are gathering speed as the pintle is opening. When the pintle is fully open the majority of the fuel is released and positions that are closer to the injector tip display a slight increase in average velocity once this happens. As measurement points move away from the injector tip a more curved profile of the mean velocity is encountered showing that the droplets are losing momentum. 20MPa in all positions is consistently has the lowest average velocity. But pressures above 20MPa have velocities with a much closer span. The clustering of velocities at raised pressures could signify that the velocity limit of this injector is being reached and where increasing fuel pressure further would not signify an increase in droplet velocity. In addition, when performing measurements close to the injector tip this difference is only slightly seen and doesn't have a significant impact as seen 40mm away from the injector tip because if the initially high kinetic energy governed by the nozzle orifice before diverging more noticeably as measurements are performed further away. Just as with Poatriotis *et al.* [78] experimentation, lower fuel injection pressures exhibit a lower velocity than those tested with higher pressures and also displaying a closing of the velocity difference which is only amplified the closer the measurement region is to the injector tip as displayed at 40mm. Suggesting that more fuel pressure can be applied as this steady plateauing of velocity would see a similar pattern to the droplet velocities seen here with the highest droplet velocity averaging about 80m/s at 60MPa compared with the ~120m/s seen with the DI injector characterised here although there is a large difference in methods of spray plume deployed.
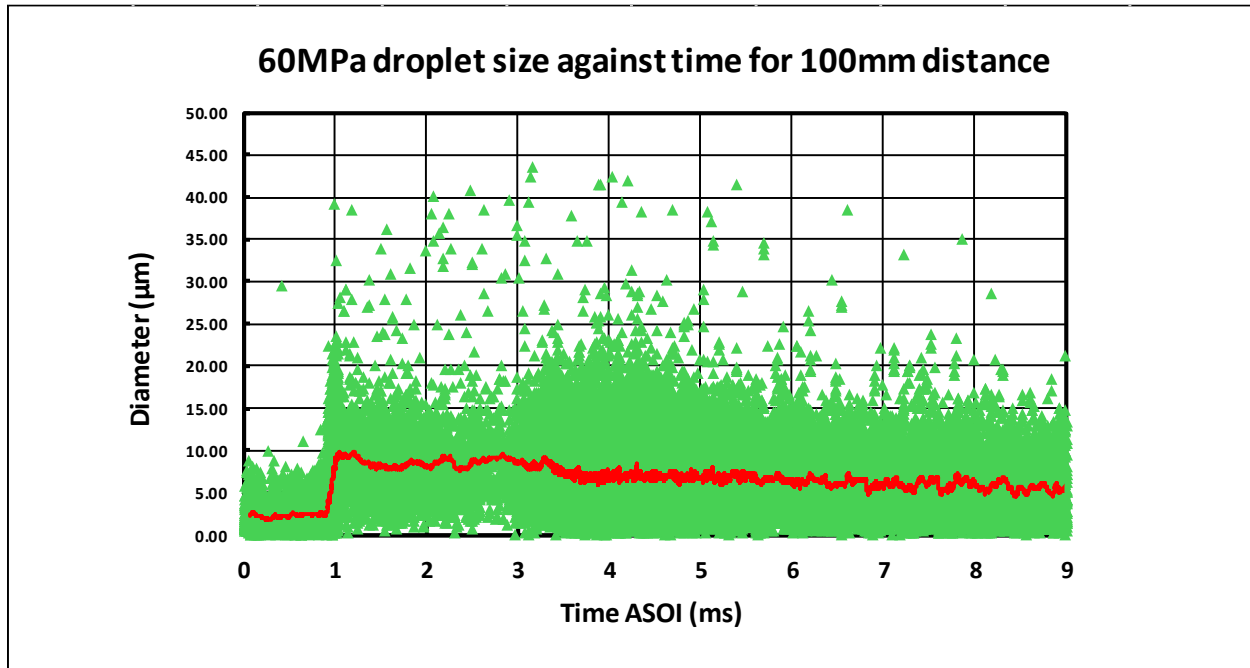
Figure 44: Droplet diameters ASOI for 60MPa at 100mm from injector tip

Having the overall droplet sizes expressed with time ASOI shown in Figure 44 correlates droplet size to when they are produced from when the injector is triggered. The droplets formed before 1ms are residual droplets that are present in the spray chamber before the delayed introduction of the measurement spray. These droplets have no velocity as can be seen in the velocity plot in Figure 43 and so they are not part of the fuel spray. When the head of the spray crosses into the measurement region at 1ms larger droplets of sub 25µm are encountered before reducing in the main body of the plume to approximately 15µm. The spray tail at 3ms sees an increase of droplet size as a result the closing of the injector needle where the injector nozzles have not optimised. The later stages of the tail after 4.25ms exhibits a reduction in droplet size and also velocity. All cases have a droplet formation behaviour but the droplet sizing varies with the peaks seen in Figure 44 depending on their pressures and at the different distances tested.

Test cases were based on a 1.5ms pulse width and looking at the velocity profiles in Figure 42 and Figure 43 the main body of the injection has the appearance of having a longer pulse width in the region of 3ms. When looking at the start of secondary peak in the droplet size against DOA, the start of the peak happens 1.5ms after the initial spray head is detected verifying that a 1.5ms pulse width was used.

5.3.3 Effect of the Injection Pressure

The measurement of droplet velocities and diameter statistics is an important part in understanding the atomisation process at high gasoline pressures, for this four different distances of 40, 60, 80 and 100mm were selected, visualised in Figure 41, with accompanying fuel injection pressures of 20, 40, 60 and 100MPa were tested with the injectors pulse width being 1.5ms.

D32

D32, saunter mean diameter, is a parameter used to characterise the average size of droplets within a distribution. The definition labels it as the diameter of a sphere that has the same volume-to-surface ratio actual droplets in the distribution and is mathematically expressed in the following equation. n represents the number of droplets of the same size grouping and d signifies the measured droplet diameter.

(3)

$$D32 = \frac{\sum n_i d_i^3}{\sum n_i d_i^2} = \frac{(D_{30})^3}{(D_{20})^2}$$

D32 is used to provide a representative value for the droplet size distribution that gives more weighting to larger droplets since it includes the cube of the diameter of the droplets.

The Sauter mean diameter profiles are reported in Figure 45 and are clearly influenced by the increase in injection pressure but only to the extent of 80MPa where after there the difference in D32 diameter becomes even with 100MPa where It could be assumed that a distribution limit for the larger D32 droplets has been reached at this point.
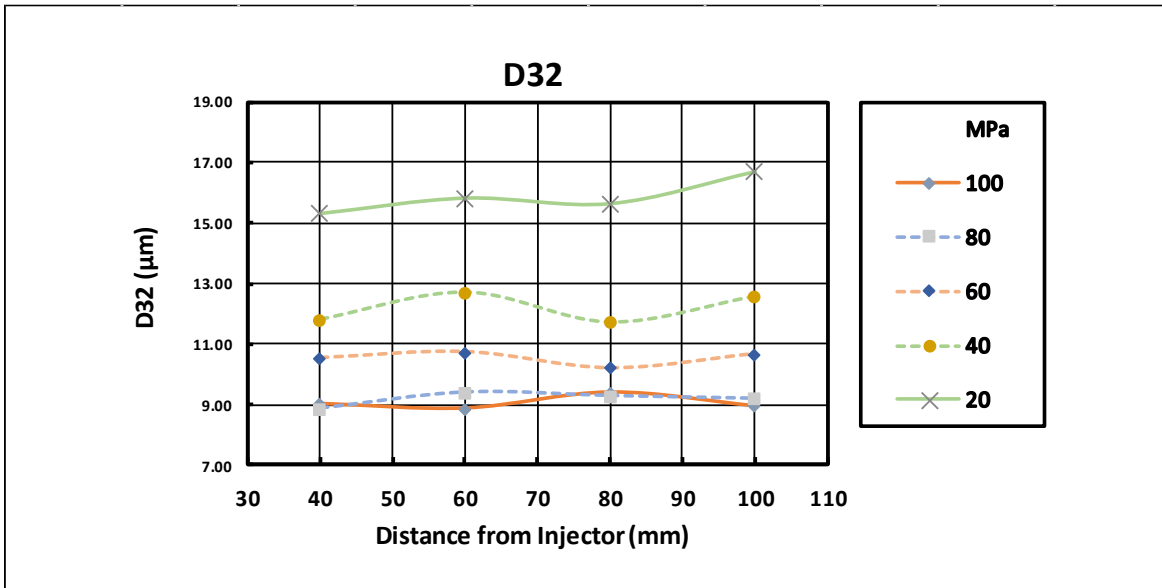
Figure 45: Sauter mean diameter profiles from the injector tip

D10

D10, arithmetic mean diameter, signifies droplet diameters that fall below 10% of the total volume of droplets in the distribution and signifies a samples mass comprised of smaller particles expressed in the following equation.

(4)

$$D10 = \frac{(\sum n_i d_i)}{N}$$

Using D10 provides information about the size of droplets in a distribution that make up a fraction of the total volume and is useful in understanding droplet distribution into smaller particles.

The arithmetic mean diameter displayed in Figure 46 shows that as the pressure increases the number of smaller droplets grows but as the distance from the tip becomes greater the fewer smaller droplets are detected. An explanation of this is that as the distance becomes greater the smaller droplets are migrating away from the main plume and the measurement region due to the turbulent diffusion at a higher rate than the larger droplets, this is also seen within the initial high-speed visualisation images. The graph demonstrates the possibility that increasing the fuel injection pressure can lead to smaller fuel droplets and as the results have not converged yet meaning the limit of smaller D10 droplets still might not have been reached unlike the D32.
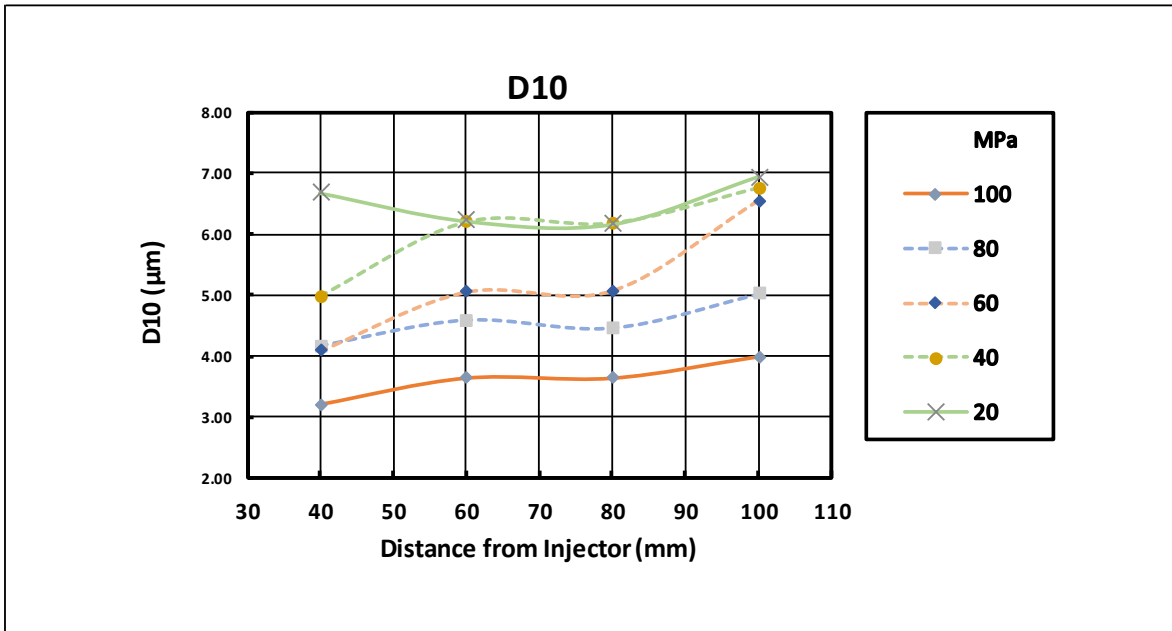
Figure 46: Arithmetic mean diameter profiles from the injector tip

Figure 45 and Figure 46 expresses D10 and D32 with relation to injection pressure, in both figures it is clearly seen that the general trend is that as injection pressure is increased the droplet diameters are reducing. As with Figure 45 the droplets start to level off at 9μm demonstrating that the injector cannot produce a smaller measure of D32 average size partials. Further increasing pressure may form a step change but more than likely is that droplet size will remain at roughly 9μm. The trend of arithmetic mean diameter against pressure in Figure 46 has a continuing downward inclination for the smaller D10 droplets and unlike the D32 graph against pressure a levelling out has not occurred yet. This could mean that the possibility of smaller D10 droplets is likely if increased pressure is applied. However, the amount of D10 droplets is due to just the pressure increase but rather a turbulent effect brought on the exiting fuel kinetic energy causing the perimeter of the fuel spray boundary to be turbulent. Future experiments focused on the D10 droplets could see a profile that levels out with further extreme gasoline fuel pressure. Owing to the fuel droplets cannot become smaller due to the turbulent effects limited by the injector orifices.

Droplet Distribution
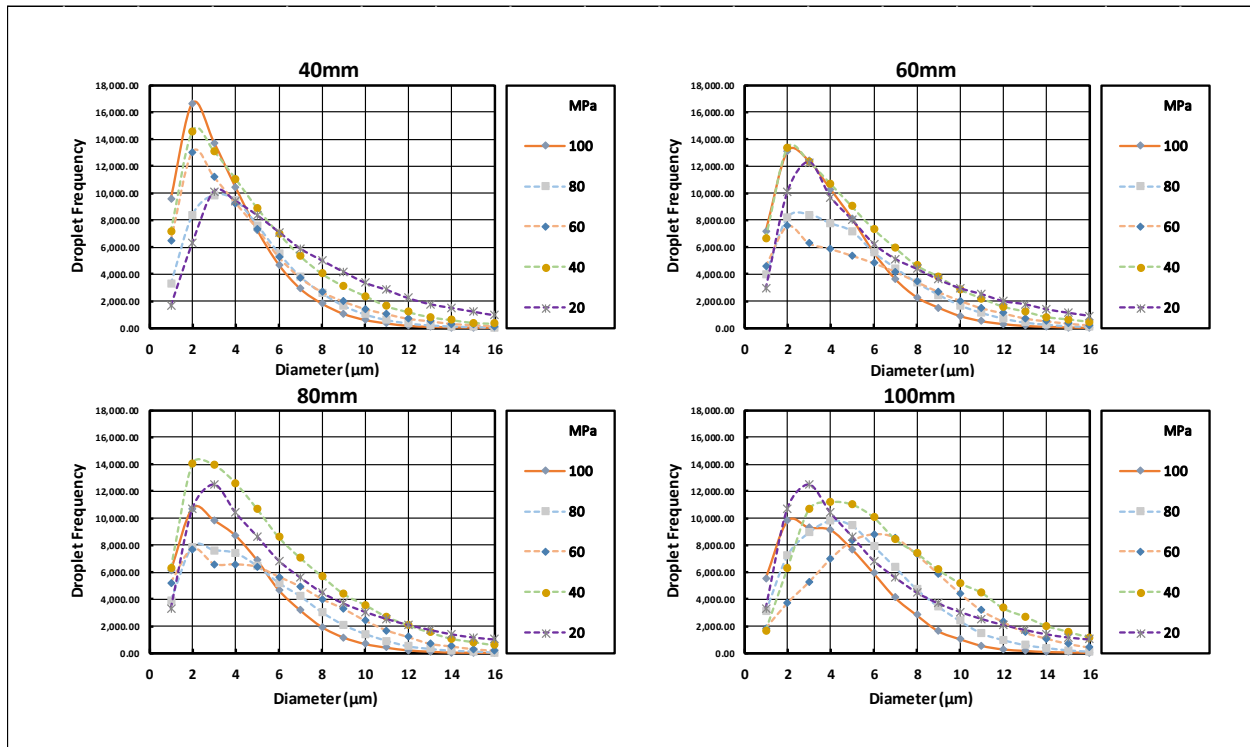
Figure 47: Histogram distributions of fuel droplets from 40, 60, 80 & 100mm away from injector tip

Histograms in Figure 47 shows the droplet distribution at different distances from the injector tip along with its injection pressure. In each case the weighting is towards a larger percentage of smaller droplets as denoted by the peaks forming on the left of the x-axis. As the D32 droplets does not need to be large to influence the partial distribution their presence could be in the centre of the spray plume and be dependent on the bore to length ratio of the injectors nozzles dimensions. For each case the weighting of droplet distribution shifted, as the pressure was raised the D32 reduced in particle size while the D10 partials increased. As the distance from the injector became further you it is evident the that the histograms in all cases, notably 80 and 100mm, begin to level expressing that the smaller droplets have migrated out of the main plume leaving larger droplets with more mass and momentum to traverse the PDPA measurement region. It is also worth noting from Figure 47 that the peaks of the histogram depiction have the tendency to happen below the number of the D10 signifying that there are smaller droplets detected in the doppler spray bursts.
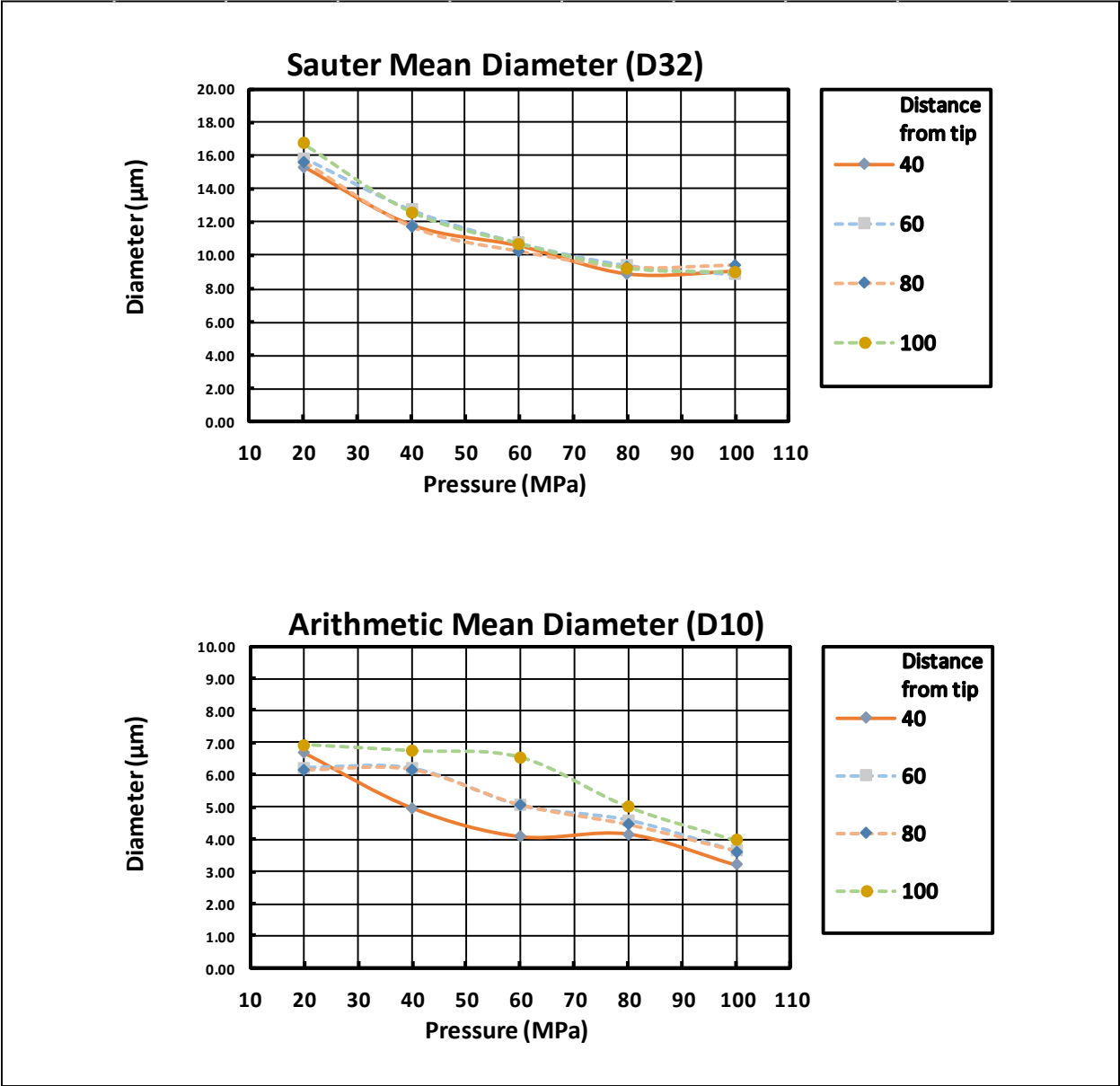
Figure 48: Arithmetic mean diameter & Sauter mean diameter against pressure

Poatriotis *et al.* [78] research into spray analysis and atomisation for a 60MPa fuel pressure included droplet sizing analysis and when comparing results, the trends for D32 and D10 shown in Figure 48 follow similar trends. However, at 20MPa the DI injector has a D32 of 16µm while for Poatriotis *D32* measures *at 22*µm. With the increased pressure of 60MPa Poatriotis *has a D32 of 8*µm while at 60MPa the DI injector is ~11µm and even with pressure at 100MPa D32 is at 9µm stating that with all the pressure increase for these different styles of injectors, 40MPa does not see substantial reduction of D32 sized droplets. When analysing both D10 results the DI injector achieves a larger number of droplets in the D10 region.

5.4 Summary

PDPA was employed to analyse the droplet sizes and velocities of gasoline sprays and how they are affected by injection pressures for a given 1.5ms pulse width. To ascertain a good numerical amount of information for each test case and position, a target of 100,000 droplet counts was set for the furthest distance from the injector knowing that a reduction in droplet count would be expected with closer proximities to the injector. This reduction would result in droplet counts of 60,000 which is still well above other studies and provides excellent data sets for the graphical information presented. Droplet distribution shown in Figure 47 shows that for the pressures tested, the weighting for smaller droplets is significant with a gradual increase in droplet size to 16μm. When comparing pressures, Figure 45 and Figure 46 show that overall as the pressure increases more smaller droplets are formed as the more kinetic energy the fuel experiences the more turbulent effect of the spray boundary is seen. This causes smaller droplets to be pulled out of the main body of the spray to create a large boundary of smaller diameter droplets. As the injector will be featured in upcoming LIF experimentations with the bore of the engine being 82mm. Droplets up to 40μm would be of more significance than those that come after as it is unsure how the droplet sizing would be affected by wall impingement and could be of significance for future study. To improve the collected data plots the repetition of the experiment should be considered in the future. Even though the droplet counts are high for the experiments, repetition would yield an even greater total number eliminating possible anomalies that could occur by having less weighting in the results. Nevertheless, PDPA has provided additional quantitative measurement data that high-speed imaging would not have been able to provide alone.

Chapter 6: In-cylinder fuel distribution measurements

6.1 High-speed LIF set up

Measuring the in-cylinder fuel distribution of ultra-high-pressure direct fuel injection was achieved with the use of a single cylinder optical research engine as described in more detail in the previous sections. The naturally aspirated spark ignition engine incorporates a quartz glass cylinder and a quartz glass flat top piston to gain additional optical access to the vertically oriented centrally mounted DI injector.

Figure 49 where the fuel spray is denoted by item number 2. The fuel spray is aligned in line with the laser sheet as to illuminate the spray formation. When the initial dense fuel spray has subsided the evolving fuel spray will still be within the laser sheet that gives rise to assess the homogeneity of the fuel mixture.

1. Injector tip
2. Fuel Spray
3. Cylinder
4. Piston
5. Laser sheet
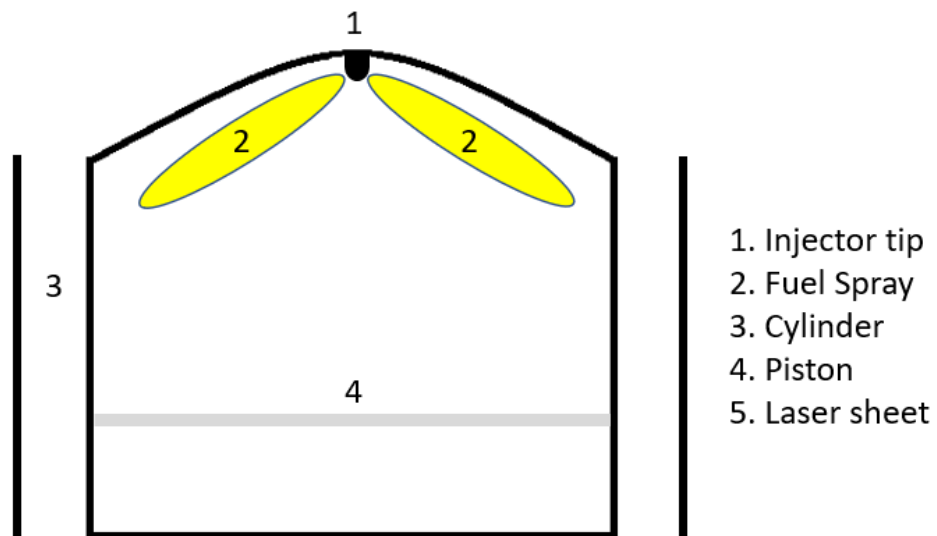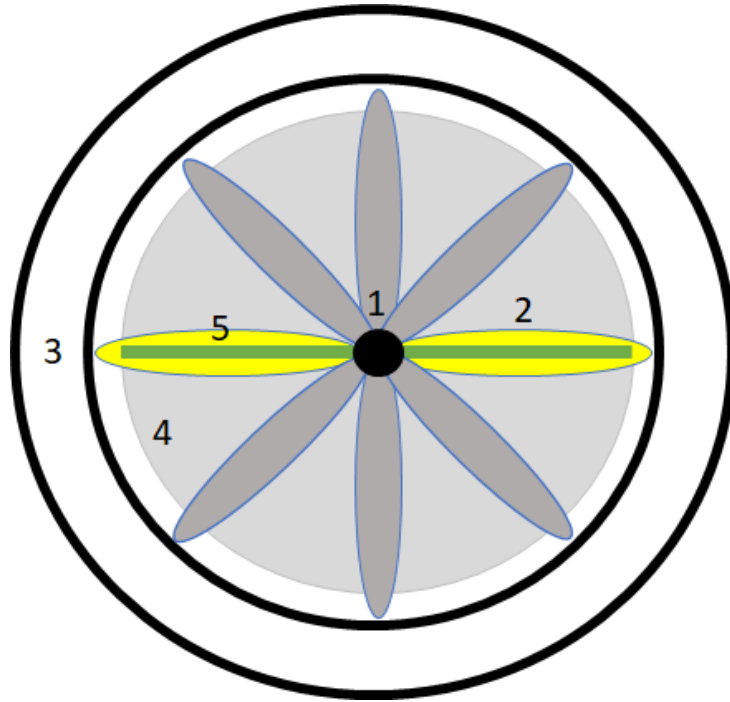
Figure 49: Diagram of the spray area within the optical engine

6.1.1 High repetition Laser

A high repetition diode-pumped solid-state laser capable of up to 12KHz was employed for the LIF testing. The Edgewave IS 400-3-L 355nm wavelength laser however has a maximum power output pulse energy of 8.24mJ at 7kHz. The emitting laser beam travels directly into a Dantec Dynamics laser guide arm that manipulates the laser light onto the Bowditch piston mirror. Using an expanding sheet optic at the end of the guide arm alters the cylindrical laser beam into a flat sheet that can acts as an excitation plane for the florescence and is less than 1mm wide.

6.1.2 Camera optics

The FASTCAM mini ax100 was once again used to capture the high-speed imagery of the experiment albeit with the addition of a Lambert instruments HiCATT 25 high-speed gated intensifier. The gating functionality signifies the ability for the intensifier to capture very fast exposure times as well as the low light will be critical in capturing the low fluorescence image. To manoeuvre around this the high-speed gate incorporates an intensifier that amplifies the light from the fluorescence. Care must be taken however to not oversaturate the intensifier as strong light will damage the intensifier and cause visually saturated artefacts or blooming. To reduce the amount of noise introduced into the recordings, as much of the fluorescing light needed to be captured by the lens. For this reason, a Nikon 50mm F1.4 lens was used, as the aperture allowed

more light to pass than one with a higher f-stop, along with a 440-510nm band pass filter to allow only the fluorescence to reach the intensifier. To also assistance in creating the most fluorescence, a 20% mixture by volume of biacetyl was added to the 95 RON gasoline test fuel and is considered to be the upper ratio limit before having an adverse effect on the gasolines characteristics.

The synchronisation and triggering of the camera, intensifier and laser was achieved by using an oscilloscope with a simplified depiction in Figure 50. This figure shows the initial laser trigger pulse, camera synchronisation trigger enveloped by the gate open time to capture the fluorescence event. Adjustment the timings were done on the veracious control software's of the equipment with the laser adjustments made on the Lambert instruments HiCATT software.

The Intensifier gate is connected to a TTL cable to the camera and is synced to the frame rate of 6800 fps which was selected in order to utilise the maximin repeated pulse energy from the laser. At this frame rate, a 1° CA between each frame could be achieve. The combined wiring of the intensifier and camera sync and trigger are show in a schematic in Figure 51.
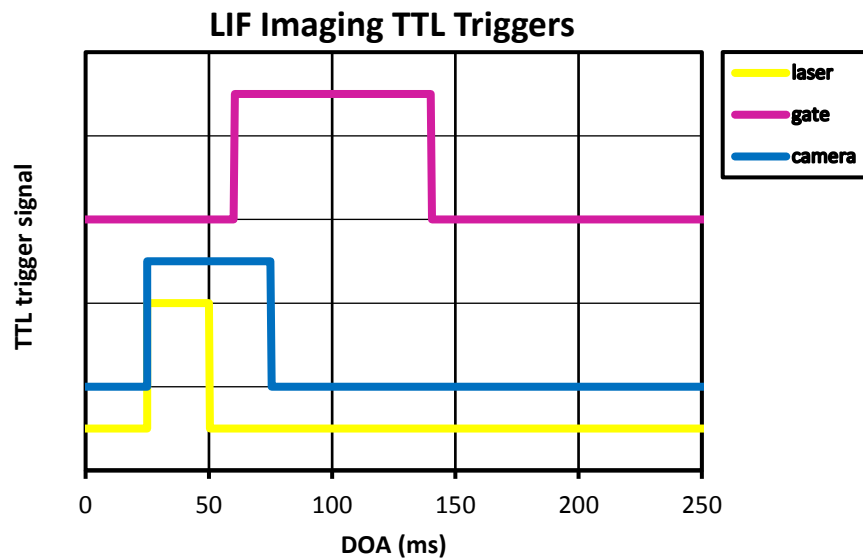
Figure 50: Simplification of TTL triggers used for LIF experiment
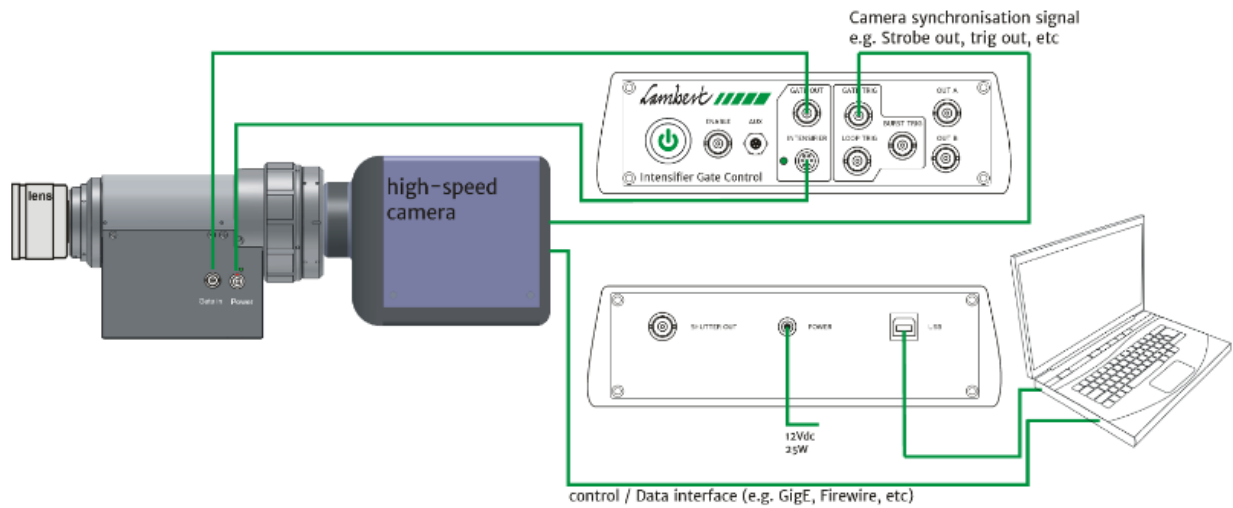
Figure 51: Wiring schematic of camera to intensifier [93]

Table 9: Optical parameters used in LIF acquisition

High-speed camera	FASTCAM Mini AX100
Pixel resolution	768x528
Frame rate	6,800fps
Lens	Nikon 50mm
Aperture	F1.4
Laser	Edgewave IS 400-3-L
Laser wavelength	355nm
Laser frequency	6,800Hz
Laser pulse energy	8mJ
LIF tracer	Biacetyl (20% by volume)

6.2 Experimental procedure

In order to take full advantage of retarded start of injection a thorough understanding of the delayed fuel mixing process needs to be understood. Test parameters are provided in Table 9 including the end of injection and fuel pressure for different fuel quantities or loads. Fuel spray behaviour can change dramatically under different engine loads when the fuel quantity is changed, effecting the spray development process, including spray penetration, cone angle, and breakup characteristics of the fuel. These changes in the amount of fuel injected can also affect the air/ mixture interaction, atomisation and distribution within the cylinder. Increased temperatures and pressures in the combustion chamber also affect airflow and combustion dynamics. To account for the different load condition the throttle is adjusted and monitored with the air intake pressure. 4.5Bar BMEP is used to create a low load condition with the intake pressure reading 0.75Bar. Part throttle load is administered by using a 7Bar BMEP with the intake pressure of 0.88 Bar. Full throttle high load conditions for the optical engine without firing operation has a maximum BMEP of 9Bar. For this, the throttle is opened fully with the engine control software reading 1.05Bar. All tests were completed at 1200rpm as the maximum operation of the engine given by its manufacture, AVL, is 3000rpm. 1200rpm also provides a finer crank resolution that is not possible with the same equipment at 3000rpm. For a comparison of later injections strategies, earlier injection needs to be obtained. Here the earliest injection considered is 90° BTDC as it is not untowardly a late injection or an early one and will give a good base for this study as to whether retarding injections are beneficial for homogeneity. As it has been shown that the injector has a linear nature using 90, 60, 30, and 10° BTDC provides an adequate resolution for these tests without the need of excluding results for clarity. EOI is used rather than SOI since the different pressures of 20, 40, 60, 80 and 100MPa require different length pulse widths to provide the same amount of fuel used for the engine load. If SOI were to be used then the end point of the pulse width and thus fuel quantity, would not be in the same place and cause an unfair comparison on injection strategies.

BMEP (Bar)	Fuel Pressure (MPa)	Pulse width (ms) (CAD)	Fuel quantity per injection event (g)	EOI (BTDC)
4.5	20	1.15ms (8.31°)	0.0113	90,60,30,10°
	40	0.65 (4.65°)		
	60	0.50 (3.60°)		
	80	0.40 (2.87°)		
	100	0.34 (2.46°)		
7	20	1.36 (9.78°)	0.0139	90,60,30,10°
	40	0.75 (5.38°)		
	60	0.57 (4.13°)		
	80	0.46 (3.29°)		
	100	0.39 (2.81°)		
9	20	1.55 (11.15°)	0.0172	90,60,30,10°
	40	0.84 (6.06°)		
	60	0.64 (4.62°)		
	80	0.51 (3.67°)		
	100	0.43 (3.13°)		

6.2.1 MATLAB and Dantec Dynamic Processing

Processing the LIF images involves several steps to enhance the quality of the images and extract the relevant information. The camera is triggered before an experiment as to acquire background images so that they can be used later to isolate the spray images in post processing. When the camera has been triggered it will record over 40 engine cycles totalling 29,106 images. Once the background and injection LIF images have been recorded. The injection events, and the corresponding backgrounds, are isolated and imported into Dantec Dynamic Studio to be averaged into singular injection and background image de-warped ensembles. From here the background is subtracted from the injection images. With applied masks to remove the unwanted areas outside of the cylinder, leaving only the fluorescing spray images.

The isolated in-cylinder spray images are then exported and organised so that MATLAB can be used to calculate the homogeneity of each case. Homogeneity is determined by the SD in an image denoting the dispersion in the pixel values in an image. Low SD indicates that data points are close to the mean value and a more uniform fuel distribution. While a high level of SD suggests that the data points are spread out over a larger range and the mixture is more inhomogeneous. Thus, higher levels of homogeneity would be indicated by lower deviation while uneven fuel mixing would be indicated with high levels of SD.

6.3 Results and Discussion

6.3.1 In-cylinder images
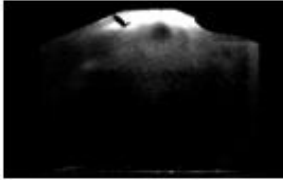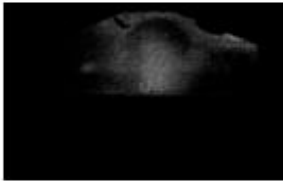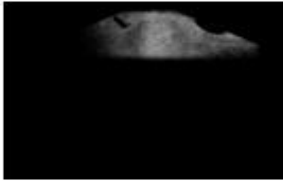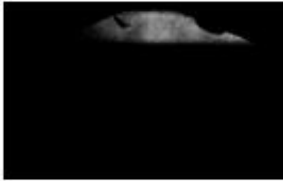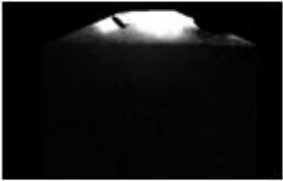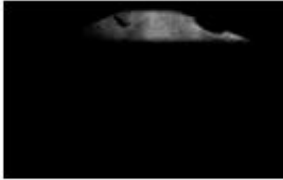
Figure 52: Mixture Development LIF images from a 7Bar BMEP load, 60MPa fuel pressure with EOIs of 90° and 10°

When observing the LIF images a characteristic trend appears for earlier injections and an insight is provided in Figure 52 shown by the 90° SOI strategy, after the injection event the fuel spray

completely impinges on the cylinder wall. As TDC approaches a turbulent effect can be seen of the fuel mixture where it ricochets off the cylinder wall before gathering centrally, seen beginning to happen here at 30° BTDC, then after being compressed into the combustion chamber. This happens with all cases but is less notable with the 10° EOI cases as there is less room for this effect to happen since the piston in near TDC. Such impingement would have an effect on the homogeneity of the air/ fuel charge on earlier EOI cases as the spray fuel initially would pool and not be as well atomised, droplets reforming after wall and piston impingement would not be as small as the initial spray event leading to insufficient mixture formation although this would need further study. As the cylinder volume is a lot smaller for a 10° EOI, impinged fuel rebounds directly back into the chamber and forgoing any turbulent effect.

6.3.2 In-cylinder Gasoline Distribution measurements
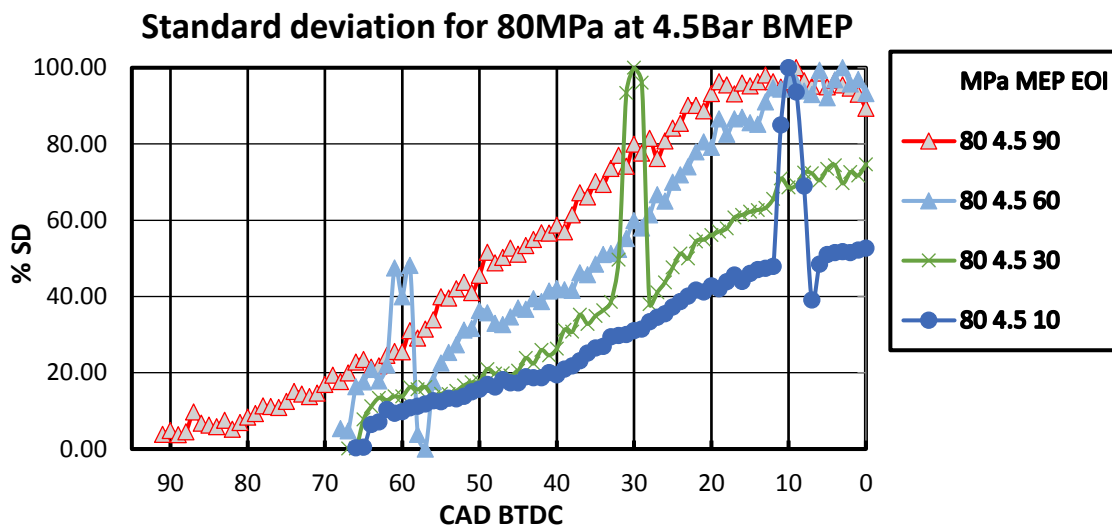
Figure 53: Standard deviation with varying EOI

Standard deviation (SD) is used as a metric to display in cylinder mixing as the images capture pixel values between 0 and 255, 0 being absent of light while a value 255 displays as white. This is calculated by using all of the processed 40 sets of images. Using the pixel values, highly concentrated areas of fluorescence shift towards a pixel value of 255 and areas with a lesser concentration converge towards 0. SD is used as a measure of the amount of fluorescence variability withing the confinements of the cylinder.

The behaviour of the SD to express homogeneity is best seen in the Figure 53 where the in-cylinder mixture has the tendency to have a greater SD when approaching TDC for earlier EOI cases as there greater space for droplets to disperse within the cylinder as opposed to later injection strategies that have a reduced capacity. The lowest SD seen in Figure 53 is of the latest

injection case where the cylinder is closeted to TDC and truss has the least amount of space. When this injection event occurs the region of interest is filled illuminated that give pixel values with less SD. Great variance can be in the level of SD between cases and could be of a result of previous visual observations where the DI injector creates an impinging turbulent fuel characteristic because of its penetration length causing poor fuel/ air mixing that is seen here with the in cylinder LIF testing. It is this effect that could be reason that the later injection strategy seen in Figure 53 prevails in having a more homogeneous mixture also seen displayed in Figure 52.

Figure 55 shows pressures from 20 to 100MPa with EOIs of 90° while Figure 57 shows EOIs of 10°. SD at 90° EOI has more of a SD spread across the range. In comparison to an EOI of 10° having less SD than their counterparts when approaching TDC. As previously mentioned, the extended penetration length likely has a great effect on this experiment that only increases with greater injection pressures. The higher penetration lengths are more likely to rebound off the cylinder wall for longer attributing to changes in SD and cannot hugely be attributed to droplet velocity as previously tested greater pressures exhibit similar maximum velocities. With a later injection strategy, fuel spray is more confined and is unable to follow the trajectories it otherwise would have seen in earlier EOIs. Instead of fuel spray rebounding and reforming centrally on the piston the LIF imaging data, when portrayed numerically shows that with a late injection strategy the injection is more homogeneous within a smaller combustion volume.

The raised step portions displayed in Figure 53 and in the 10° EOI cases in Figure 57 is due to the high concentration of fuel near the tip of the injector as it has not yet sufficiently mixed with the cylinder. As the dense fuel spray in this area and in the laser plane it appears as high SD while also having an effect a few degrees after the EOI and happens on all cases with varying degree.

When comparing SD within the 10° EOI cases, as the BMEP decreases from 9 to 4.5Bar SD begins to rise approaching TDC. This indicates that at higher or part throttle load are able to mix or disperse the fuel more evenly than at lower load conditions. This being the case the increased air introduced could have amplified turbulent air flow from the valves although would have also created a more defined trend in the visual images of the spray and in the earliest EOI cases. The reasoning could be observed in the first high-speed imaging experiment where the fuel quantity for an engine load of 4.5Bar BMEP is not sufficient to form a fine boundary lay of droplets as the needle isn't open for a long enough time to accommodate this. While at higher BMEPs more fuel is introduced to counter this effect.

Figure 55 and Figure 56 represent for EOIs of 60 and 30°, respectively. These are the intermediary results between the two extremes of 90 and 10° EOI and show a pattern for the

reduction of SD as the injection strategy becomes later. For 9Bar BMEP at a 60° EOI, 20MPa is the highest at roughly 95% for a 30° EOI 20MPa is again the highest at roughly 47%. 20MPa also gives the highest SD for a 90°EOI. For pressures above 20MPa at 60° and 30° EOI the level of deviation remains at a dramatically lower value of near 30%. The difference in percentage is quite notable. When referring back to an even earlier EOI, the second highest level of SD is seen for 100MPa while later EOIs do not have this intermediately and 100MPa follows more in line with pressures 40MPa and up. This signifies that this high load case of 9Bar that lower pressures are not favourable for retarded start of injection. Likewise, for an earlier injection a high pressure of 100MPa is not suitable for this injector. Further in cylinder PDPA studies could unearth how the droplet sizing is affected. For a 7Bar BMEP EOIs 90 and 60° are mostly consistent in their position and spread in terms of SD. After 60° EOI there is a dramatic shift towards a more homogenous mixture suggesting that there is a major shift in behaviour of the spray characteristics that remains consistent till the latest injection strategy of 10° EOI to below 30%.

The lowest BMEP tested here of 4.5Bar BMEP does not lend itself well to low SD seen in other cases although notably 60MPa has the lowest deviation from 60 to 10°EOI. For 4.5Bar BMEP 40MPa is ranked second lowest behind 60MPa, ranked third is 20MPa. This could imply that the at this load, and with other load cases, that pressure is not acting linearly or predictable but rather has a concave trend. When isolating 40MPa in the different load and EOI cases it is consistently one of the lowest for SD. Inspecting Figure 47, the histograms of fuel droplet distribution, could reveal the answer as the frequency for smaller droplet sizes are uniformly higher on average than others and when operating within the confines of in-cylinder conditions, rebound off the cylinder wall with favourable droplet size and kinetic energy that it coincidently creates the optimum homogeneous fuel/ air mixture for the setup and the condition tested.
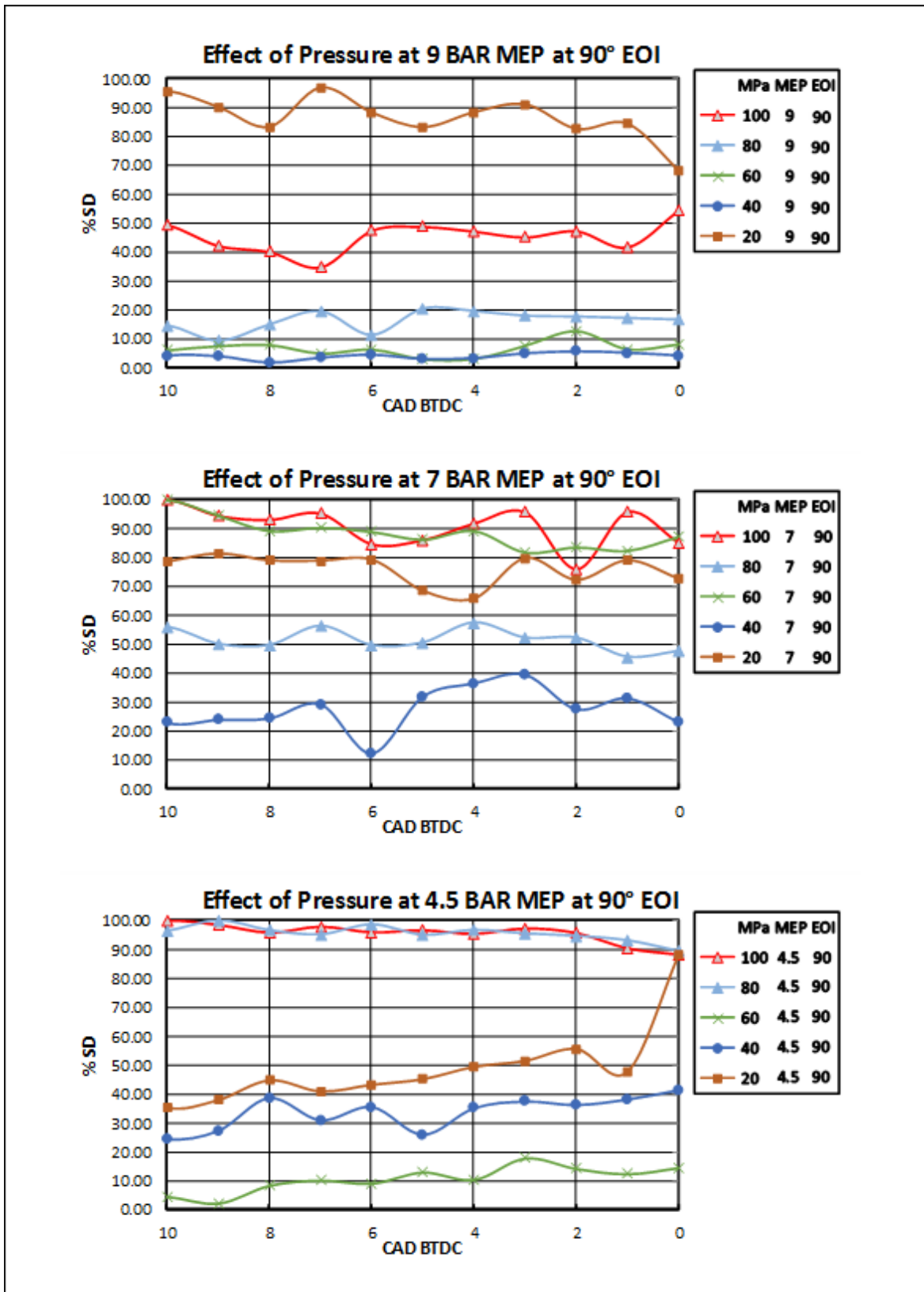
Figure 54: Effects of injector pressure at 90° EOI cases
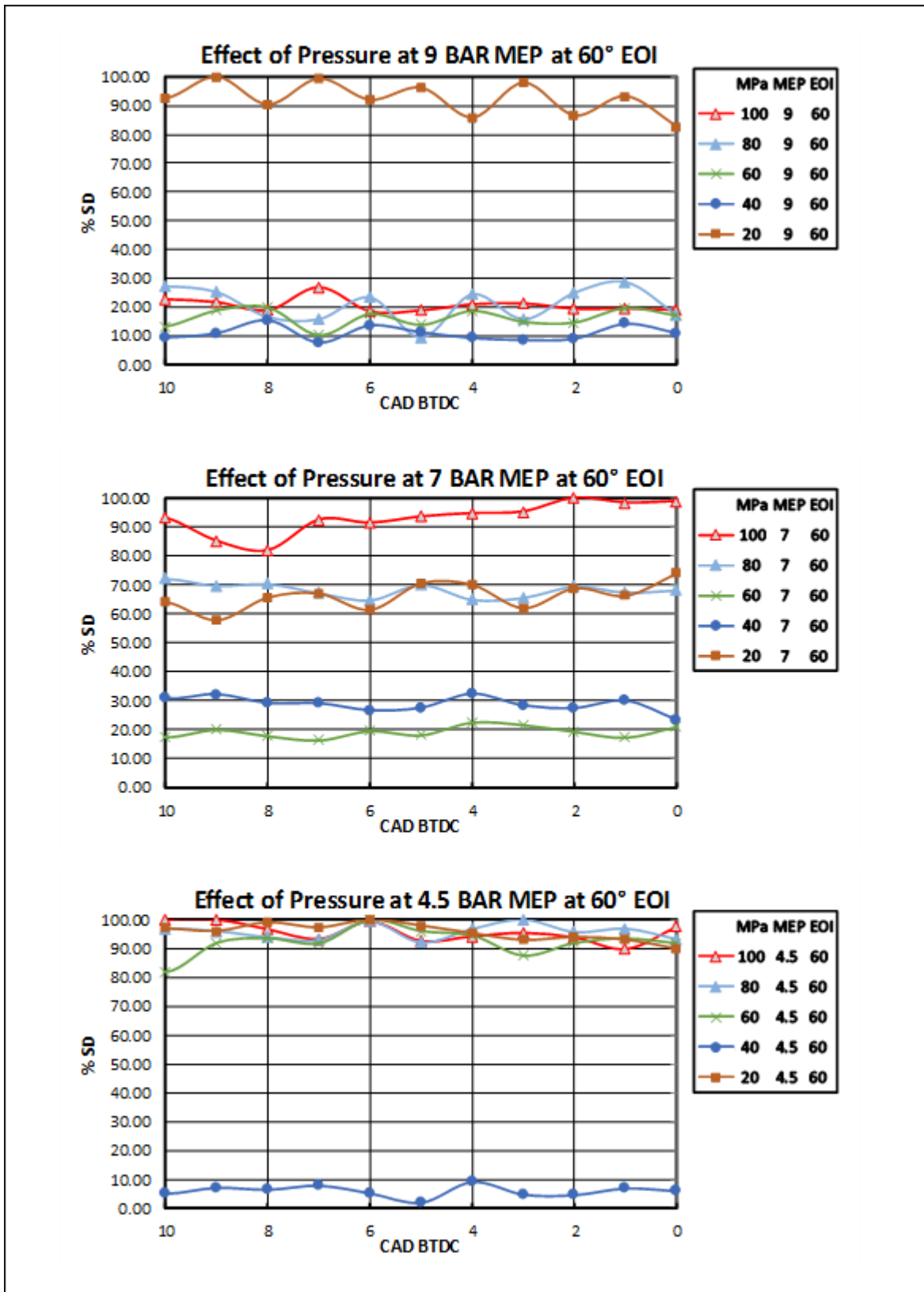
Figure 55: Effects of injector pressure at 60° EOI cases
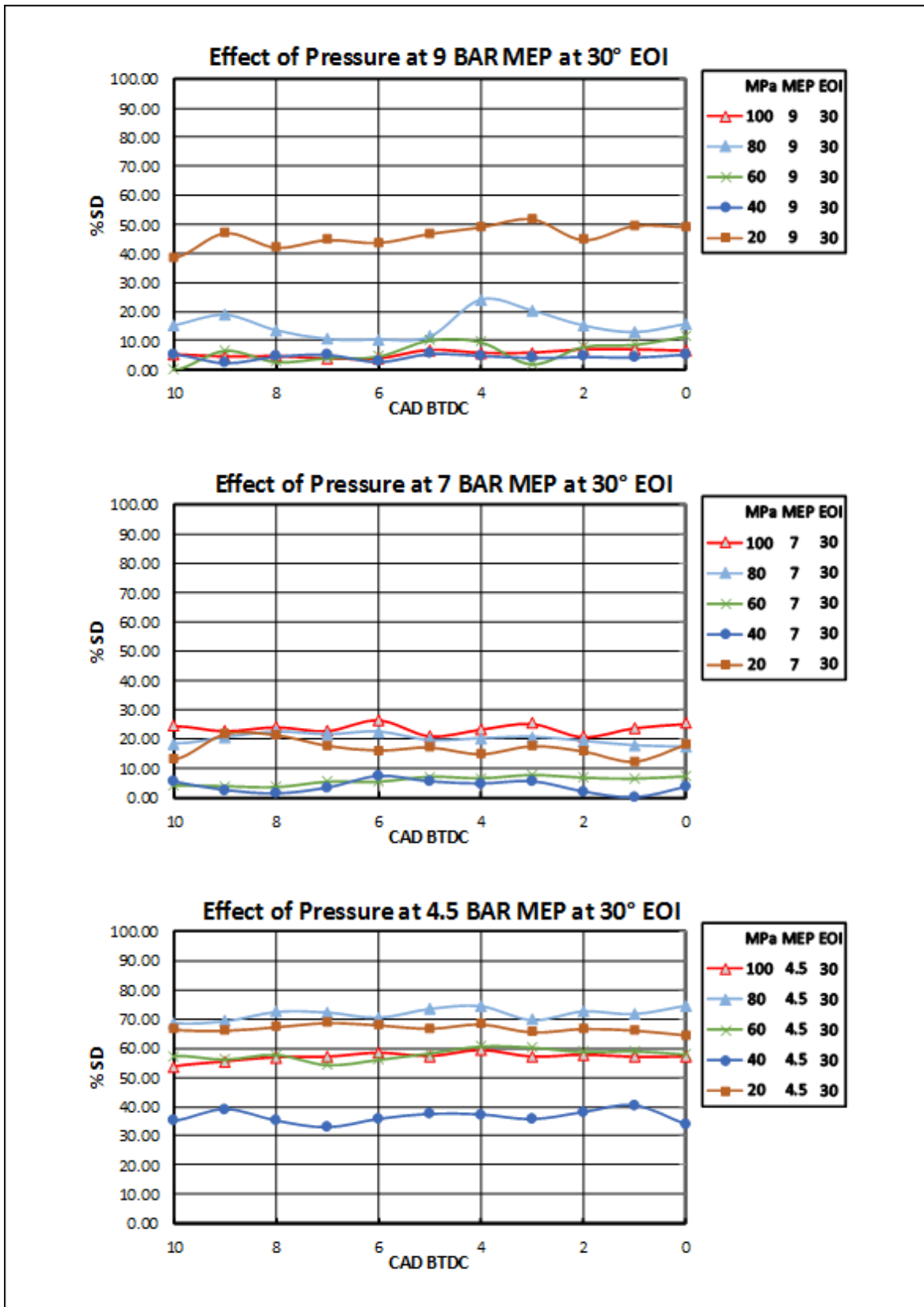
Figure 56: Effects of injector pressure at 30° EOI cases
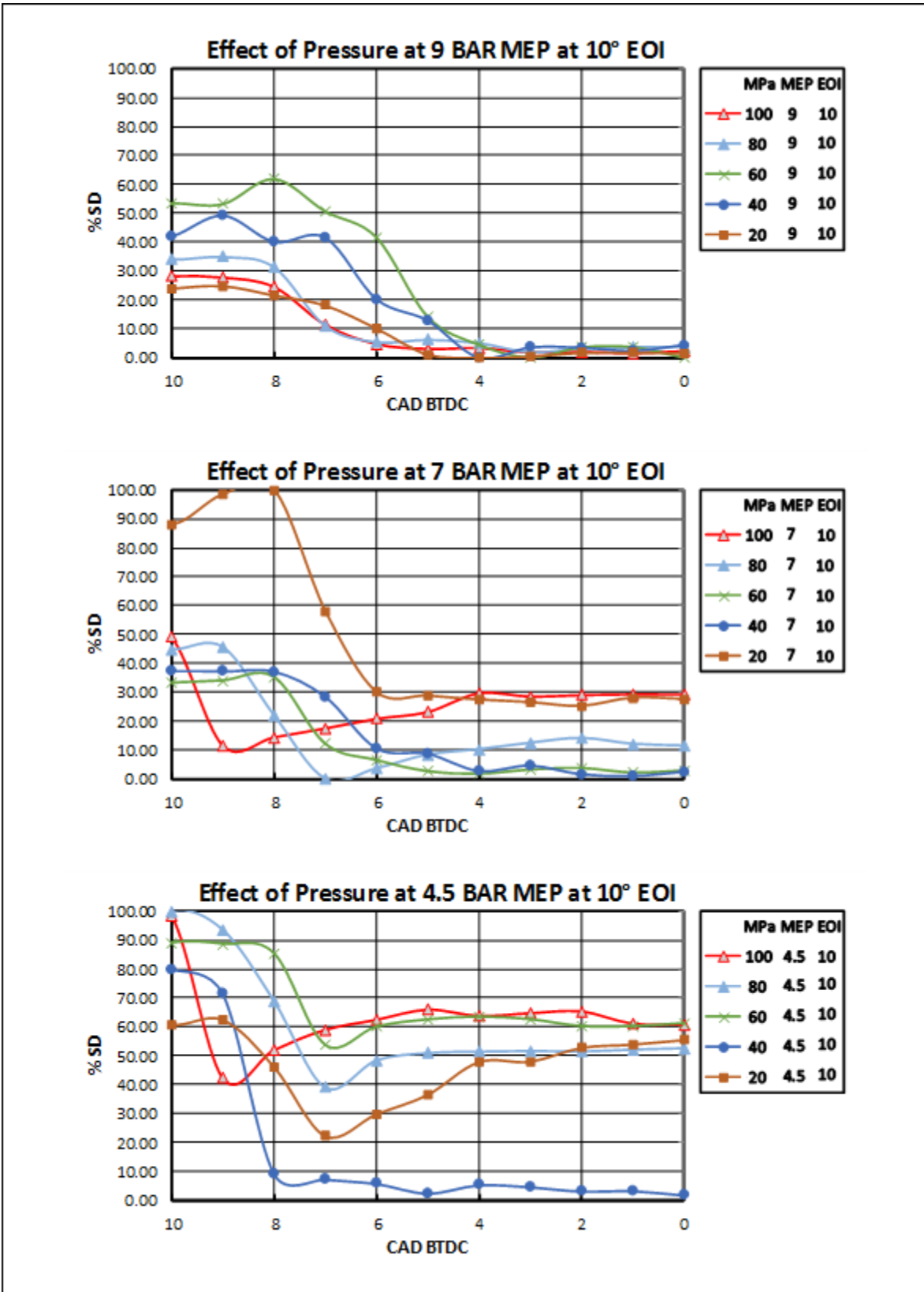
Figure 57: Effects of injector pressure at 10° EOI cases
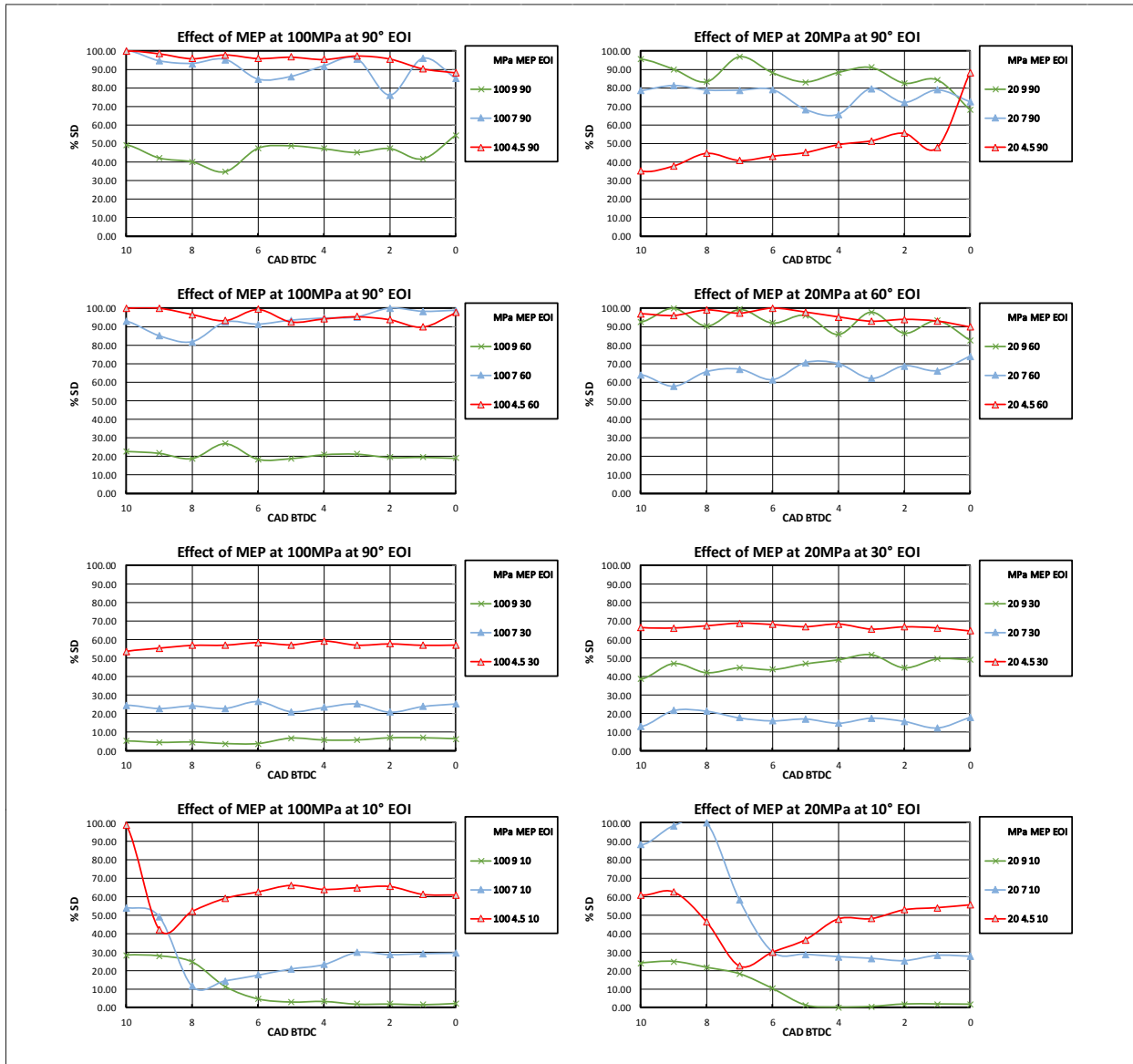
Figure 58: Effects of MEP at 90°, 60°, 30° & 10° EOI for 100 & 20MPa injection pressures

Figure 58 shows a series of graphs that corresponds to 100 and 20 MPa from 4.5 to 9Bar BMEP with EOI events from 90° to 10°. Observing these graphs relating to MEP an overall trend can be seen whereas the injection timing is increasingly retarded the SD for most cases decreases at TDC. As the fuel pressure lowers this trend is still observed, however the SD becomes more erratic and less clear. A reasoning is that as the pulse widths for higher loads and lower pressures are longer the volume of fuel is also increased producing differing penetration lengths that impinge on the cylinder glass. The different fuel quantity sprayed into the cylinder would influence the homogeneity by means of creating turbulent mixing that alters with injection timing and engine load.

6.4 Summary

High-speed Laser induced fluorescence has been used to record the in-cylinder fuel distribution at ultra-high injection pressure with retarded start of injection. High, medium and low engine conditions were also tested to provide an insight into how spray characteristics effect the mixture preparation in an optical research engine at 1200rpm. The use of a high repetition 355nm laser operating at 6800Hz coupled to a high-speed camera of the same frame rate is sufficient to measure the temporal fuel distribution with a one crank angle resolution. These LIF images are post processed using a bespoke MATLAB programme and Dantec Dynamics BSA flow software to convert the images into numerical data regarding the SD of fuel concentration within the cylinder.

Scrutinising the experimental data reveals that the injection pressure does not increase the atomisation and mixture homogeneity linearly as seen with previous experiments. Several cases are seen to have the intermediate fuel pressure, notably 40MPa, displaying the least amount of SD and thus most homogeneous mixture distribution. The variance of the exhibited information can vary dramatically when the EOI is at 90° BTDC. But when seen as a whole picture several trends present themselves. For this specific experimental setup earlier injection strategies give a wide assortment of values symbolising that more factors are attributing to mixture formation such as the wall impinging tumble of the fuel spray seen in the high-speed images. As the injection strategies become more retarded the SD for all loads becomes more condensed and follow each other more closely in an overall decline. A contributing factor to this would be the reduction in in-cylinder volume where fuel spray ricochets more aggressively back onto itself dispersing to form a much more homogenous mixture. This suggests that the penetration length plays a substantial roll in homogeneity at the expense of wall impingement and occurs with all pressures tested. As the load increases from 4.5 to 9Bar BMEP for 10° EOI cases SD decreases further notably for all pressures. The larger pulse widths and fuel quantities that accompany the higher loads could be exacerbating the homogeneity by its own fuel spray turbulence.

Laser induced fluorescence has been able to provide insight into in-cylinder characteristics of ultra-high-pressure gasoline with different engine conditions and injection strategies. For this experiment a retarded injection strategy is beneficial to mixture homogeneity. Although previous PDPA experiments show that the frequency of smaller droplet sizes is exhibited with higher fuel pressure but whether this translates to smaller in-cylinder droplets is unknown due to significant cylinder wall impingement playing a major factor.

Chapter 7: Summary and Conclusions

The aim in this project was to assess the characteristics of ultra-high-pressure gasoline fuel injection for its potential use in retarded injection strategies to supress engine knock. Higher injection pressures are expected to produce improved atomization, faster breakup, greater dispersal, and accelerated combustion. To evaluate retarded start of injection, systematic experiments were undertaken that visualise and quantitatively analyse the fuel spray evolution, atomisation and cylinder homogeneity. Summaries of the findings and the main conclusion of this experimental works are presented in this chapter, followed by the recommendation for future works.

7.1 Summary of findings for high-speed backlit illumination images

To understand the effects fuel pressure and pulse widths has on the penetration length of the fuel spray, high-speed imaging was used to investigate the macroscopic spray evolution of a high-pressure DI fuel injector. Fuel injection pressures ranged from 20 to 100 MPa with fuel quantities ranging from 0.01 to 0.05g per injection. The recorded images show distinctive features that correspond to varying fuel pressures and pulse widths. Analyses of the spray images suggest that a liquid fuel jet resides at the spray's core, yet its impact diminishes as the fuel pressure escalates to 100 MPa. At this heightened pressure, the liquid fuel at the periphery interacts with the surrounding air, manifesting a visibly broader cone angle. The high-speed imaging shows escalated fuel pressure resulting in smaller fuel droplets by air entrainment on the boundary of the fuel spray, albeit raising concerns about potential wall impingement in forthcoming in-cylinder experiments. To measure penetration length, test cases were repeated 30 times to obtain an average penetration length for each fuel injection case. Noticeable shifts in penetration length emerge with increased fuel quantities. This divergence arises from an extended injector pulse duration, that enables the fuel to harness more kinetic energy, propelling it over greater distances. Escalating the fuel pressure while keeping the fuel quantity constant requires a reduction in pulse width. This supplies the fuel spray with an equivalent kinetic energy for comparable penetration lengths between fuel quantities regardless of pressure.

Contrary to expectations, altering fuel pressure doesn't significantly amplify the total penetration length for a given fuel quantity. Instead, it accelerates the rate of injection when active, owing to the increased kinetic energy. These insights into spray dynamics offer valuable viewpoints at a macroscopic level for optimising fuel injection in the context of engine performance.

7.2 Summary of findings for droplet size and velocity measurements

Determining the droplet sizes and velocities of ultra-high-pressure fuel spray required the use of a PDPA system inside a constant volume chamber. Using this system to measure at different distances from the injector tip quantifies the atomisation process along the spray plume and to see the effects fuel pressure has in terms of droplet size and velocity. For this experiment a 1.5ms pulse width was selected with injection pressures ranging from 20 to 100MPa with measurements taken at 40, 60, 80 and 100mm away from the injector tip along the spray plume. To obtain acceptable results a target of over 30,000 droplet counts for each case was set. However, a persisting count of 60,000 to 100,000 droplets were achieved and used for analysis. The droplet size distribution showcased a pronounced inclination towards smaller droplets with higher injection pressures, exhibiting droplets enlarging up to 16µm. Comparisons amid pressures indicated that heightened pressures yielded smaller droplets to migrate towards the spray boundary due to higher kinetic energy creating a more turbulent spray boundary that is apparent with higher fuel pressures. As fuel pressure rises a decrease in D32 is seen up until 80MPa where from there no further decrease is seen at 100MPa suggesting that a hard mass flow limit has been reached suggesting that the number of D32 sized particles cannot be increased thereafter. However, as mentioned, as the fuel pressure increases the D10 sized particles surge and continue to do so to no such limitation in comparison to D32 as the enhanced kinetic energy creates boundary layer turbulence creating a migration of smaller D10 fuel droplets from the main spray plume to the outer edges. PDPA delivers quantitative measurements about droplet behaviour that extend beyond the capabilities of high-speed imaging alone.

7.3 Summary of findings for in-cylinder homogeneity images and measurements

High-speed Laser-induced fluorescence was employed to examine the in-cylinder homogeneity of ultra-high-pressure direct fuel injection with a retarded start of injection strategy in an optical engine operating at 1200rpm. High, medium, and low engine conditions engine conditions were explored using a high repetition 355nm laser and a high-speed camera to achieve fine resolution figures at 1 CAD. MATLAB and Dantec Dynamics BSA flow software were used for the post-processing, converting images into numerical data regarding the SD of the fluorescing fuel particles within the cylinder.

The experimental data exposed non-linear behaviour of the injection pressure on the in-cylinder mixture formation process. Intermediate fuel pressure, particularly at 40MPa, exhibited the least SD, indicating better homogeneity at certain test cases. Several other trends also emerged, with earlier injection strategies showing a broad range of values, suggesting that wall impingement is affecting mixture formations. Retarded injection strategies lead to in condensed SD across all

loads, indicating a more homogenous mixture due to fuel spray ricocheting in the reduced cylinder volume. This emphasised the role that penetration length and the ensuring spray impingement on piston and cylinder liners have on the mixture formation process with the current injector that was designed for a diesel engine. As load increased from 4.5 to 9Bar BMEP for 10° EOI cases, SD decreased further, likely influenced by the larger pulse widths and fuel quantities exacerbating homogeneity through increased fuel spray turbulence. In-cylinder Laser-induced fluorescence can play a major role into understanding combustion chamber conditions and injection strategies. A retarded injection strategy can promote mixture homogeneity though ultra-high direct fuel injection, though the impact of smaller droplet sizes on in-cylinder behaviour remains uncertain due to the significant cylinder wall impingement observed across many of the cases tested.

7.4 Recommendation for future works

It was observed that with higher fuel pressures that the cone angle of the spray plume became wider. Using MATLAB, it would be possible to segment the images into section at even intervals to determine the volume of the plume. With a known fuel quantity, a plume volume to fuel ratio can be calculated giving another spray characteristic to examine and would be another level deeper in the macroscopic spray details of the DI injector giving an indication of spray diffusion.

As wall impingement is highlighted to be a continues problem. The droplets that are measured by the PDPA after 40mm are not representative to the in-cylinder droplets. Moving the PDPA into the cylinder will give an insight to how wall impingement is affecting droplet sizing.

Split injection strategies can also be investigated as a counter to wall impingement and its affects can also be examined with LIF in the same fashion. Several smaller injection pulses individually delivering small amounts of fuel could see the penetration length minimised as seen with smaller pulse widths here although appropriate time for the injections to occur will need to be accounted for when injecting into the cylinder.

The in-cylinder PLIF measurements demonstrated the presence of significant wall wettings by use of the current injector that was designed for a diesel compression ignition engine. It would be necessary to redesign the injector in order to take advantage of the better atomisation of ultra-high injection sprays for retarded injection in a spark ignition engine. Furthermore, with the interest in alternative fuels for the use in SI engines for widespread adoption, it would only be a matter of time since they are scrutinised and the need for more fuel efficient alternative fuelled SI engines are called for. Understanding how these fuels react to these experiments in comparison to gasoline is advantageous for manufactures in the imminent future.

References

[1] T. Smith, A. Jones and B. Johnson, "The Impact of Automotive Emissions on the Environment," *Environmental Science: Processes & Impacts,* vol. 20, no. 2, pp. 229-246, 2018.

[2] IEA, "Global EV Outlook 2020," IEA, Paris, https://www.iea.org/reports/global-ev-outlook-2020, License: CC BY 4.0, 2020.

[3] R. Stolkin and e. al., "A Review of Alternative Jet Fuels," *Energies,* vol. 12, no. 19, pp. 36-55, 2019.

[4] J. Haywood, Internal Combustion Engine Fundementals (second edition), London: McGraw-hill Education, 2018.

[5] N. Fraser, H. Blaxill, G. Lumsden and M. Bassett, "Challenges for Increased Efficiency through Gasoline Engine Downsizing," *SAE Int. J. Engines,* vol. 2, no. 1, p. 991–1008, 2009.

[6] J. Turner, A. Popplewell, R. Patel, T. Johnson and e. al., "Ultra Boost for Economy: Extending the Limits of Extreme Engine Downsizing," *SAE Int. J. Engines,* vol. 7, no. 1, pp. 387-417, 2014.

[7] B. Singh and S. Shukla, "Experimental analysis of combustion characteristics on a variable compression ratio engine fuelled with biodiesel (castor oil) and diesel blends," *Biofuels,* vol. 7, no. 5, pp. 471-477, 2016.

[8] M. Shelby, T. Leone, K. Byrd and F. Wong, "Fuel Economy Potential of Variable Compression Ratio for Light Duty Vehicles," *SAE Int. J. Engines 10(3):817-831, doi: 2017-01-0639,* 2017.

[9] E. Toulson, H. Schock and W. Attard, "A Review of Pre-Chamber Initiated Jet Ignition Combustion Systems," *SAE Technical Paper: 2010-01-2263, doi: 10.4271/2010-01-2263,* 2010.

[10] Energy Information Administration, "Today in Energy," 22 08 2022. [Online]. Available: https://www.eia.gov/todayinenergy/detail.php?id=53539. [Accessed 16 10 2023].

[11] L. Richard and P. Beachtold, Alternative Fuels Guidebook, Warrendale, PA, USA: SAE International, 1997.

[12] B. He, J. Wang, J. Hao, X. Yan and J. Xiao, "A study on emission characteristics of an EFI engine with ethanol blended gasoline fuels," *Atmospheric Enviroment,* vol. 37, pp. 949-957, 2003.

[13] S. Taniguchi, K. Yoshida and Y. Tsukasaki, "Feasibility study of Ethanol Applications to A Direct Injection Gasoline Engine," *SAE Technical Paper No. 2007-01-2037,* 2007.

[14] D. Bresenham and J. Reisel, "The effect of High Ethanol Blends on Emissions from Small Utility Engines," *SAE Technical Paper No. 1999-01-3345,* 1999.

[15] T. Wallner and S. Miers, "Combustion Behaviour of Gasoline and Gasolinel/Ethanol Blends in a modern Direct-Injection 4-Cylinder Engine," *SAE Technical PaperNo. 2008-01-0077,* 2008.

[16] U.S. Department of Energy, ""Assesment of Costs and Benefits of Flexible and Alternative Fuel Use in the U.S. Transportation Sector"," *Technical Report Three: Methanol Production and Transportation Costs,* 11 1989.

[17] U.S. Enviromental Protection Agency, "Mobile Source-Related Air Topics Study," *as reported in "The Clean Fuels Report",* 9 1993.

[18] U.S. Department of Energy, ""Alteranatives to Traditional Transportation Fuels - Volume 2: Greenhouse Gas Emissions"," *Energy Information Administration, Report No. DOE/EIA-0585(94)/1, Febuary 1996,* 1992.

[19] M. Wang, "Development and Use of the GREET Model to Estimate Fuel-Cycle Energy Use and Emissions of Various Transportation Technologies and Fuels".*Arrgonne National Laboratory, Argonne, Ill, USA.*

[20] U.S. Department of Energy, ""Assesment of Costs and Benefits of Flexible and Alternative Fuel Use in the U.S. Transportation Sector Technical Progress Report One: Context and Analytical Framework"," *DOE/PE-0080,* 1 1988.

[21] G. Zacharakisjutz, *Performance Characteristics of Ammonia Engines Using Direct Injection Strategies. Ph.D. Thesis,* Ames, IA, USA: Iowa State, 2013.

[22] R. Liu, D. Ting and M. Checkel, "Ammonia as a Fuel for SI Engine," SAE Technical Paper; SAE, Warrendale, PA, USA, 2003.

[23] C. Mounaïm-Rousselle and P. Brequigny, "Ammonia as Fuel for Low-Carbon Spark-Ignition Engines of Tomorrow's Passenger Cars," *Front. Mech. Eng,* vol. 6, no. 70, p. doi: 10.3389/fmech.2020.00070, 2020.

[24] E. Koch, "AMMONIA-A FUEL FOR MOTOR BUSES," *J. Inst. Petroleum,* vol. 31, pp. 213 - 223, 1949.

[25] S. Maity, K. Gayen and T. Bhowmick, Hydrocarbon Biorefinery, Amsterdam: Elsevier, 2021.

[26] H. Hientzsch, "How to Make eFuels Truly Sustainable," *Porsche Magazine, Christophorus No. 407,* pp. 42-50, 2 2023.

[27] R. Stone, Introduction to internal combustion engines, Basingstoke: Palgrave Macmillan, 2012.

[28] SmellPetrol, "Combustion in IC SI Engines," 2019. [Online]. Available: http://petrolsmell.com/2012/07/02/combustion-in-ic-si-engines/. [Accessed 12 04 2019].

[29] V. Hassan, "A study of pre-ignition and knock in an optical spark ignition engine," *Brunel University Research Archive (BURA),* vol. Brunel University London, 2018.

[30] W. Pulkrabek, Engine Fundamentals of the Internal Combustion Engine, Upper Saddle River, N.J.: Pearson Education, Inc, 2004.

[31] Simple Digital Systems, "Pushing it Too Far," 29 02 2000. [Online]. Available: http://www.sdsefi.com/meltdown.htm. [Accessed 03 04 2019].

[32] Applied Chemical Specialties Inc, "Fall 2012," 2012. [Online]. Available: https://www.no-rosion.com/fall2012.htm. [Accessed 26 09 2020].

[33] J. Linengood and P. Wu, "Correlation of autoignition phenomenom in internal combustion engines and rapid compression machines," *Proc 5th International Symposium on Combustion,* no. ISSN 0082 0784, pp. 347-56, 1955.

[34] E. Forlani and E. Ferrati, "Miccroelectronic ignition - status and evolution," *Paper 87002 ISATA Procedings,* 1987.

[35] E. W. Meyer, R. Green and M. Cops, "Austin-Rover Montego Programmed ignition system," in *VECON '84 Fuel Efficent Power Trains and Vehicals*, London, 1984.

[36] A. Isenstadt, J. German, M. Dorobantu, D. Boggs and T. Watson, "Downsized, boosted gasoline engines," *ICCt, Working paper 2016-22,* 2016.

[37] H. Zhao, in *Advanced direct injection combustion engine technologies and development*, H. Zhao, Ed., Sawston, Cambridge, Woodhead Publishing Limited, 2009, p. 2.

[38] U. Meinig, "One Hundred Years of Gasoline Direct Injection Part 2.," in *MTZ worldwide. 77. 30-37. 10.1007/s38313-016-0130-2.*, 2016.

[39] J. Haywood, Internal Combustion Engine Fundamentals (second edition), London: McGraw-Hill Education, 2018.

[40] U. Montanaro, A. di Gaeta and V. Giglio, "An MRAC Approach for Tracking and Ripple Attenuation of the Common Rail Pressure for GDI Engines," in *Preprints of the 18th IFAC World Congress*, Milano, 2011.

[41] A. Kalwar and A. Agarwal, Overview, Advancements and Challenges in Gasoline Direct Injection Engine Technology. In: Singh A., Sharma N., Agarwal R., Agarwal A. (eds) Advanced Combustion Techniques and Engine Technologies for the Automotive Sector. Energy, Environment, and Sustaina, Singapore: Springer, 2020.

[42] H. Badshah, D. Kittelson and W. Northrop, "Particle Emissions from Light-Duty Vehicles during Cold-Cold Start," SAE Internation, London, 2016.

[43] R. Stone, B. Williams and P. Ewart, "Optical Techniques that can be Applied to Investigate GDI Engine Combustion," *SAE Technical Paper 2017-24-0046,* 2017, doi:10.4271/2017-24-0046.

[44] P. Bielaczyc and J. Merkisz, "Cold Start Emissions Investigation at Different Ambient Temperature Conditions," *SAE Technical Paper 980401,* 1998, doi:10.4271/980401.

[45] I. Whelan, W. Smith, D. Timoney and S. Samuel, "The Effect of Engine Operating Conditions on Engine-out Particulate Matter from a Gasoline Direct-injection Engine during Cold-start," *SAE Technical Paper 2012-01-1711,* 2012, doi:10.4271/2012-01-1711.

[46] J. Laurikko, "Ambient temperature effect on automotive exhaust emissions: FTP and ECE test cycle responses," *Sci. Total Environ 169:195-204,* 1995, doi:10.1016/0048-9697(95)04648-K.

[47] P. Mulawa, S. Cadle, K. Knapp, R. Zweidinger, R. Snow, R. Lucas and J. Goldbach, "Effect of ambient temperature and E-10 fuel on primary exhaust particulate matter emissions from light-duty vehicles," *Environ. Sci. Technol. 31(5):1302-1307, 1997,* 1997, doi:10.1021/es960514r.

[48] P. Bielaczyc, A. Szczotka and J. Woodburn, "Excess Emissions and Fuel Consumption of Modern Spark Ignition Passenger Cars at Low Ambient Temperatures," *SAE Technical Paper 2012-01-1070,* 2012, doi:10.4271/2012-01-1070.

[49] K. Tong, B. Quay, J. Zello and D. Santavicca, "Fuel Volatility Effects on Mixture Preparation and Performance in a GDI Engine During Cold Start," *SAE Technical Paper 2001-01-3650,* 2001, doi:10.4271/2001-01-3650.

[50] G. Taylor and S. Stewart, "Cold Start Impact on Vehicle Energy Use," *SAE Technical Paper 2001-01-0221,* 2001, doi:10.4271/2001-01-0221.

[51] R. Kassel, P. Couch, M. Conolly and A. Hammer-barulich, "Ultrafine Particulate Matter and the Benefits of Reducing Particle Numbers in the United States," *MECA Report,* 2013.

[52] G. Fiengo, A. di Gaeta, A. Palladino and V. Giglio, "Common Rail System for GDI Engines," Springer, London, 2013.

[53] E. Stevens and R. Steeper, "Piston Wetting in an Optical DISI Engine: Fuel Films, Pool Fires, and Soot Generation," in *SAE Technical Paper Series: 2001-01-1203, SAE World Congress*, Detroit, Michigan, 2001.

[54] J. Jose, A. Parsi, S. Shridhara, M. Mittal and e. al., "Effect of Fuel Injection Timing on the Mixture Preparation in a Small Gasoline Direct-Injection Engine," *SAE Technical Paper 2018-32-0014, https://doi.org/10.4271/2018-32-0014,* 2018.

[55] M. Costa, L. Marchitto, S. S. Merola and U. Sorge, "Study of mixture formation and early flame development in a research GDI (gasoline direct injection) engine through numerical simulation and UV-digital imaging," *Energy,* vol. 77, pp. 88-96, 2014.

[56] P. Richardson, J. Gu and G. Di Liberto, "Knock Prevention by Retarded Injection with Ultra-High Pressure and Fuel injector Nozzle Development," *28th Achen Colloquium Automobile and Engine Technology 2019,* pp. 1103-1128, 2019.

[57] M. A. Attara, M. R. Herfatmaneshb, H. Zhao and A. Cairns, "Experimental investigation of direct injection charge cooling in optical GDI engine using tracer-based PLIF technique," *Experimental Thermal and Fluid Science,* vol. 59, pp. 96-108, 2014.

[58] E. Kasseris and J. Heywood, "Charge Cooling Effects on Knock Limits in SI DI Engines Using Gasoline/Ethanol Blends: Part 1-Quantifying Charge Cooling," *SAE Technical Paper 2012-01-1275, http://dx.doi.org/10.4271/2012-01-1275,* 2012.

[59] J. B. Haywood, INTERNAL COMBUSTION ENGINE FUNDAMENTALS, New York: Mcgraw-hill, 1988.

[60] G. Konig and C. Sheppard, "End gas autoignition and knock in a spark ignition engine," *SAE No. 902135,* 1990.

[61] R. R. Maly, "State of the art and future needs in S.I. engine combustion," in *25th Symposium Internal on Combustion/The Combustion Institute*, 1994/pp. 111-124.

[62] U. Spiecher, L. Speigel and B. Reggelin, "Investigation into applicability of an optical fiber sensor for knock detection and knock control system," *SAE No. 922370,* 1992.

[63] T. Kaminaga, K. Yamaguchi, S. Ratnak and J. Kusaka, "A Study on Combustion Characteristics of a High," *SAE International,* pp. 2019-24-0106, 2019.

[64] K. Kuwahara, K. Ueda and H. Ando, "Mixing Control Strategy for Engine Performance Improvement in," *SAE International,* p. 980158, 1998.

[65] T. Li, K. Nishida, Y. Zhang and H. Hiroyasu, "Effect of split injection on stratified charge formationof direct injection spark ignition engines, DOI: 10.1243/14680874JER02106," *Int. J. Engine Res. Vol. 8,* pp. 205-219, 2006.

[66] K. Li, K. Nishida, Y. Ogata and B. Shi, "Effect of flat-wall impingement on diesel spray combustion," *Proceedings of the Institution of Mechanical Engineers, Part D: Journal of Automobile EngineeringVolume 229, Issue 5,* pp. 535-549, 2015.

[67] R. Kiplimoa, E. Tomitaa, N. Kawaharaa and S. Yokobe, "Effects of spray impingement, injection parameters, and EGR on the combustion," *Applied Thermal Engineering,* pp. 165-175, 2012.

[68] H. Badshah, D. Kittelson and W. Northrop, "Particle Emissions from Light-Duty Vehicles during Cold-Cold Start," *SAE International,* pp. doi:10.4271/2016-01-0997, 2016.

[69] Z. Feng, C. Zhan, C. Tang, K. Yang and H. Z., "Experimental investigation on spray and atomization characteristics of," *Energy,* pp. 549-561, 2016.

[70] R. Payri, J. Gimeno, P. Marti-Aldaravi and G. J.S., "Methodology for Phase Doppler Anemometry Measurments on a Multi-hole Diesel Injector," *Exp Tech, DOI 10.1007/s40799-016-0154-1,* p. 95–102, 2017.

[71] C. Jiang, M. Parker, A. Spencer, G. Wigley, G. C.P. and H. J., "Droplet Size Development in a DISI Injector Fuel Spray," *18th International Symposium on the Application of Laser and Imaging Techniques to Fluid Mechanics,* 2016.

[72] S. Lee, Y. Oh and S. Park, "Characterization of the spray atomization process of a multi-hole gasoline direct injector based on measurements using a phase doppler particle analyser," *Proc IMechE Part D: J Automobile Engineering,* vol. 7, no. 227, pp. 951-965, 2013.

[73] S. Lee and S. Park, "Experimental study on spray break-up and atomization processes," *International Journal of Heat and Fluid Flow,* vol. 45, pp. 14-22, 2014.

[74] B. Stiebels, R. Krebs and E. Pott, "FSI - Gasoline direct injection engines from Volkswagen," in *Proc. of GPC Global Powertrain Congress June 2001, Vol a: Advanced engine design & performance*, Detroit, USA, 2001.

[75] K. Hiraya, I. Hotta, E. Takahashi, H. Tsuchida and T. Urushihara, "A Study of a DISI Engine with a Centrally Located High-pressure Fuel Injector. SAE Technical paper: 2004-01-2944," SAE International, Warringdale, Pennsylvania, USA, 2004.

[76] E. Karaiskos, C. Arcoumanis and T. Hale, "Flow and Spray Investigation in Direct Injection Gasoline Engines. SAE Technical paper: 2002-01-0832," SAE International, Warrendale, Pennsylvania, USA, 2002.

[77] S. Soichi, S. Hitoshi, O. Masahiro and M. S., "Evolution of Gasoline Direct Injection System for Reduction of Real Mode Emission," *SAE Technical Paper 2019-01-0265,* pp. doi:10.4271/2019-01-0265, 2019.

[78] L. Postrioti, A. Cavicchi, G. Brizi, F. Berni and S. Fontanesi, "Experimental and Numerical Analysis of Spray Evolution, Hydraulics and Atomization for a 60 MPa Injection Pressure GDI System," *SAE Technical Paper 2018-01-0271,* pp. doi:10.4271/2018-01-0271, 2018.

[79] R. Ochoterena, A. Lif, M. Nyden, S. Andersson and I. Denbratt, "Optical studies of," *Fuel,* vol. Vol. 89, no. 1, pp. 22-132, 2010.

[80] J. shao and Y. Yan, "Digital Imaging Based Measurement of Diesel Spray Characteristics," in *IEEE Instrumentation and Measurement Tech. Conf. Proceedings*, Sorrento, Italy, 2006.

[81] S. Lee and S. Park, "Spray atomization characteristics of a GDI injector equipped with a group-hole nozzle," *Fuel 137,* pp. 50-59, 2014.

[82] J. Hwang, J. Ha and S. No, "Spray Characteristics of DME in Conditions of Common Rail Injection System (II)," *International Journal of Automotive Technology,* vol. 4, no. 1, pp. 119-124, 2003.

[83] H. Zhao, Laser Diagnostics and Optical Measurement Techniques in Internal Combustion Engines, Warringdale, Pennsylvania USA: SAE International, 2012.

[84] A. Coghe and G. Cossali, "Quantitative optical techniques for dense sprays investigation: A survey," *Optics and Lasers in Engineering,* vol. 50, pp. 46-56, 2012.

[85] L. Araneo, V. Soare, R. Payri and J. Shakal, "Setting up a PDPA system for measurments in a Diesel spray," *Journal of Physics: Conference Series,* vol. 45, no. 85, 2006.

[86] H. P. Fuchs and E. Winklhofer, "Diesel fuel spray visualisation by laser induced fluorescence," FLuid Mechanics Research Department, AVL LIST GmbH, Graz, Austria, 1991.

[87] J. Smith and V. Sick, "Crank-angle resolved imaging of biacetyl laser-induced fluoresence in an optical internal combustion engine," *Appl. Phys.,* vol. 81, no. B, pp. 579-584, 2005.

[88] T. Heinze and T. Baritaud, "Gasoline Distribution Measurments with PLIF in a SI Engine," *Section 3: JOURNAL OF ENGINES,* vol. 101, pp. 2035-2047, 1992.

[89] J. Smith and V. Sick, "Quantitative, dynamic fuel distribution measurements," *Proceedings of the Combustion Institute,* vol. 31, pp. 747-755, 2007.

[90] D. Hung, D. Harrington, A. Gandhi and a. et, "Gasoline Fruel Injector Spray Measurment and Charicterization - A New SAE J2715 Recomended Practice, 2008-01-1068," SAE International, Warringdale, Pennsylvania, 2008.

[91] M. Dhanji and H. Zhao, "Effect of a split-injections strategy on the atomisation rate for charge stratification using a high pressure gasoline multi-hole injector," *SAE Technical Paper 2019-01-2248,* 2019.

[92] J. Changzhao, "OPTICAL INVESTIGATION ON THE SPRAY AND COMBUSTION CHARACTERISTICS OF THE FURAN BIO-FUELS," *PhD thesis, School of Mechanical Engineering, The University of Birmingham, Birmingham, England,* 2014.

[93] Lambert Instruments, *HiCATT 25 User's Manual,* Groningen: Lambert Instruments B.V., N.D.

[94] R. Ochoterena, A. Lif, M. Nyden, S. Andersson and I. Denbratt, "Optical studies of spray development and combustion of water-in-diesel emulsion and microemulsion fuels," *Fuel,* vol. Vol. 89, no. 1, pp. 22-132, 2010.

[95] L. Postrioti, A. Cavicchi, G. Brisi, f. Berni and e. al, "Experimental and Numerical Analysis of Spray Evolution, Hydraulics and Atomization for a 60 MPa Injection Pressure GDI System," *SAE Technical Paper 2018-01-0271,* 2018, doi:10.4271/2018-01-0271.

[96] J. Dharmalingam, "Knocking in spark ignition and compression ignition Engines," 2019. [Online]. Available: https://inspirationaltechnology.in/knocking-in-spark-ignition-and-compression-ignition-engines/auto/. [Accessed 19 01 2020].

[97] D. Ludykar, R. Westerholm and J. Almén, "Cold start emissions at +22, -7 and -20°C ambient temperatures from a three-way catalyst (TWC) car: Regulated and unregulated exhaust components," *Sci. Total Environ. 235(1-3):65-69,* 1999, doi:10.1016/S0048-9697(99)00190-4.